Open Research Online

The Open University's repository of research publications
and other research outputs

Electroplated titanium coatings

Thesis

How to cite:

Bettley, Alison (1992). Electroplated titanium coatings. PhD thesis The Open University.

For guidance on citations see FAQs.

© 1992 The Author

https://creativecommons.org/licenses/by-nc-nd/4.0/

Version: Version of Record

Link(s) to article on publisher's website:
http://dx.doi.org/doi:10.21954/ou.ro.00010168

Copyright and Moral Rights for the articles on this site are retained by the individual authors and/or other copyright owners. For more information on Open Research Online's data policy on reuse of materials please consult the policies page.

oro.open.ac.uk

UNRESTRICTED

DX97856

ELECTROPLATED TITANIUM COATINGS

Alison Bettley B.Sc

offered for the degree of Ph.D.

Discipline: Chemistry

Date of Submission: 31 March 1992

Date of submission: 30th April 1992
Date of award : 3rd July 1992

ProQuest Number: 27758383

All rights reserved

INFORMATION TO ALL USERS
The quality of this reproduction is dependent on the quality of the copy submitted.

In the unlikely event that the author did not send a complete manuscript
and there are missing pages, these will be noted. Also, if material had to be removed,
a note will indicate the deletion.

ProQuest 27758383

Published by ProQuest LLC (2019). Copyright of the Dissertation is held by the Author.

All Rights Reserved.
This work is protected against unauthorized copying under Title 17, United States Code
Microform Edition © ProQuest LLC.

ProQuest LLC
789 East Eisenhower Parkway
P.O. Box 1346
Ann Arbor, MI 48106 - 1346

ELECTROPLATED TITANIUM COATINGS

Alison Bettley

ABSTRACT

Electroplated titanium coatings on substrates such as steels have many potential industrial applications. The low cost of the substrate is combined with the excellent corrosion-resistance of the coating. However, titanium cannot be electrodeposited from aqueous systems because the hydrogen evolution reaction is always preferred. Proton-free media must be used. The electrodeposition of titanium from molten chlorides is well-known: large-scale titanium electrowinning processes have been operated, to produce high quality particulate material in an energy efficient way. The production of thick compact electroplates, however, has not been demonstrated consistently. It was therefore the objective of this work to determine the principal operating parameters for a titanium electroplating process based on a molten chloride (LiCl-KCl) bath.

Studies of substrate oxide film reduction, the electro-reduction of divalent titanium, the nature of electrodeposits produced under various plating conditions, and the behaviour of the dissolving titanium anode have been undertaken.

The following have been identified as the most important factors:

(1) Substrate pre-treatment

(2) Melt composition (titanium concentration, average valency, level of oxygen contamination)

(3) Electrochemical parameters (chosen so as to combine good nucleation characteristics with avoidance of mass transport control effects)

It has been demonstrated that thick, adherent, relatively smooth, compact coatings of titanium can be produced from molten chlorides at 450^{0}C. Pulse plating and periodic current reversal are the most promising techniques for future optimisation with the objective of developing a commercial process.

CONTENTS

LIST OF TABLES

LIST OF FIGURES

CHAPTER 1

INTRODUCTION

1.1. Titanium as a coating material

Titanium metal is remarkable for two principal characteristics: its excellent corrosion-resistance, particularly in oxidising environments; and a high strength-to-weight ratio. Applications for the metal can be divided into two broad areas, reflecting the exploitation of these properties: aerospace where the metal's mechanical properties are advantageous; and non-aerospace uses such as chemical plant construction where corrosion-resistance is the most important attribute. Its use is generally limited by cost (it is still a relatively expensive metal, typically £5000 per tonne for sponge metal in 1990) and by ease of fabrication. Sheet and tube fabricated from titanium are about four times as expensive as the same parts made in stainless steel, and perhaps ten or fifteen times the cost of mild steel; titanium components such as bolts may be ten times as expensive as stainless steel[110].

It is the corrosion-resisting properties which are of value in considering titanium as a coating material. Coatings are applied where the surface characteristics of the coating material need to be combined with other properties of the substrate. Frequently a cheap substrate can be imbued with more exotic surface properties by applying the appropriate coating. Examples include silver and gold electroplating for decorative purposes; zinc coatings (electro- or hot dip galvanising) on steels for corrosion-resistance; PTFE coatings for lubrication or non-stick attributes. Titanium coatings on cheaper substrates such as steels would provide the excellent

corrosion-resistance of titanium without the excessive cost. Examples of potential uses are given in table 1.1.

The reason for titanium's excellent corrosion-resisting performance is the presence of a tenacious and self-healing oxide layer on the metal's surface. Whenever the oxide layer is breached, perhaps by mechanical damage to the surface, it is immediately re-formed by reaction of the clean metal with oxygen in the atmosphere. It is only under conditions where this oxide itself is broken down that corrosion-protection fails.

In many instances of applying coatings for corrosion-protection the "galvanic effect" is relied upon. This is the fact that the relative reduction potentials of the coating and substrate materials in the corrosive medium are such that corrosion of coating takes place in preference to corrosion of the substrate. This is true for zinc-coated steel in air, for example. However, the combination of titanium with most other likely substrates leads to the reverse situation: the substrate will tend to corrode preferentially[34]. This places additionally rigorous requirements on the coating characteristics: it must have negligible porosity and be relatively thick in order to perform adequately.

There is currently no commercial process for the application of titanium coatings to foreign substrates. Flame spraying techniques using titanium dioxide powders produce a rather porous coating, incapable of supplying the degree of corrosion-resistance sustained by the metal itself[58]. Cladding is widely used, in which a thick sheet of titanium is bonded to a substrate material (usually steel) for the construction of such items as tubing and vessels for the

chemical industry. However, costs are high, not least because of the substantial thicknesses of titanium which are used.

Electroplated titanium coatings are therefore potentially very useful. Many aqueous electroplating systems are capable of yielding uniform, thick, continuous and pore-free coatings, widely used for a variety of coating metals and substrates for a range of purposes. Electroplating is just one of four specific types of electrodeposition process:

electrowinning: particulate solid or liquid metal product; metal compound feedstock.

electrorefining: particulate solid or liquid product; impure metal feedstock as dissolving anode.

electroplating: continuous compact solid coating product; dissolving anode or metal salts feedstock.

electroforming: similar to electroplating but substrate removed to leave free-standing electroform.

1.2. The electrodeposition of titanium - the state of the art

1.2.1. Aqueous solution

Titanium cannot be electrodeposited from aqueous solution because the hydrogen evolution reaction is thermodynamically preferred. Low titanium alloys can be produced but their properties are not comparable with those of pure titanium. There are some claims in the literature for titanium electrodeposition from aqueous solution[1]-[5]. These frequently depend on the use of various means of suppressing the hydrogen evolution reaction by the inclusion of

complexing agents. However usually only thin deposits are claimed, and evidence of true metal formation (as opposed to oxides or other compounds) is generally absent.

1.2.2 Organic Solvents

Many of the more common organic solvents, such as alcohols, offer similar opportunity for cathodic hydrogen discharge as water, and are therefore not useful alternative media. Aprotic solvents, such as ethers, acetonitrile, dimethyl sulphoxide, etc. have been studied widely as prospective solvents for the electrodeposition of metals which cannot be electrodeposited from aqueous solution[6]-[12]. Such liquids are very stable electrochemically, but have the disadvantage of generally being poor electrical conductors. Support electrolyte salts must often be added to improve this characteristic. However, even with this modification, current densities sustained by these systems are relatively low, making organic media generally inappropriate for primary metal production or refining purposes. Consequently most work is directed towards electroplated coatings, or, indeed, merely the verification that metal deposits (of any kind) can be produced.

In spite of the huge effort which has been put into these investigations, few useful plating baths have been developed, and none capable of producing titanium coatings. Some of the most promising results have been obtained in dimethyl sulphoxide[7]-[9].

This may, at first sight, seem surprising, in view of the fact that the alkali metals themselves can be electrodeposited from such media. Indeed, many modern battery systems are based on that

reaction[49]. However while lithium can be electrodeposited from propylene carbonate, for example, titanium cannot, although the latter's reduction potential is the less negative. This is because of the capacity of the transition metal ion to form a coordination complex with the solvent molecules. The transition metal is stabilised in solution as a result, and a more negative potential would be required to discharge the metal. The deposition potential is therefore shifted to a value more negative than the decomposition potential of the solvent itself, and no metal deposition takes place. Lithium, having no d-orbital bonding, does not exhibit such a potential shift, and its discharge remains possible. Using a less coordinating solvent (such as an aromatic compound, for example) to avoid excessive stabilisation of the metal ion is usually not appropriate because such a liquid has less capacity to dissolve metal salts and neither sufficient solute concentration nor electrical conductivity can be built up[48].

The most commercially significant developments of aprotic organic plating baths have been aluminium plating systems[13]-[14]. The REAL (Room temperature Electroplated ALuminium) process employs $AlCl_3$ and $LiAlH_4$ dissolved in tetrahydrofuran and must be operated in a dry inert atmosphere[13]. The SIGAL process, using triethyl aluminium dissolved in toluene, has been demonstrated on the production scale and operates at about 100 C in a nitrogen-blanketed plating line[14].

Similar analogous titanium systems have been studied but to date little success has been reported. A recent Japanese patent reports titanium coatings electrodeposited onto steel from alkyl pyridinium halide systems, either with or without the incorporation of an

organic solvent such as toluene[12]. The operating temperature was between 20 and 150°C. Current efficiencies of almost 100% are claimed, but the coatings produced appear to be thin, of the order of 5-6 microns.

The preferred feedstock for most of these studies has been titanium chlorides: either $TiCl_3$ or $TiCl_4$. Organotitanium compounds have also been used[15].

1.2.3 Molten Salts

The second class of aprotic solvents of potential use for the production of electrodeposited titanium is molten salts. This is by far the greatest field of endeavour for titanium electrodeposition, most of the work having been directed towards titanium electrowinning.

1.2.3.1. Electrowinning

Titanium is conventionally produced by chemical reduction of the tetrachloride using either sodium or magnesium metals. Electro-reduction techniques offer potential savings in both energy use and capital costs[16]. Preliminary work began in the 1940's and culminated in the commissioning of the D-H Titanium Company plant in the U.S.A in 1980[16]-[23]. The process is based on the lithium chloride-potassium chloride eutectic melt containing 4 % titanium at a temperature of 520°C. Titanium tetrachloride is the feedstock and the anode (graphite) and cathode compartments are separated by a metal diaphragm to prevent back-oxidation of the lower valent titanium species produced at the cathode. The product metal is particulate in form (resembling the sponge product of the

conventional routes) and is periodically scraped from the cathode during the continuous process. The process operates under an inert atmosphere. Although subsequently the process was abandoned, this was for market reasons rather than because of technical or economic shortcomings. Indeed, there is now renewed interest in titanium electrowinning plant construction in both Europe and the U.S.A.[24],[25]. These processes are essentially similar to the D-H process, although modifications to the initial reduction of the $TiCl_4$ feedstock are incorporated. In one, two reductions to the metal are employed, the first producing a relatively impure material and the second refining the product to the highest degree.

It is noteworthy that the product in all cases is particulate metal. It might be imagined that compact metal would be a preferred product form: the problems and additional process costs of separation of the metal from the salts, and of melting to produce ingot, might be avoided. However, the advantages of the particulate form are dominant:

* similar to conventional (e.g. Kroll process) product
* easy to mix alloy components
* high current densities (high rates of production) can be used

In Japan, however, the Sony Corporation have taken the view that the process cost savings to be derived from compact product are more important, and they have devoted huge efforts to the demonstration of a titanium electrowinning process to produce such material. A series of patents spanning more than 20 years describes the various process conditions adopted to this end[26]-[33]. Careful control of

electrodeposition from various molten chloride baths allowed thick, compact titanium deposits to be produced on a considerable scale. The various process conditions applied include :

* the co-deposition of magnesium (imparting some magnesium content to the product in spite of a re-dissolution mechanism intrinsic to the process mechanism).

* the maintenance of two temperature regimes to control the formation of solids in suspension in the melt, claimed to be desirable near the cathode surface.

* introduction of inert solid particles

* pulsed current regimes to control solids precipitation near the cathode and to allow magnesium deposition.

* cathode agitation or rotation

The underlying process mechanisms determining these conditions are not well-defined. The creation of a viscous "polarisation" layer close to the cathode, in which melt composition deviates from the bulk very considerably, is discussed. This layer is said to consist of either viscous liquid or suspended solids. Control of this layer is the rationale for many of the process modifications. Mass transport effects are obviously important but are not well-characterised.

1.2.3.2. Electrorefining

The recycling of scrap titanium has always been a very important part of the titanium industry. Scrap material is re-melted and forms

a large proportion of the primary ingot produced. However rigorous procedures are adopted world-wide to ensure that only clean, uncontaminated single alloy scrap is re-used in this way. In particular so-called high density inclusions (silica or tungsten carbide particles, for example) must be eliminated, to prevent catastrophic failure of engine parts made from titanium ingot. This requirement, imposed by the major end-user of the metal, the aerospace industry, severely limits the types of scrap which can be recycled. Most scrap cannot be re-melted, and consequently has a very low value.

Electrorefining could potentially deal with this sort of material, allowing a large part of the titanium value otherwise lost to be recovered. However it appears that only in the USSR does any such process take place on a commercial scale.

In electrorefining the impure material forms the dissolving anode, and pure metal is electrodeposited at the cathode. Studies of the behaviour of some of the major contaminants have been made[1][35]-[38]. Alkali metal chloride-titanium chloride melt compositions were used, usually at about 800°C. Nitrogen content can be dramatically reduced, nitrogen accumulating in the anode scale which consists essentially of Ti_2N. Oxygen, iron, molybdenum, vanadium and chromium could also be practically eliminated. Two-stage processes have been found to be beneficial in some cases. Manganese, a common alloying element, was found to co-deposit with titanium and could not therefore be removed. Hydrogen and chlorine content also were little affected by the refining process. When an element accumulated in solution in the melt then eventually problems in its continued removal were found. When the contaminants collected in anode residue

cell operation was more successful. This had some dependence on the phase of the titanium metal (alpha or beta, the latter being stable above 882°C) being refined. Some contaminants become concentrated in the beta phase which oxidises less readily than the alpha phase.

1.2.3.3. Electroplating

The most significant development of electroplating using molten salt baths was made by Union Carbide in the 1960's. They found that the FLINAK melt (a eutectic mixture of the fluorides of lithium, sodium and potassium) could be used at about 700-800°C to produce compact electrodeposits of several refractory metals[39]-[41]. Excellent quality electroplates and electroforms were produced for niobium, tungsten, molybdenum, tantalum, chromium and zirconium. The process has been scaled up and used commercially for some metals, notably tantalum plating operated currently by Degussa in Germany. However, titanium was not amenable to the same treatment: only powders were produced. The reasons for this anomalous behaviour were not unequivocally identified. It was thought that titanium formed a particularly strong fluoride complex such that pre-deposition of the alkali metal took place allowing chemical reduction of the titanium species to form powdery metal.

Other workers have since used similar fluoride melts with some degree of success, however. Compact coatings on iron, nickel, copper and steels are possible[42]-[44],[137],[138] at operating temperatures of between 600 and 800°C. It is significant that the coatings generally consist in part of diffusion alloys, the titanium content increasing with increasing distance from the interface with the substrate. Once pure titanium is being electrodeposited a

tendency to dendrite formation is usually observed. Such coatings should perform well as a corrosion-resistant barrier. Indeed the adhesion of this type of coating can be expected to be exceptionally good because of the intermetallic diffusion layer. However high temperature and probable dependence on the nature of the substrate both militate against commercial exploitation. This process should perhaps not be considered true electroplating, but rather diffusion alloying with finite restrictions on coating thickness.

Based on the efforts to develop electrowinning processes, chloride melts have received some attention with the intention of using these systems for electroplating. They are more attractive than fluoride melts for this purpose because of the possibility of significantly lower operating temperatures: typically the 400-500^{o}C range becomes accessible. Thus a wider range of substrates becomes employable and engineering problems are reduced. In general, however, adaptation of winning processes for plating has not been successful. The most significant work is the Sony Corporation's electrowinning process, also demonstrated as a means of producing titanium coatings, discussed above.

A Russian patent identifies a current density range of 0.08-0.15 A.cm^{-2} in the LiCl-KCl-$TiCl_2$ melt at 400-450^{o}C as suitable for coating production[45]-[46]. Ductile, adherent coatings up to 0.3 mm thick are claimed. An average titanium valency of 2.1 was necessary. Outside the preferred current density range, and at higher temperatures, powders resulted.

Use of a high temperature chloride system (NaCl-KCl-$TiCl_2$ at 700-900^{o}C) resulted in the formation of protective titanium coatings at

1 $A.cm^{-2}$[47]. It seems likely that diffusion alloying also plays a role in this system.

The problems of obtaining good electrode coverage in attempts to produce titanium coatings from chloride melts have been noted by several workers[45-46][68][139][140]. In general higher temperatures and current densities appear to provide the most favourable conditions, but tend to produce coarse-grained or dendritic deposits. The need to maintain a low average valency (as close to 2 as possible) has also been widely recognised as an essential characteristic. The work of Duan and Inman [139] has identified the need to ensure adequate nucleation of the metal before continued growth to the required coating thickness. They found that various pulse regimes were useful in achieving this end. Oxygen contamination has been linked with the production of poor quality, non-continuous, porous deposits from fluoride melts[137].

1.3. The choice of plating bath

While organic liquids are attractive prospective plating media in comparison with most molten salts because of the possibility of near ambient temperature operation, the problems of refractory metal deposition from highly coordinating solvents have not been overcome. Indeed this may be a fundamentally intractable problem. The use of more novel approaches may ultimately prove fruitful, but to date successes have been few[48].

In comparison, the extensive background of work supporting electrowinning processes makes molten salts, and in particular chlorides (as the lower temperature option), a better prospect. The

literature contains studies of various chloride melt compositions, with no consensus as to which might be the most suitable for plating, as opposed to electrowinning, purposes. Melts other than halides have been little studied; all those of potential interest because of lower operating temperatures have drawbacks such as oxygen content rendering them unsuitable for the purpose[50].

A general feature of metal electrodeposition from molten salts is that the metal is usually produced (if solid) in particulate form. The Union Carbide plating process is the exception to the rule. The factors influencing metal electrodeposition from molten salts need to be examined in more detail[51]-[53].

1.3.1. The causes of particulate electrodeposits

There are several possible causes of particulate electrodeposits:

* mass transport control of the deposition reaction leads firstly to dendritic or nodular growth and ultimately to powders.

* prior discharge of the alkali metal may result in chemical reduction of the solute metal species to metal powder.

* disproportionation reactions of lower valent species to yield metal powder.

* the presence of impurities which influence the growth of the electrodeposit by adsorption or inclusion.

The general consensus of opinion concerning deposition from molten salts is that at the high temperatures involved electron transfer is

very fast, such that mass transport is likely to be the rate determining step. Thus deposits tend to be rough or powdery. Specific findings for titanium electrodeposition, in particular the Sony electrowinning process development, indicate that this is an important factor. However, the description of results in the literature suggests that this is not the dominant mechanism in all instances. For example, the observation that low current densities lead to powders while higher ones lead to compact deposits cannot be rationalised by this argument. It is therefore probable that one or more additional mechanisms are also important.

The success of the Union Carbide plating process, and of certain others such as molybdenum deposition from molten chlorides[56], depends on a process other than mass transport determining deposition rate. Where a relatively slow decomposition reaction precedes the final reduction to the metal, then this preceding reaction is the rate determining step, and compact deposits are possible. The formation of complex species in solution is usually considered a necessary pre-condition for this type of process.

The chemical reduction of low valent titanium species by lithium metal discharged at the cathode was once considered to be the main mechanism for metal production by electrolysis of chloride melts[54]. However it is now recognised that this is not generally the case. Such a reaction would be expected to produce fine powders throughout the bulk of the melt, although powder formation may in practice be confined to the cathode region, the site of lithium metal formation. The separation of the lithium and titanium reduction potentials (see table 1.2) suggests that such a mechanism

can only be important at very high current densities. However, some depolarisation of lithium discharge on titanium has been observed[55]. Some specific interaction of lithium and titanium deposition may therefore be significant.

Disproportionation reactions are common for metals which can exist in various valencies. In the case of titanium several equilibria can be set up (see below). Where titanium metal is produced by such reactions, it is in finely divided form. Again the formation of the metal product throughout the bulk of the melt can be expected, unless the conditions favouring that decomposition are confined to a specific region close to an electrode. $TiCl_2$, for example might build up near a cathode, leading to disproportionation to TiIII and Ti0 only in that region of the melt.

The presence of impurities can influence the nucleation and subsequent growth of an electrodeposit very significantly. Specific adsorption effects, and co-deposition of hydrogen are familiar mechanisms in aqueous solution capable of producing powdery electrodeposits[57]. It has also been postulated that colloids of metals or their compounds can form aggregate particles on the electrode surface where they form centres of crystallisation[57]. The growth of 1-dimensional needle-like structures (forming a porous and friable mass) is a common mode of growth when adsorbed material interferes with the electrocrystallisation process[132].

1.3.2. The chemistry and electrochemistry of titanium in molten chlorides

In order to predict the best approach to the development of a titanium plating bath the chemistry and electrochemistry of these

systems must be understood.

Titanium can exist in chloride melts in three different valence states: 2, 3 and 4[1]. Various complex species have been proposed to explain chemical and electrochemical behaviour as well as spectral data.

The electronic absorption spectrum of Ti^{3+} in LiCl-KCl at $400^{0}C$ was examined by Gruen and McBeth[59] and it was concluded that octahedral coordination dominated. That is, the following equilibrium lay well to the left hand side:

$$[TiCl_6]^{3-} = [TiCl_4]^{-} + 2Cl^{-} \quad ....(1.1)$$

octahedral tetrahedral

Further evidence of the importance of complexes was provided by activity coefficient data for TiIII and TiII in LiCl-KCl[66]. The greater the extent of complexation, the lower the activity coefficient is likely to be. Activity coefficients for both species increased with temperature but remained less than 1. More extensive complexation was indicated for TiIII than TiII.

Chassaing et al investigated the Raman spectra of TiIII chlorides as a function of cation composition of the melt[60]. In pure CsCl a spectrum similar to the compund Cs_3TiCl_6 was determined. On the addition of lithium salts, however, an additional band appeared as well as shifts in other bands. This was attributed to a change in symmetry of the TiIII species as a result of the following equilibria:

$$[TiCl_6]^{3-} = [TiCl_4]^{-} + 2\ Cl^{-} \quad ...(1.2)$$

$$2\ [TiCl_6]^{3-} = [Ti_2Cl_9]^{3-} + 3\ Cl^{-} \quad ...(1.3)$$

With increased lithium content the solvent becomes more acid, i.e. a more powerful chloride ion acceptor, and the above equilibria move to the right. The extra line in the spectrum is thought to represent the extra octahedral species: $[Ti_2Cl_6]^{3-}$ consisting of two $TiCl_6$ octahedra joined by one face.

TiII species are best described as $[TiCl_4]^{2-}$ species (tetrahedral) in LiCl-KCl although hexa-coordination has been found in chloroaluminate melts[61].

The equlibria set up between the various valence states has been studied by Chassaing et al[62]. Melts of various cation composition containing dissolved titanium were held at 700°C in the presence of titanium metal and analysed at constant composition. Disproportionation reactions of the following types are important:

$$2\ TiIII + Ti = 3\ TiII \qquad (1.4)$$

$$2\ TiIII = TiIV + TiII \qquad (1.5)$$

$$4\ TiIII = Ti + 3\ TiIV \qquad (1.6)$$

$$2\ TiII = Ti + TiIV \qquad (1.7)$$

In melts with small cations (such as Li^+, Na^+) (1.4) and (1.5) are more important as little powdery titanium metal was observed. In such melts TiIV is not stabilised by complex formation and titanium is lost from the melt as a result of the formation of volatile $TiCl_4$. In LiCl-KCl, however, TiIV is stabilised by the formation of K_2TiCl_6 and less titanium is lost. Large cations de-stabilise TiII and (1.7) shifts to the right. This effect is counter-balanced by the stability of TiIV in such melts causing (1.6) to shift to the left. Consequently more TiII and TiIII stay in the melt than might be expected. Disproportionation of TiII (such as via the reverse of (1.4)) is favoured at high temperatures[1].

The electrochemical reduction of TiIV has been observed to occur in a stepwise manner[63]:

TiIV + e -> TiIII (at +500 or -100 mV vs Ag^+/Ag)

TiIII + e -> TiII (at -500 mV vs Ag^+/Ag)

TiII + 2e -> Ti (at -1.15 V vs Ag^+/Ag)

Additional reduction waves at -1.0 V vs Ag^+/Ag have sometimes been observed and are attributed to either the behaviour of impurities or the presence of complex species. The final reduction to the metal has been found to take place at potentials only 100mV more positive than alkali metal reduction[63].

Ferry et al have also studied the sequence of electrochemical reduction reactions[141][142] and have determined the following standard reduction potentials at 470°C versus the standard chlorine electrode:

Ti/Ti^{2+}.....-2.053 V

Ti^{2+}/Ti^{3+}...-1.938 V

$Ti^{3+}/TiCl_4$..-0.67 V

Here too, additional waves were observed, this time attributed to adsorbed TiII and TiIV species. Precipitated $TiCl_2$ was produced when the TiII content of the melt was above 0.07 $mol.kg^{-1}$. However, the effect of disproportionation of TiII was considered negligible.

Lithium metal discharge at various cathode materials has been examined[55]. Both titanium and vitreous carbon show significant depolarisation of the alkali metal deposition reaction over other metals such as iron, nickel and tungsten:

vitreous carbon -0.8 V vs Ag/AgCl

titanium	-2.0 V vs Ag/AgCl
iron	-2.3 V vs Ag/AgCl
tungsten	-2.3 V vs Ag/AgCl
nickel	-2.4 V vs Ag/AgCl

Intercalation compound formation of lithium with vitreous carbon explains this observation, but the reason for the effect on titanium is unknown. Some specific interaction or alloying of lithium with titanium might be postulated. The solubility of lithium metal in chloride melts can result in depolarisation of the deposition potential from the thermodynamic value[64].

The effect of altering melt cation composition or temperature indicates that different forms of titanium's valence states can exist. The equilibrium:

$$K_2TiCl_6 = 2KCl + TiCl_4 \qquad ...(1.8)$$

is proposed to explain the different reduction potentials observed under different conditions[55]. In $BaCl_2$-KCl-LiCl the first reduction occurs at +500mV vs Ag^+/Ag and is thought to be:

$$[TiCl_6]^{2-} + e \rightarrow [TiCl_6]^{3-} \qquad ...(1.9)$$

At a higher temperature, or in the absence of the potassium ion, the first reduction takes place at -100mV vs Ag^+/Ag and represents:

$$TiCl_4 + e \rightarrow [TiCl_4]^- \qquad ...(1.10)$$

because under these conditions $[TiCl_6]^{2-}$ is not formed. Both reductions can occur in some circumstances.

A single step reduction, TiIII-> Ti, can occur where the TiII ion is not sufficiently stabilised: i.e. in CsCl-LiCl at 400^0C[62].

Anodic dissolution of titanium has not been widely studied. $TiCl_2$ is considered to be the main product[1] but passivating films have been

observed at current densities of 0.15 to 0.3 $A.cm^{-2}$ [65].

Diffusion coefficients for Ti^{2+} and Ti^{3+} in LiCl-KCl have been determined in the range 10^{-4} to 10^{-6} cm^2sec^{-1}, for example:

Temp., ^0C	D, Ti^{2+}, cm^2sec^{-1}	D, Ti^{3+}, cm^2sec^{-1}	Reference
400	3.5×10^{-6}		65
500	1.5×10^{-5}		65
450	$1-3 \times 10^{-5}$		68
450	5.2×10^{-5}	3.2×10^{-5}	140
450	1.25×10^{-5}		143

The presence of black and/or grey "corrosion product" in titanium-containing chloride melts is repeatedly commented upon. The identity of this material has been variously determined as metallic titanium[141], Li_2TiO_2[67], TiO_2[66], TiO[66], and $TiO_{0.198}$[68]. It is sometimes associated with the dissolving anode reactions in a titanium deposition cell[68].

1.3.3 LiCl-KCl-$TiCl_2$-$TiCl_3$ as plating bath

There are strong indications that with proper process control the LiCl-KCl melt, the preferred choice for titanium electrowinning, could be used as the basis of a titanium plating bath. It has the following advantages:

* small cations, favouring stabilisation of TiII species, avoiding cluster compound formation of lower valent species.

* presence of K^+ stabilises TiIV

* relatively low operating temperature (compared to other molten salts), desirable for both kinetic and practical reasons as well as for avoiding diffusion alloy formation

* well-characterised melt system

* relatively cheap

* good solvent for TiII and TiIII

Its disadvantages include:

* need for rigorous purification and drying (lithium salts are very hygroscopic)

* relatively high operating temperature (compared to ambient)

* need for cell operation under dry, inert atmosphere

Operating conditions must be chosen which comply with the following criteria.

1) Titanium electrodeposition should take place at potentials well-separated from alkali metal discharge.

2) Mass transport control of the electro-reduction process must be avoided.

3) The contribution of other mechanisms likely to produce particulate deposits (e.g. disproportionation reactions, impurities) should be minimised.

4) Process design should allow for the use of dissolving titanium

TABLE 1.1
POTENTIAL APPLICATIONS OF ELECTROPLATED TITANIUM COATINGS

APPLICATION	SUBSTRATE	COMMENTS
chemical plant components	steels	to replace bulk Ti to improve substrate performance
valve and pump parts	steels	to replace bulk Ti to improve substrate performance as alternative to Ti cladding
tubing/pipework	steels	to replace bulk Ti to improve substrate performance as alternative to Ti cladding
electrode materials	mild steel copper	to replace bulk Ti
heat exchanger plates for food industry	mild steel	to replace bulk Ti to improve substrate performance
components for marine environments	steels	as an alternative coating material
electric current carriers	copper aluminium	to improve substrate performance as alternative to Ti cladding
aircraft components	aluminium alloys	to improve substrate performance to replace bulk Ti

TABLE 1.2

STANDARD REDUCTION POTENTIALS IN LiCl-KCl AT 450 C [73] [50]

REDOX COUPLE	STANDARD REDUCTION POTENTIAL vs Ag/AgCl(1m) (V)
Li(I)/Li(0)	-2.593
Mg(II)/Mg(0)	-1.853
OH^-/O_2	-1.567
Al(III)/Al(0)	-1.04
Ti(II)/Ti(0)	-1.01
Cr(II)/Cr(0)	-0.698
H_2O/OH^-	-0.657
Ti(III)/Ti(II)	-0.61
Fe(II)/Fe(0)	-0.445
Ni(II)/Ni(0)	-0.068
$HCl(g)/H_2(g)$, Pt	+0.017
Pt(II)/Pt(0)	+0.727
Fe(III)/Fe(II)	+0.797
$Cl_2(g)$,C/Cl	+1.033

CHAPTER 2

EXPERIMENTAL

The details given in this chapter relate to general features of experimental procedure, concerned with melt preparation, analysis and so on. Experimental details specific to particular experiments are given in the pertinent chapter.

2.1. Preparation and purification of the lithium chloride potassium chloride eutectic

The eutectic composition of the salt mixture is 59 mole % lithium chloride, 41 mole % potassium chloride. The chemical nature of the melt and the electrochemistry to be investigated both demand that rigorous purification procedures be carried out.

2.1.1. The importance of melt purity

1. The salts constituting the melt system are used in a very concentrated form. This contrasts with typical aqueous systems, for example, where the reactants, together with their associated contaminants, are substantially diluted by a solvent obtainable in very pure form. In a molten salt mixture the level of impurity in the salts themselves is maintained in the solvent system.

2. The most significant aspect of this particular system with respect to purification requirements is the hygroscopic nature of lithium salts. Left in the average laboratory atmosphere, such salts rapidly absorb enough moisture for a paste-like consistency to be achieved. Rigorous measures are therefore necessary to dry the salts initially and to maintain moisture-free conditions. If moisture remains when fusion takes place lithium oxides and/or hydroxides are

produced in the melt.

3. Gross contamination with water could lead to hydrogen discharge at the cathode instead of the desired reaction.

4. The nature of the titanium salts to be added to the mixture is also pertinent to the purification measures taken. Lower valent titanium and, indeed, titanium metal itself, will react with any oxygen present to form titanium oxides. At the extreme, the formation of such compounds diminishes the titanium present in a form suitable for cathodic discharge, or the presence of insoluble material may have an unpredictable influence over electrodeposition processes.

5. The quality of the product may be critically dependent on the system's purity: the mechanical properties of titanium are very sensitive to trace components, such as oxygen, hydrogen, and metals such as iron.

6. Investigations of electrochemical characteristics need to be carried out in a pure system to avoid the masking or modification of the observed behaviour by electrode reactions of contaminants.

7. Damp LiCl-KCl melts etch pyrex containers very much more rapidly than dry ones[69]. This can lead to the failure of the container within a few hours.

2.1.2. Types of impurity

These are:

1. Water, which exists largely in its undissociated form and as the

products of hydrolysis of the melt components, i.e. oxides, hydroxides and hydrogen ions.

2. Oxyanions, such as SO_4^{2-}, NO_3^-.

3. Heavy metal ions.

4. Organic residues.

5. Particulate matter such as dust and carbon particles.

The purification and ancillary procedures adopted were designed to deal with all these classes of contaminant, moisture removal being the most important consideration.

2.1.3 The behaviour of water in melts

The moisture present in molten salts is not driven off during heating, as might be supposed. Water can have significant solubility in melts and the hydrolysis of melt components becomes important at elevated temperatures[70][71].

Water's "solubility"[72] in this context can be either:

(a) a physical interaction, with the water molecule occupying a void in the melt structure, possibly including hydrogen bonding of H_2O to Cl^-.

or (b) a chemical interaction (hydrolysis) with the formation of oxides or hydroxides, likely to be relatively more prevalent at higher temperatures.

The interaction of the lithium cation with the water molecule is strong because of the highly polarising nature of the lithium ion.

The effect is to stabilise the water molecule in the melt and reduce the magnitude of the equilibrium constant for water dissociation:

$$H_2O = H^+ + OH^- \qquad ...(2.1)$$

However, H^+ and OH^- can react as follows[70]:

$$Li^+ + nH_2O = Li(H_2O)_n^+ \qquad ...(2.2)$$

$$Li^+ + OH^- = LiOH \qquad ...(2.3)$$

$$H^+ + 2Cl^- = HCl_2^- \qquad ...(2.4)$$

$$LiOH + 2LiCl = Li_2O + HCl_2^- + Li^+ \qquad ...(2.5)$$

Supporting evidence for this sort of scheme lies in the experimental observation that HCl is found in melts with significant water vapour pressures.

The equilibrium:

$$2OH^- = O^{2-} + H_2O \qquad ...(2.6)$$

lies well to the left; i.e. hydroxide ions dominate.

Peroxides and superoxides (O^-, O_2^{-}) may form in some melts in the presence of oxygen.

The importance of moisture control from a practical viewpoint is exemplified in the reactions of silica-containing glasses:

$$nSiO_2 + O^{2-} \rightarrow (SiO_2)_nO^{2-} \qquad ...(2.7)$$

$$nSiO_2 + OH^- + Cl^- \rightarrow (SiO_2)_nO^{2-} + HCl\uparrow \qquad ...(2.8)$$

In LiCl-KCl the effect of the lithium ion is dominant in determining water's behaviour: KCl appears to act only as a physical diluent[72].

The electrochemical behaviour of water in melts has been

studied[70], [72]. Reduction reactions are:

$H_2O + e \rightarrow OH^- + 1/2\ H_2\uparrow$ -1.69V vs Cl_2[73],[74]

$OH^- + e \rightarrow O^{2-} + 1/2\ H_2\uparrow$ -2.60V vs Cl_2[73],[74]

In HCl-containing melts, reduction of H^+ as HCl^{2-} has been observed at -0.86V vs $Pt/Pt^{2+}(1M)$[70].

Oxidation of the oxide ion occurs:

$O^{2-} \rightarrow 1/2\ O_2 + 2e$ -0.54V vs $Pt/Pt^{2+}(1M)$[70]

The electrochemical behaviour of the species associated with the presence of water in melts can be used as a means of assessing purity. Peak heights in linear sweep voltammetry have been shown to be proportional to H_2O, OH^- and O^{2-} concentrations[75][76].

2.1.4. Purification methods

The following procedure was adopted for preparation of the LiCl-KCl mixture. This uses techniques adapted from recommended practice discussed in references (76) and (77) and elsewhere and combines various methods to cope with the full range of possible contaminants.

2.1.4.1. Rough vacuum drying

The salts used were BDH AnalaR anhydrous. The individual salts were vacuum dried at about 0.1 mbar in a vacuum oven at 100°C for several hours. The salts were then combined in the appropriate proportions (59-41 mol% LiCl-KCl, 45-55 weight % LiCl-KCl) using a motorised mortar and pestle mill and the mixture further vacuum dried in the vacuum oven. The pre-dried mixture was then stored either in the

vacuum oven or in a dry inert atmosphere glove box (Faircrest model 4A fitted with recirculation set). The conditions within the glove box were a nitrogen atmosphere maintained at </= 20 ppm H_2O and </= 20 ppm oxygen.

2.1.4.2 Apparatus preparation

All glassware to be brought into contact with the molten salts was pre-cleaned by leaching with a 50/50% mixture of concentrated nitric and sulphuric acids, rinsing and vacuum drying. The salts (about 300g charge typically) were loaded into a pyrex container with a thin dimple in the base (see figure 2.1) within the glove box. The container was then removed from the box and loaded into the filtration assembly held within the furnace and attached to a vacuum/argon line, as illustrated in figure 2.2.

2.1.4.3 High vacuum drying

This was carried out first at ambient temperature, then at 300 ^{o}C using an Edwards combined 2-stage rotary and 63 mm "Diffstak" oil diffusion pump system. Pirani and Penning gauge heads fitted in the line allowed pressure to be monitored. Pumping was continued until a pressure of 6.5×10^{-4} mbar was reached. Typically this took 48 hours. See figure 2.2.

2.1.4.4. Hydrogen chloride treatment

The temperature of the salts was raised to above the melting point and held at 450^{o}C. HCl gas was then bubbled through the melt for 1-2 hours. This was followed by an argon sparge to remove traces of HCl. This treatment is designed to remove oxide and hydroxide ions

present in the melt:

$$O^{2-} + 2HCl \rightarrow H_2O + 2Cl^- \quad ...(2.10)$$

$$OH^- + HCl \rightarrow H_2O + Cl^- \quad ...(2.11)$$

The water formed is carried out of the melt by the flow of gas.

2.1.4.5 Pre-electrolysis

A constant voltage of 2.7 V was applied between a tungsten rod cathode and vitreous carbon anode during argon gas sparging of the melt. The current was monitored and the electrolysis terminated when the current had fallen to about 0.1 $mA.cm^{-2}$. Periodically, the potential of the cathode was measured against a silver/silver chloride reference electrode to check that the applied potential is not so great that lithium discharge can occur.

This treatment is to remove impurities such as heavy metal ions which are electrodeposited at the cathode. Oxyanions are also destroyed.

2.1.4.6. Filtration

The melt was then filtered by breaking the dimple in the base of the melt container with the breaker rod (figure 2.1) and applying vacuum to the lower compartment of the filtration cell (figure 2.2). The melt was filtered through the medium porosity (4) glass frit and collected in a receiver vessel. The apparatus was allowed to cool under either argon or vacuum, and the solidified melt billet stored within a storage jar in the inert atmosphere glove box.

2.1.5. Verification of melt purity

Although it might be possible to assume that, provided the above

procedures were carried out carefully, the melt purity should be adequate for the intended purpose, some independent method of assessing this was thought desirable. Although a variety of impurities may be treated, the most important are oxide and hydroxide species formed as a result of contamination by moisture. It is convenient to determine the extent of their presence by electrochemical techniques.

It has been suggested that cyclic voltammograms at a sweep rate of 100 $mV.sec^{-1}$ between stated potential limits be used for this purpose[76]. It can be shown that peak heights of 1 $mA.cm^{-2}$ correspond to concentrations of the order of 10^{-6} $mole.cm^{-3}$.

To determine voltammograms of this sort a tungsten wire electrode, sealed into glass, of 0.5 mm diameter was used as working electrode. The reference was a silver/silver chloride electrode and the counter electrode was a vitreous carbon rod. A Thompson ministat together with a Hi-Tek waveform generator was used to impose the potential ramp of 100 $mV.sec^{-1}$ between 0 and usually about -2.0V vs Ag/Ag^{+}.

The effect of various stages of the purification procedure are shown in figure 2.3. The importance of both the vacuum drying and the HCl treatment are evident.

The target for melt purity was that contaminant concentration should be two orders of magnitude less than the concentration of the added solute[70]. If the latter is 0.05 $moles.l^{-1}$, then impurities should be less concentrated than 5×10^{-4} $moles.l^{-1}$ Peak currents must therefore be less than 0.5 $mA.cm^{-2}$. This is the level reached using the procedure described above.

2.2. Making up the titanium-containing melt

The solidified melt billet, prepared as described above, was loaded into the experimental cell within the inert atmosphere glove box. The cell was sealed and transferred to the laboratory where it was attached to the gas/vacuum line (similar to that used for melt preparation, as shown in figure 2.2). The cell was evacuated and back-filled with argon at least three times to replace the nitrogen atmosphere with argon. The cell head was fitted with an inlet tube in the central port (figure2.4).

The cell was heated to 450^{o}C with argon flow through the cell. The required amount of titanium trichloride (Aldrich Chemical Co.) was weighed within the glove box into a Schlenk tube. The tube was sealed and transferred out of the glove box. It was then attached to the inlet tube in the cell, using an argon flush to prevent air ingress. The Schlenk tube was rotated through 180^{o} so that the titanium trichloride contents fell into the cell via the inlet tube (figure 2.4). Argon flow through the melt was used to stir the contents and aid dissolution. Titanium metal (rod or sheet) was then lowered into the melt and the argon sparge continued. Reaction of the titanium metal with Ti^{3+} takes place according to the equilibrium:

$$Ti + 2Ti^{3+} = 3\ Ti^{2+} \qquad ...(2.12)$$

which lies towards the right hand side. It was found useful to "activate" the titanium metal by applying a polarisation of +300mV vs a titanium rod to ensure smooth dissolution took place. This process of reducing the average valency as close to 2 as possible

was assisted by electrolysis between a titanium anode and a suitable cathode (e.g. a tungsten rod). This was carried out at constant current density of typically 30 $mA.cm^{-2}$. At the cathode the reactions Ti^{3+}-->Ti^{2+} and Ti^{2+}-->Ti occur; at the anode Ti-->Ti^{2+} takes place.

Occasionally an alternative method of adding titanium was adopted: the reaction of titanium metal with HCl gas. The gas is bubbled through the LiCl-KCl melt with a piece of titanium metal immersed in it. The following reactions are thought to take place[78]:

$$2HCl + Ti \rightarrow TiCl_2 + H_2 \qquad ...(2.13)$$

$$3HCl + Ti \rightarrow TiCl_3 + 3/2\ H_2 \qquad ...(2.14)$$

$$4HCl + Ti \rightarrow TiCl_4 + 2\ H_2 \qquad ...(2.15)$$

Subsequent reduction to approach a nearly entirely divalent melt is necessary as described above.

The melt was then allowed to stand for 24 hours before experimental work was commenced. This was found to be necessary for the production of good quality electrodeposits and is discussed further later.

2.3. Electrochemical techniques and instrumentation

The required potentiostatic or galvanostatic conditions were imposed on the working electrode by either a Thompson ministat or a Wenking ST72 potentiostat. Occasionally a programmable Kepco power supply was used in constant current mode. Either a Hitek waveform generator or an Electroman (a Uman computer-based system) waveform generator were used to impose particular waveforms (pulses and/or ramps). The current or potential response was recorded using either: a Chessel

linear chart recorder; a Brians X-Y recorder; or a Nicolet model 4094A digital storage oscilloscope. In the case of the last of these, data was stored on floppy disks, and subsequently transferred to a Prime computer for processing and/or output to Hewlett Packard or Calcomp digital plotters. Total charge passed was controlled by either reference to a Hitek digital integrator or by imposing a known total charge in the waveform applied from the Electroman system. The latter allowed a pre-determined number of cycles of the particular waveform to be output, giving precise delivery of a known amount of charge.

Specific techniques are discussed under descriptions of particular experiments in later chapters.

Temperature was checked by means of a thermocouple probe and a Kane-May digital thermometer. Control was typically +/- 1^{o}C whichever furnace type was used.

2.4. Electrodes

Two types of working electrodes were used: wires and flags. The former were constructed by using 0.5 mm diameter wire which was threaded through alumina tubing, of bore slightly greater than the wire's diameter. The wire was sealed into the alumina at the upper end with araldite to prevent movement. Various metals were used depending on the particular experiment carried out, all from Goodfellow Metals. Flags were constructed using a square piece of sheet material (again from Goodfellow metals) spot welded to a nickel wire (0.5 or 1mm diameter) held within an alumina tube as before. All materials were ultrasonically degreased in trichloro

ethane before use. Additional pre-treatments are described for specific experiments.

The preferred reference electrode was silver/silver chloride. This was constructed as shown in figure 2.5. The design was adapted from that described by Bockris et al[79]. A silver wire (BDH Chemicals) dips into a 1% solution of silver chloride (BDH analaR) in LiCl-KCl (purified eutectic mixture). The liquid junction is thin pyrex glass. This was found to be stable for several days, but after that length of time immersed in a titanium-containing melt the potential was no longer reliable.

In some cases a titanium rod immersed in the bulk melt was used as a quasi-reference electrode. This was adequate for checking cathode or anode potentials during plating runs, for example.

Vitreous carbon rods (Le Carbone), tungsten rods, or titanium rods or sheet (all Goodfellow metals) have all been used as counter electrodes, depending on the experiment.

2.5. Experimental cells and ancillary apparatus

A typical experimental cell is shown in figure 2.6. The specific cell components differ depending on the particular experiment. The outer vessel is silica and the inner crucible alumina. The various cell components were constructed of either pyrex or alumina. The cell head was constructed from a pyrex disc with various ports (Quickfit screw thread joints or standard cone/socket joints) and gas or vacuum connections (ball/socket joints). The cell head was clamped to the outer vessel flange together with a Viton O ring.

The cell was located within either a specially adapted Statim metal

block bath or in a port in the top of a Lenton high temperature oven.

2.6. Analytical techniques

Samples of the melt were taken using a conventional pipette filler attached to a glass tube of 5mm internal diameter. The tube was acid-washed and vacuum dried before use. The tube was inserted into the cell through one of the ports in the cell head. The pipette filler was used to flush the inside of the tube with argon several times before immersing the tube-end into the melt and withdrawing the liquid into the tube. This solidifed rapidly. The samples were stored within the glass tubes, sealed at both ends by rubber bungs, until analysis was carried out. No significant deterioration of the material took place even over very extended time periods. The solid cylinder of the salt mixture could then easily be removed from the glass tube and broken up as necessary for the analytical technique to be applied. Some or all of the following determinations were made on each sample.

2.6.1. Determination of $[Ti^{2+}]$ (80)

The method depends on the reaction of divalent titanium with dilute acid :

$$TiCl_2 + HCl \rightarrow TiCl_3 + 1/2\ H_2 \qquad ...(2.16)$$

The volume of hydrogen evolved was measured under known pressure and temperature conditions. To prevent errors arising from the solubility of hydrogen in the acid solution, the solution was saturated with hydrogen gas before use. Titanium metal in the sample

also introduces error as absorption of hydrogen by the metal to form titanium hydride can take place[81].

Figure 2.7 shows the apparatus used.

The procedure was as follows.

a) The acid reservoir was filled with hydrogen-saturated 0.02M HCl. The acid solution was drawn up, using the vacuum pump, into the burette as far as the upper stop-cock. Both stop-cocks were then closed.

b) About 10 g of ground sample salt material was weighed and introduced into the acid reservoir beneath the bell. The lower stop-cock was opened and the magnetic stirrer activated to encourage dissolution of the salts.

c) The H_2 gas evolved displaced acid in the burette. When this had ceased the lower stop-cock was closed. The solution appeared a violet-blue colour due to the presence of the trivalent titanium complex $[Ti(H_2O)_6]^{3+}$. The levelling tube was adjusted to equate the pressure of hydrogen to atmospheric pressure. The gas volume was read from the graduations on the burette.

d) Atmospheric pressure and temperature were noted.

e) The concentration of divalent titanium in the salt sample was calculated as follows.

P = pressure, mm Hg (barometric - water vapour pressure at T).

T = temperature, K

V = volume H_2 gas, cm^3.

w = weight of sample, g.

x = concentration TiII, wt. %.

$$\frac{P_s V_s}{T_s} = \frac{PV}{T} \quad \text{(s denotes standard conditions)} \qquad \ldots(2.17)$$

$$P_s = 760 \qquad V_s = \frac{PV}{T} \cdot \frac{273}{760} \ldots(2.18)$$

$$T_s = 273$$

The experimentally measured value V can be converted to the equivalent volume at standard temperature and pressure, V_s.

$$V_s \text{ cm}^3 H_2 = \frac{V_s}{22410} \text{ moles } H_2 \qquad \ldots(2.19)$$

$$TiII + H^+ \rightarrow TiIII + 1/2\ H_2 \qquad \ldots(2.20)$$

$\frac{V_s}{22410}$ moles H_2 produced by $\frac{2V_s}{22410}$ moles TiII

and $\frac{2V_s}{22410} = \frac{2V_s}{22410} \times 47.9$ g TiII

$$= \frac{x.w}{100} \text{ g}$$

$$\text{i.e. } x = \frac{2\ V_s .\ 47.9}{22410} \cdot \frac{100}{w} \ldots(2.21)$$

Substituting for V_s gives :

$$x = \frac{2PV}{T} \cdot \frac{273}{760} \cdot \frac{47.9}{22410} \cdot \frac{100}{w} \qquad \ldots(2.22)$$

$$x = 0.1536 \frac{PV}{Tw} \qquad \ldots(2.23)$$

2.6.2. Determination of $[Ti^{3+}]$

"Total" titanium (i.e. the sum of divalent and trivalent forms) was determined by titration with ferric ions using a thiocyanate indicator.

$$Ti^{3+} + Fe^{3+} \rightarrow Fe^{2+} + TiIV \qquad \ldots(2.24)$$

Any divalent titanium is also included in the reaction because it is oxidised to TiIII immediately on dissolution in the acid solution. [TiIII] is therefore obtained by subtracting a value for [TiII] determined as described in the previous section from the total concentration determined by titration.

The end point of the titration is a permanent red colouration due to ferric thiocyanate.

Titanium in metallic form or as TiIV species is not recognised by this method.

The procedure was as follows.

a) About 5 g of the sample material was accurately weighed and dissolved in 50 cm^3 of 0.2 M HCl solution continuously purged with argon.

b) 10 cm^3 of ammonium thiocyanate solution was added, and the solution was titrated against 0.1 M ammonium ferric sulphate to the first permanent orange-red colouration. The titre volume was noted.

c) The total (TiIII + TiII) titanium concentration was calculated as follows.

x = TiII concentration in sample, wt. %.

y = TiIII concentration in sample, wt. %.

w = weight of sample, g.

t = titre volume, cm^3.

w g sample contains $\frac{(x + y)}{100} \cdot \frac{w}{47.9}$ moles Ti.

This is equal to $\frac{0.1}{1000} \cdot t$ moles ferric ions in titre.

i.e. $(x + y) = 0.479 \frac{t}{w}$ ...(2.25)

2.6.3. Determination of total titanium by atomic absorption spectrophotometry

This method includes contributions from titanium species not included in the titrimetric method, because all material is brought into solution initially.

Standards were made up by dissolving titanium wire (Goodfellow Metals) in HCl using an appropriate background concentration of LiCl and KCl to match the sample material.

An appropriate weight of sample material was dissolved usually in 10 % HCl, but stronger solutions were necessary if titanium metal, for example, was present.

2.6.4. Determination of total oxygen

The Leco TC-136 Oxygen/Nitrogen Determinator was used. This instrument measures via an infra-red detector the amount of CO_2 given off when a specimen is heated to high temperature in a graphite crucible within an EF-100 electrode furnace. The instrument is calibrated using standards of known oxygen content.

The method adopted for carrying out this determination on samples of the chloride plating electrolyte was as follows.

The melt was sampled in the usual way. The salts were ground in a mortar and pestle mill. About 0.1 g was weighed into a pre-weighed tin capsule. The capsule was sealed by crimping and folding the

ends, and stored in a desiccator prior to the analysis.

An empty graphite crucible was outgassed in the furnace within the instrument. The tin capsule was then placed within a zinc basket and this sample assembly loaded into the crucible. The crucible was sealed from the outside atmosphere and completely flushed by carrier gas. The current is passed through the crucible to heat the contents. Oxygen from the sample combines with carbon from the graphite crucible forming CO which is then converted to CO_2 by passage through heated rare earth copper oxide. This is detected in the IR cell. Results are automatically calculated by the machine from the input of sample weights.

Investigation of the effect on oxygen determination of sample preparation and handling was made. No effect was found of using ground or unground material. Melt samples can be stored in their sample tubes for extended periods without any moisture pick-up or other oxygen contamination. A relatively large number of determinations on any one sample is desirable. Using four repeats typical precision was only +/- 10%.

FIGURE 2.1

MELT PURIFICATION CELL

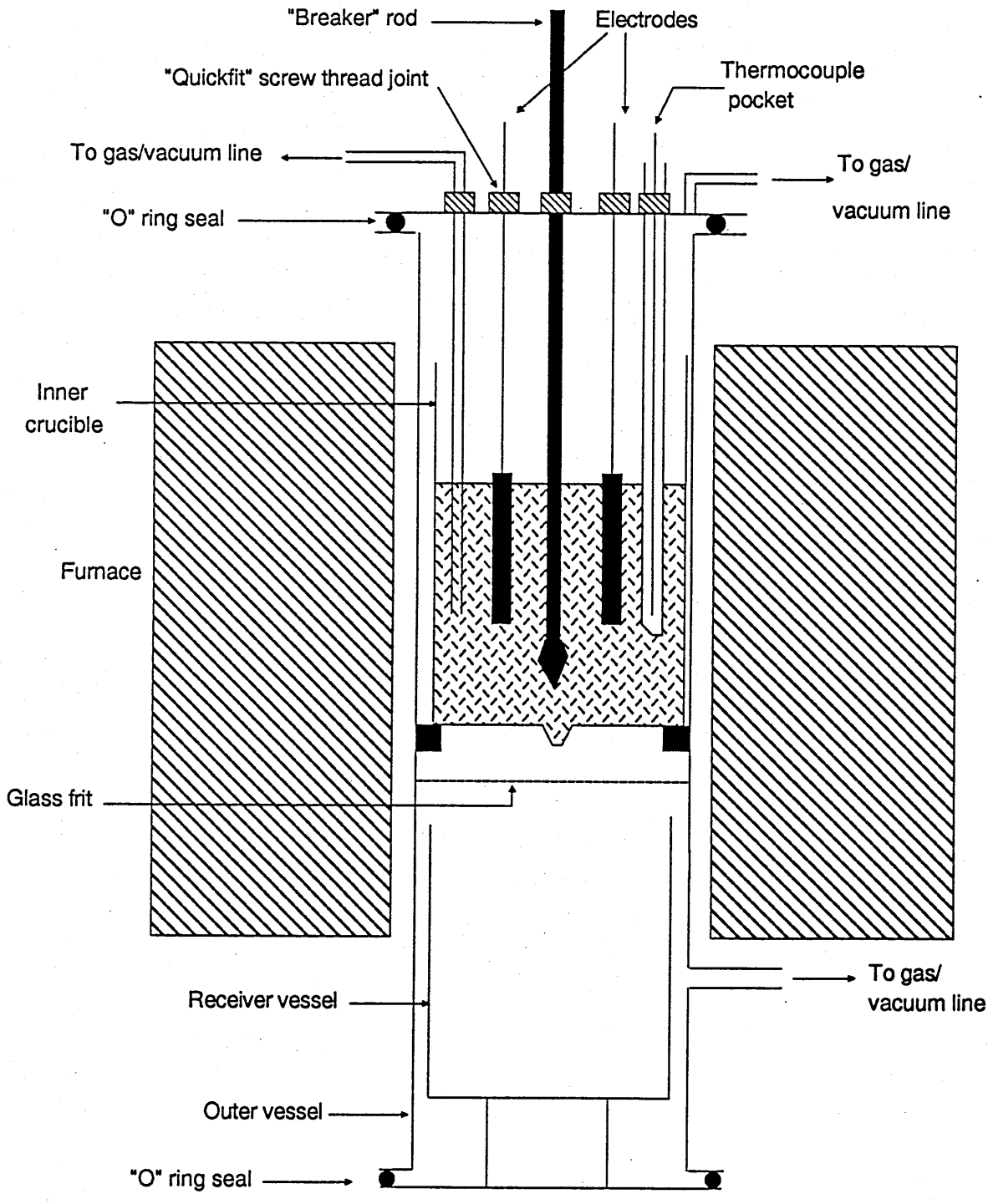

FIGURE 2.2

GAS/VACUUM LINE FOR PURIFICATION CELL

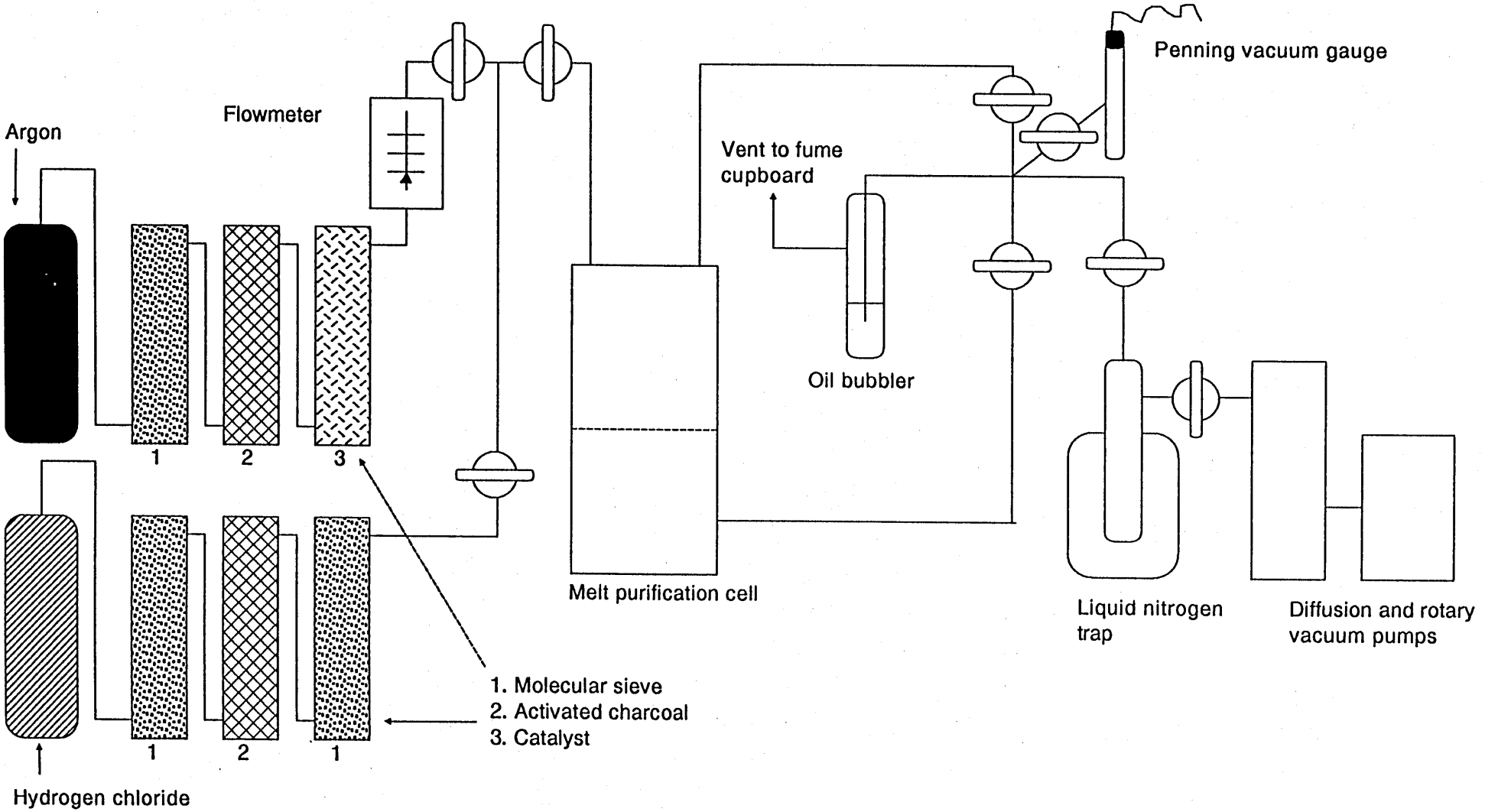

FIGURE 2.3

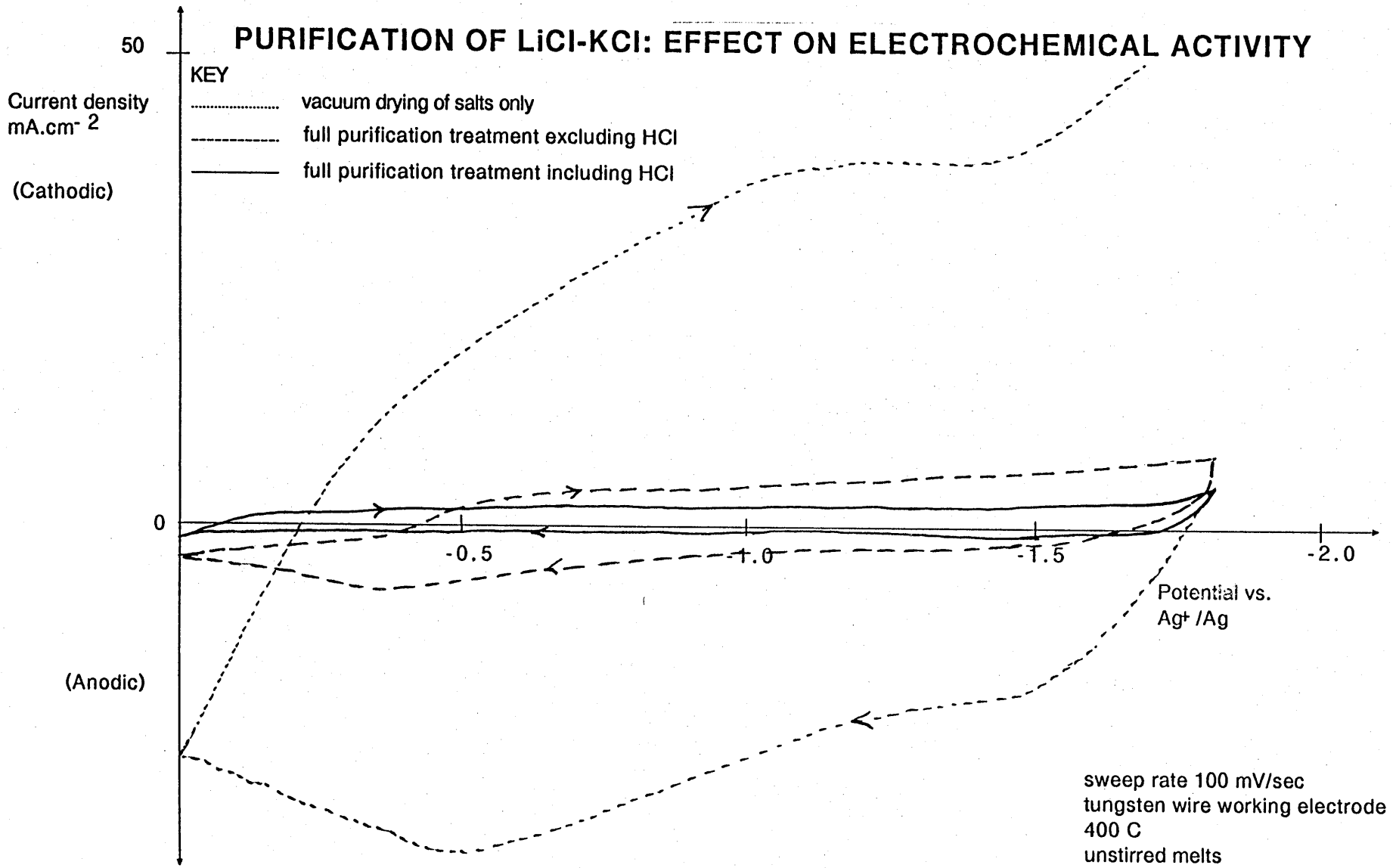
PURIFICATION OF LiCl-KCl: EFFECT ON ELECTROCHEMICAL ACTIVITY
50
KEY
vacuum drying of salts only
full purification treatment excluding HCl
full purification treatment including HCl
Current density
mA.cm- 2
(Cathodic)
0
-0.5
-1.0
-1.5
-2.0
Potential vs.
Ag+ /Ag
(Anodic)
sweep rate 100 mV/sec
tungsten wire working electrode
400 C
unstirred melts

FIGURE 2.4

ADDITION OF SALTS TO CELL

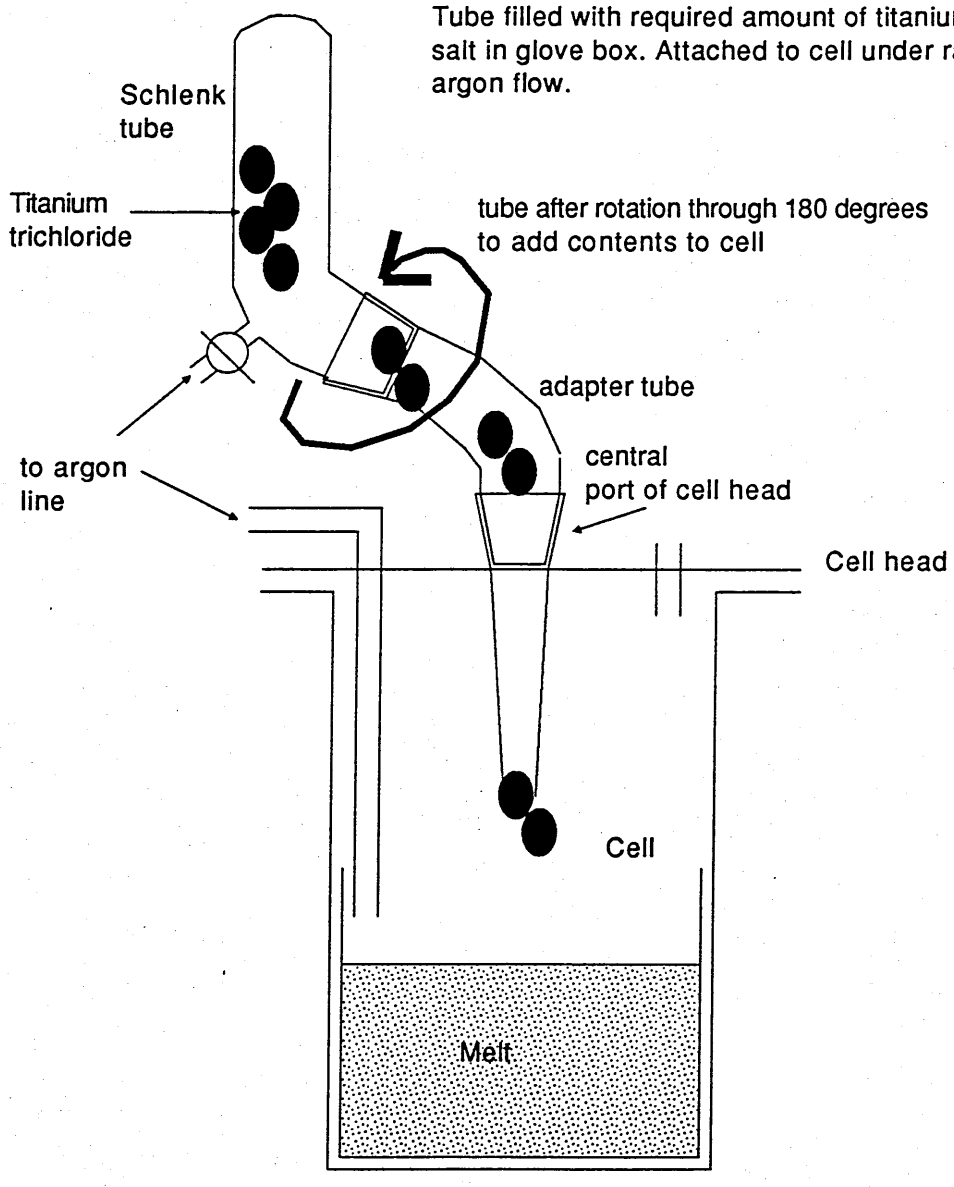

FIGURE 2.5

REFERENCE ELECTRODE

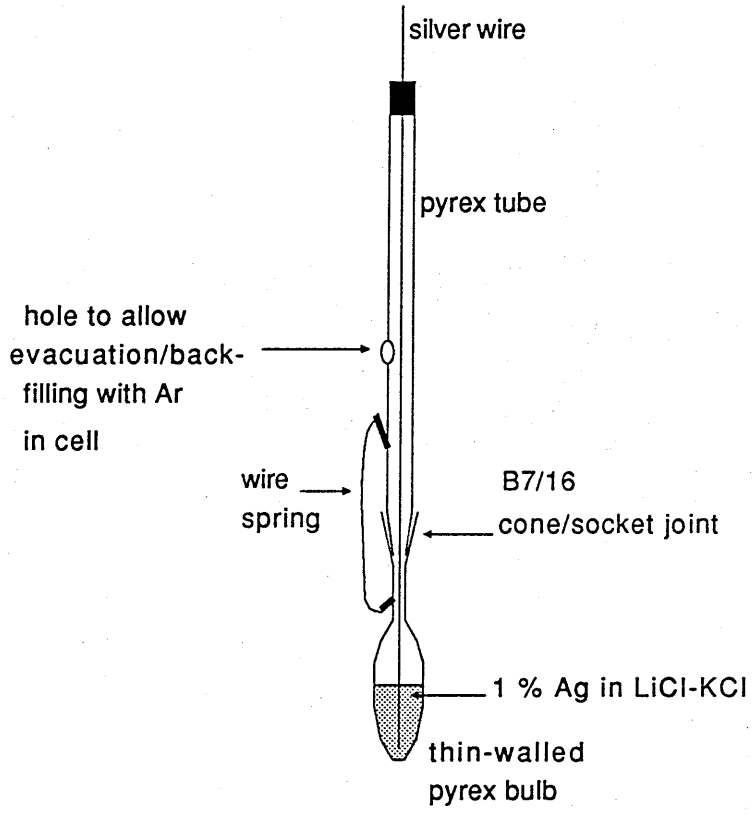

FIGURE 2.6

TYPICAL EXPERIMENTAL CELL

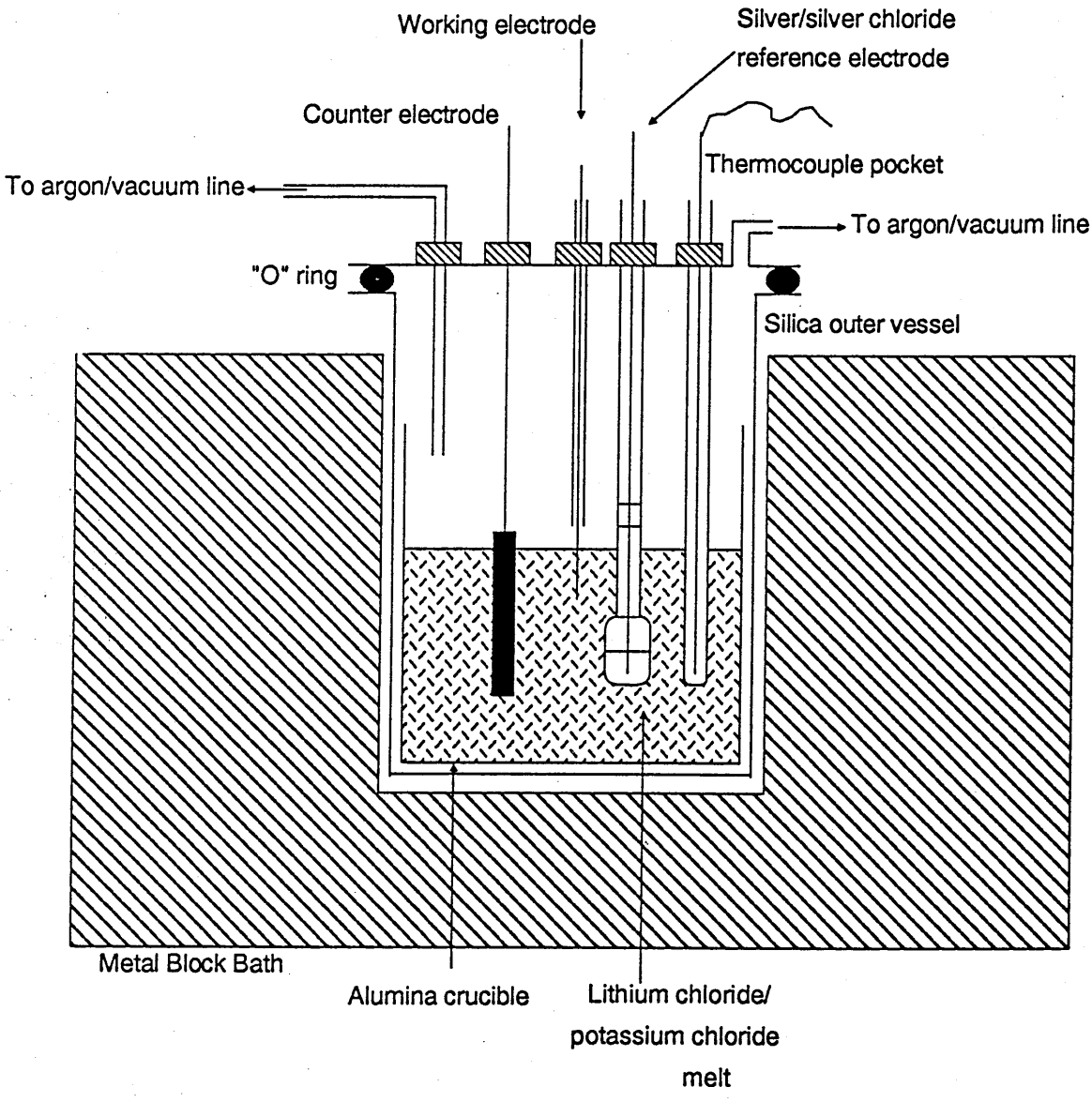

FIGURE 2.7

APPARATUS TO DETERMINE DIVALENT TITANIUM CONCENTRATION

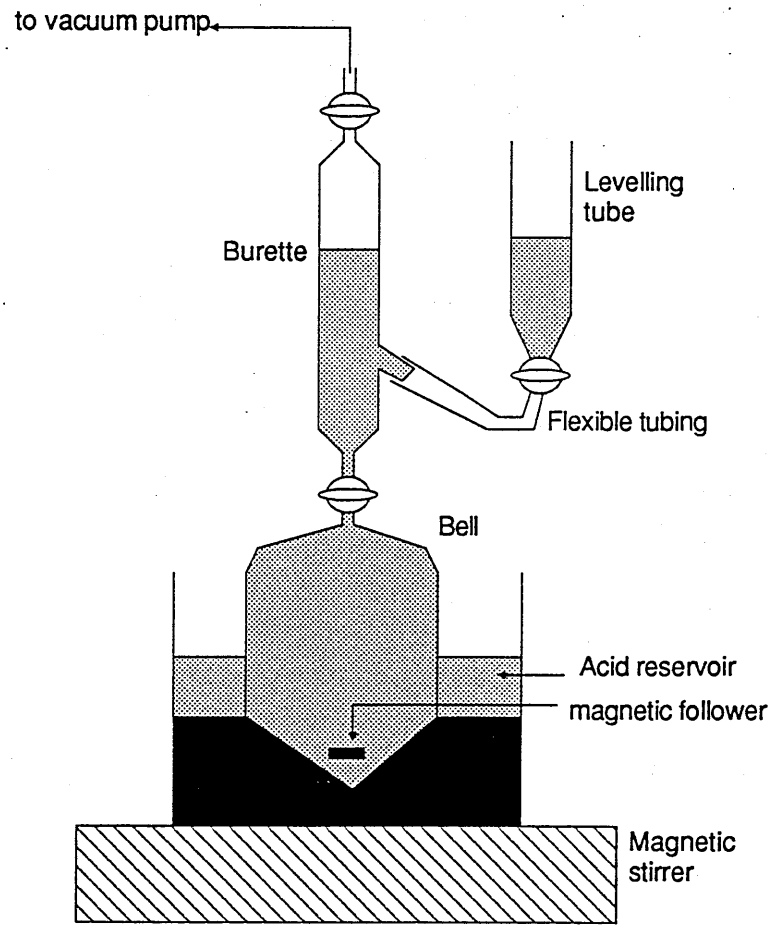

CHAPTER 3

THE ELECTROCHEMICAL REDUCTION OF OXIDES ON IRON AND STEEL ELECTRODES

3.1. Introduction

During electrodeposition experiments under controlled potential conditions on stainless steel electrodes (see later chapter) considerable irreproducibility in the nature and appearance of the deposits was observed. The only possible explanation appeared to be the state of the electrode surface prior to deposition. It had been asssumed initially that the flux action of the melt would produce essentially identical surface conditions. However, it was found necessary to prepare the substrate much more carefully in order to obtain reproducible results. Indeed surface preparation of the stainless steel substrate was found to be a very important factor: it is capable of strongly influencing the nature of the deposit formed, and, in extreme cases, determines whether an adherent deposit is produced at all. Although standard procedures capable of allowing reproducible results to be obtained in deposition experiments were successfully developed, the importance of this factor merited a closer study of these effects.

Stainless steel was the selected substrate because it was considered that there would be a significant number of applications for titanium coated stainless steel. Stainless steel is often used as a cheaper alternative to titanium in the chemical process industries. It performs less well in most corrosive environments. A coating of titanium would enhance its performance, but stainless rather than mild steel as substrate would avoid disastrous consequences if the coating was breached.

It is generally well-known that plating on stainless steel requires prior "activation" of the substrate surface, i.e. removal of surface oxide. See for example reference 82. The composition of passive oxide films on iron and on stainless steel alloys has been the subject of a considerable amount of investigation. Most information has been derived from electrochemical reduction experiments in aqueous media in conjunction with various spectroscopic investigations[83]-[96]. In spite of this there is still some controversy as to the exact nature of these films.

It is fairly widely thought [83]-[86] that air-formed and anodically generated oxides on iron are similar and consist mostly of gamma Fe_2O_3 (i.e. cubic close-packed array of oxide ions with FeIII distributed randomly among the octahedral and tetrahedral interstices). It has been observed that the ferrous ion content increases from the outer surface to the metal/oxide interface. This is sometimes described in terms of an inner Fe_3O_4 layer. Cathodic polarisation of the oxide films in aqueous media causes reduction to Fe^{2+} in solution and to Fe metal. This is a 2-stage process. The exact mechanisms of these reactions are disputed. The relative proportions of the product Fe and Fe^{2+}(solution) have been shown to depend on pH, more Fe metal being produced at relatively high pH values [85]. The involvement of hydroxy species and the hydrogen ion in reaction mechanisms is frequently proposed. There is a reasonable consensus that the initial stage of the reduction can be described as[83],[85] :

$$Fe_2O_3 + 6H^+ + 2e \rightarrow 2Fe^{2+} + 3H_2O \qquad ...(3.1)$$

although an alternative has also been suggested[84] :

$$Fe_2O_3 + 6H^+ + 4e \rightarrow Fe^{2+} + Fe + 3H_2O \quad ...(3.2)$$

The second stage of reduction to Fe metal is more contentious still. Fe_3O_4 reduction has been proposed[83][86]:

$$Fe_3O_4 + 8H^+ + 8e \rightarrow 3\ Fe + 4H_2O \quad ...(3.3)$$

or simply: $$Fe^{2+} + 2e \rightarrow Fe. \quad ...(3.4)$$

The absence of ferrous species in the oxide film on passivated iron is claimed by Sato et al [87]. The excess oxygen content of the film is explained in terms of bound water : hydrous ferric oxide. FeOOH has also been detected by others[88]-[90] mainly in the outer portion of oxide films. Conditions of film formation can also be significant in affecting reduction characteristics[93]. A summary of the various interpretations of electrochemical reduction investigations is included in a review of the subject[91].

Relatively high chromium content steels rely for their corrosion resistance on a chromium oxide (Cr_2O_3) film[92],[94]-[97]. This is often described as "self-healing" because of its propensity to re-form (in the presence of oxygen) after mechanical or other damage exposing the substrate alloy. Under most conditions this film contains little iron. Formation of chromium oxide causes a depletion of chromium in the alloy near the metal/oxide interface. If the film is then breached (as can readily occur during heat treatment, for example) very rapid corrosion of the iron-rich portion of the substrate metal takes place (with formation of iron-rich oxides) until a sufficient chromium concentration in the metal is re-established. Cr_2O_3 then forms again. At high temperatures this cycle can continue, to produce a layered oxide structure on the steel surface[94], which constitutes surface "scale". The various components (in addition to Cr_2O_3) may be iron oxides or mixed

(duplex) iron/chromium oxides[92] [94]. Nickel is found to be present in the oxide film only in very much smaller proportions than the bulk metal alloy composition[97] and does not seem to be a significant component of the film. The precise composition of oxide films on stainless steels is very dependent on the conditions under which the films were formed[97]. A film produced by anodic passivation has been found to have a chromium cation concentration of about 70 % (atomic concentration)[92]. Chromium enrichment of the oxide layer close to the metal/oxide interface has been observed[95] [96] for both thermally and anodically generated films. It has not been possible to identify individual oxide components of the film with oxides of the alloy's constituent metals[95]. Electrochemical reduction characteristics determined for stainless steel in aqueous solution have been interpreted (in a similar way to iron) as consistent with the reduction of ferric oxide, Fe_2O_3, and to a lesser degree, Fe_3O_4[95] [96] [98] [99]. Solid state valence transitions of chromium and nickel have also been proposed[95]. Chromium oxide is assumed to remain un-reduced[95].

The difficulties encountered in determining the exact composition of these oxides can be attributed to the fact that they are so thin (typically 20 A); their variable composition; and the problems of either examination in situ or transfer of the specimen to the investigation environment without significantly affecting the film[91]-[92].

Electrochemical reduction of these oxides in molten salts does not seem to have been studied. It was therefore decided to undertake experimental investigation of stainless steel and iron electrodes in the lithium chloride - potassium chloride eutectic at 450 C. The

objectives were to identify the potentials at which reduction of oxide takes place (particularly in relation to metal deposition potentials); to determine the approximate extent of oxide coverage under these conditions; and to determine the best substrate pre-treatment regime for plating processes in molten salts.

3.2. Experimental

3.2.1. Galvanostatic reduction

The technique used for the investigation was galvanostatic reduction. This would give information on the potentials at which the various reduction reactions took place, as well as provide a measure of the amount of material available for reduction. Comparison of the behaviour of substrates prepared in different ways should therefore allow selection of the most appropriate pre-treatment regime.

A cathodic galvanostatic pulse was applied to the working electrode held in the experimental cell (similar to that illustrated in figure 2.6), using a Wenking ST72 potentiostat in conjunction with a Hi-Tek waveform generator, and the potential-time response recorded on a Nicolet 4094 digital storage oscilloscope. The data were stored on floppy disks and later transferred to the site Prime (9755) computer for subsequent processing, analysis and output either to a Hewlett Packard 7475A or Calcomp plotter. The initial potential step at very short times attributable to the ohmic drop in the system was determined. This was then used to correct all data for this effect. The data were subsequently integrated to give charge-potential information.

3.2.2. Electrodes and pre-treatment

Stainless steel working electrodes were constructed from 0.5 mm diameter wires of Goodfellow Metals AISI 302 stainless steel with a typical analysis as follows :

chromium 17-20 %

manganese < 2 %

nickel 7-11 %

carbon < 1600 ppm

iron, the remainder.

The wires were straightened before use and were mounted in alumina tubes of bore just slightly greater than 0.5 mm for immersion in the melt. The alumina tube was secured in the central port of the cell head using a specially made PTFE washer with a Quickfit screw cap joint.

The immersed electrode area was about 0.3 cm^2 in each case.

Electrodes were used either in their "as-received" state, with no pre-treatment except for degreasing in an ultrasonic bath using trichloroethane, or after undergoing one of the following treatment schedules.

1) Anodic etching, in a 30 % sulphuric acid solution, applying between 4 and 5 volts between the wire and a platinised titanium counter electrode. This was followed by rinsing in distilled water, then ultrasonic cleaning in trichloroethane.

2) Grit-blasting with alumina grit (180/220 high purity

grade), followed by ultrasonic cleaning in trichloroethane.

3) Grit-blasting and cleaning as in 2) followed by anodic etching as in 1) above.

Pure iron and pure nickel wires were also employed. These were also 0.5 mm in diameter and were Goodfellow Metals pure material (>99.9 %).

The counter electrode used throughout was a vitreous carbon rod (Fluorocarbon).

A silver/silver chloride reference electrode was used, constructed as shown in figure 2.5 and as described previously.

3.3. Results

3.3.1. The general form of the reduction : a comparison of iron, stainless steel and nickel

The reduction of each material (un-treated except for degreasing) at 85 $mA.cm^{-2}$ is shown in figure 3.2. Data in this and subsequent similar figures in this chapter have been plotted in the same way : the drawn curves represent more than 300 data points. The symbols on each curve, although they do represent a small sample of actual data points, are present only to allow discrimination between the various curves.

Nickel exhibits no features in its potential-charge response, the potential rapidly reaching about -2.38 V vs Ag/AgCl, the lithium discharge potential[50]. In the case of iron, however, there are two distinct arrests in the potential-charge curve. The potential decays rapidly at first to about -1.2 V. The fall in potential then slows

considerably so that there is almost a level plateau until about -1.4 V when the potential falls rapidly once more. A second such "wave" occurs at more negative potentials, before the final steady lithium discharge potential is reached. The stainless steel electrode shows behaviour lying somewhere between iron and nickel: at least one wave is present, but it is ill-defined.

The position of each wave can be characterised conveniently by the point of maximum slope occurring at the end of the plateau region. These end-points were determined by plotting differentiated potential/charge data (calculated for groups of data points shifted one point at a time along the entire potential-charge curve) against both potential and charge. The points of maximum slope were identified as minima in these plots (see figure 3.3). It was necessary to alter the differentiation parameters (i.e. the number of data points, n, in the groups of points used to calculate the potential/charge slope values) to deal adequately with the different waves. The end-point charge and potential values were determined with a precision of approximately +/- 5 %. The charge passed in each wave was determined by simple subtraction of end-point charge values. The results are presented for iron and stainless steel in tables 3.1 and 3.2 respectively. The waves are labelled and referred to by their end-points, A, B, C, etc. as described in figure 3.1. The various waves in the reductions are henceforward referred to in the text by their end-point potentials.

The potential-time responses obtained on iron and stainless steel were found to be sensitive to the immediate history of the electrode, for example the length of time it had been held above the

melt surface within the inert gas envelope, etc. (The individual effects are discussed below). Consequently considerable effort was expended in determining the procedures required to ensure good reproducibility of results. With very careful control of pre-treatment procedures, the time spent at high temperature before immersion in the melt, and the time allowed to elapse from the electrode's immersion to the application of the reduction step, reproducibility of better than +/- 2 % was achieved. This represents the scatter of the values of the charge passed before the final steady lithium discharge potential is reached.

Thus the waves for iron (see figures 3.3 and 3.4) have end-points at -0.9V, -1.5 V and -2.2 V. There is a shoulder on the -1.5 V wave at about -1.85 V. This is obvious as a distinct wave in some reductions, particularly at low current density and is discussed later. Stainless steel shows similar -1.5 V and -2.2 V waves but the -0.9V wave is absent. The absence of these waves in the case of nickel confirms that these features are the result of processes peculiar to the electrode materials and not the reactions of species dissolved in the melt.

3.3.2. The effect of current density

The results are illustrated in figures 3.4, 3.5 and 3.6 for iron, and stainless steel (degreased only and anodically etched) respectively. Superficially the trend in each case is similar. At low currents (< 15 $mA.cm^{-2}$) the amount of charge passed before lithium discharge takes place falls with increasing current density. At higher current the effect becomes negligible.

The results for iron differ from those for stainless steel in that

at low currents an additional wave appears in the reduction process at about -1.8 V. This feature remains evident at higher currents in the differentiated potential/charge data where it manifests itself as a shoulder on the previous wave. See, for example, figure 3.3. No such extra feature is present for stainless steel reduction. This additional wave is largely responsible for the current dependence of the total charge at low currents. Charge associated with the -1.5 V wave is current independent except at the lowest current densities.

On stainless steel nearly all the increased charge passed at low current density is associated with the final wave. Current dependence is much less marked for the etched surface.

3.3.3. Repeated reduction of the same electrode

Repeating the reduction on the same electrode after the potential had been allowed to decay back to its rest value at open circuit resulted in different effects for stainless steel and iron (figures 3.7 and 3.8). On the stainless steel electrode the -2.2V wave remains, and indeed, after the first reduction, becomes better-defined, whereas for iron the wave essentially disappears.

Repeated reductions on stainless steel gradually reduce the charge required for "complete" reduction (i.e. the charge passed before the final lithium discharge potential is reached), but even after four consecutive reductions this charge is still substantial. Another effect is observed on stainless steel : the first wave disappears after the first reduction but is replaced by a wave at about -1.8 V (table 3.2). This persists with repeated reduction. Repeated reduction on iron results in the disappearance of all features in

the potential-charge curve.

"Partial" reductions were carried out, both potentiostatically at -1.8 V for 1 minute, and galvanostatically at 1 $mA.cm^{-2}$. In the latter case the constant current was applied and the potential-time response monitored to allow termination of the reduction before the final transition to the lithium metal discharge potential took place. For iron, subsequent galvanostatic reduction showed in both cases a diminution in the charge required to effect "complete" reduction. However, in the case of potentiostatic pre-reduction, the charge associated with the final wave remained unchanged while that of the -1.5 V wave diminished considerably (table 3.1). With galvanostatic pre-reduction both waves were dramatically reduced in charge, behaviour resembling that following full pre-reduction.

On stainless steel the -1.8V wave, persistent during repeated "full" reductions, disappeared after partial reduction at 1 $mA.cm^{-2}$. Only the -2.2 V wave remained, albeit with less charge than even the 4th consecutive full reduction.

3.3.4. The effect of holding the electrode at elevated temperature in the cell inert atmosphere

The electrodes were held for various periods of time just above the melt surface before immersion in the melt and reduction. Each electrode was therefore exposed to an argon atmosphere at 450 C during this period. The effects are shown in figures 3.9 and 3.10.

A steady increase in the charge associated with the -1.5 V wave is observed for iron. The charge in the final wave remains essentially unchanged except for the longest time experiment. The first -0.9 V

wave remains very small throughout. Stainless steel shows enhanced charge values (associated with both waves) only at very long exposure times (above 600 seconds).

3.3.5. The effect of immersion in the melt

With increasing time of immersion in the melt before reduction, the iron electrode requires less charge to effect reduction as far as lithium discharge (figure 3.11). This is consistent with dissolution of oxide from the electrode surface. Stainless steel, however, shows a different trend : charge for "complete" reduction increases with immersion time (figure 3.12). Most of this increase is associated with the final wave.

3.3.6. The effect of surface preparation

Figure 3.13 compares the reduction at 80 $mA.cm^{-2}$ of stainless steel electrodes pre-treated in various ways. It is evident that grit-blasting increases the charge necessary to effect complete reduction, while anodic etching leads to a considerable decrease in the charge requirement.

3.4. Discussion of results

The observed behaviour of the reduction of iron and stainless steel electrodes in the molten chloride electrolyte is consistent for the most part with reduction reactions of their surface oxides. The two materials exhibit similar but not identical reduction characteristics.

This is to be expected because of the different compositions of the

oxide films covering each material, as discussed in section 3.1. The film on pure iron at the oxide/air interface can be thought of as essentially Fe_2O_3 with perhaps some contribution from hydrated species such as FeOOH. An increased concentration of ferrous ions is likely towards the oxide/metal interface.

It is more difficult to estimate what is the most likely composition of the oxide film on the stainless steel electrodes. Following the simple degreasing pre-treatment it is likely to be mostly Cr_2O_3 with possibly some Fe_2O_3 and Fe_3O_4 also present, particularly if the wire had undergone any heat treatment. The etched wires will probably have an oxide film consisting almost entirely of the chromium oxide.

The electrochemical reductions reported here can be summarised as a series of waves corresponding to the following approximate end-point potential values vs Ag/AgCl :

Iron : -0.9 V, -1.5 V, (-1.8 V), -2.2 V

Stainless steel : -1.5 V, (-1.8 V), -2.2 V

The final steady potential attained on each is -2.38 V, the lithium discharge potential. The -1.8V is enclosed in parentheses to denote this wave's less distinct nature.

3.4.1. The -0.9 V wave on iron

The wave at -0.9 V is always a minor contribution to the total charge for reduction and is present only for pure iron. This could possibly arise from the presence of a small amount of hydrated oxide on the outer film surface. The phenomenon is somewhat similar to that observed by Ehrenfreund and Leibenguth in their study of ferric oxide films on platinum[90][93]. They attributed this "extra"

reduction wave to reaction of FeOOH formed on the surface of Fe_2O_3. This feature was not always observed in the present studies, but this would be consistent with slight variations in experimental technique leading to more or less hydration of the outer surface. The effect was never observed for stainless steel. This may lend support to other evidence that there is little ferric oxide making up its oxide film.

3.4.2. The -1.5 V wave on iron and stainless steel

The -1.5 V wave is characterised by the current-independence (except at the lowest current densities) of the charge associated with it (see tables 3.1 and 3.2); its disappearance following the first reduction of any electrode; its gradual diminishment with increased immersion time before reduction; the increase in the charge associated with it with increased time of holding the electrode above the melt surface. All this evidence is consistent with reduction of oxide on the surface of the electrode.

The solution of Fe_2O_3 in these melts has been observed before[100], [101]. Other oxides (FeO and Fe_3O_4) are considered insoluble[101]. The most likely mechanism for this solubility is a reaction of the type[102]:

$$\underset{\text{in oxide film}}{Fe} + 2Fe^{3+} \dashrightarrow \underset{\text{in solution}}{3\ Fe^{2+}} \qquad \ldots(3.5)$$

The increase in the charge of this wave with increased exposure to the cell atmosphere prior to immersion and reduction suggests that the oxide can grow under these conditions. In turn, this implies

that oxygen is present to fuel such growth. Contamination of the cell's argon atmosphere with low levels of oxygen can be expected from air ingress during exchange of electrodes, and possibly from oxygen/moisture adsorption on the electrode surface itself.

Two possibilities for reactions represented by this wave are :

$$Fe_2O_3 + 6e \rightarrow 2Fe + 3O^{2-} \quad \text{.....(3.6)}$$

$$Fe_2O_3 + 2e \rightarrow 2Fe^{2+} + 3O^{2-} \quad \text{.....(3.7)}$$

The current independence of the charge associated with the wave (at all but the lowest current densities) suggests a non-diffusion controlled reaction. This in turn may indicate that reaction (3.6) is the best description of behaviour because of the absence of involvement of ferrous ions in solution.

The charges associated with the -1.5 V wave correspond to the following oxide film thicknesses if reaction (3.6) is an accurate description.

Material	Charge in -1.5V wave, C/cm2	Calculated film thickness,nm
Degreased iron	0.0135	7.1
Degreased steel	0.0035	1.8
Etched steel	0.0005	0.26

These values have been calculated assuming that the density of the film equals that of compact gamma Fe_2O_3, 5.24 $g.cm^{-3}$ (the density of Cr_2O_3 is very similar at 5.21 $g.cm^{-3}$)[103]. Typical thicknesses for oxide films on iron and stainless steel given in the literature are 2-5 nm[92]. The results are therefore completely consistent with the anticipated thicknesses of ferric oxide films on the electrodes studied.

The observation of much increased charge passed following grit-blasting of the stainless steel surface (figure 3.13) may be the result of an increased amount of ferric oxide in the oxide film. Surface roughening will also contribute to the observed effect. Surface treatments can have a marked effect on the composition of oxide films on stainless steels[92][104]. Mechanical polishing has been shown to produce a film consisting largely of ferric oxide while other (electrochemical) pre-treatments produce a chromium-rich film on chromium containing steels[92]. Anodically etching the electrode leads to much lower charge requirements, because of the much thinner oxide film covering the electrode surface. The etching process will remove all previous oxide , such that the freshly prepared surface will have an air-grown film, with no contribution from oxide growth as a result of heat or other treatments. This demonstrates the efficacy of the preferred substrate pre-treatment method.

It is significant that the standard reduction potentials and therefore the deposition potentials of many metals are more positive than the potentials associated with this wave[50]. It must therefore be assumed that oxide reduction does not take place in preference to metal deposition during passage of current for electrodeposition. Strong influence of the substrate's oxide film on electro-crystallisation is therefore possible. Removal of the oxide film before electroplating and related processes is therefore preferred. This will be particularly important for systems containing metals with as strong an affinity for oxygen as titanium.

3.4.3. Other reduction processes

Assuming the hypothesis described above, the remaining charge passed during the reductions of iron and steel electrodes must be attributed to reactions other than oxide reduction. Additional evidence for the importance of other reduction processes is provided by the persistence of the -2.2 V wave on stainless steel, even after repeated reductions. Also the relationship of the charge values associated with the two most significant waves is not a constant one : a simple stepwise reduction of a particular species cannot therefore be important. This is demonstrated in figure 3.5: potentiostic pre-reduction of iron at -1.8 V causes the -1.5 V wave to be much diminished but does not affect the final -2.2 V wave. The relative contributions of the -1.5 V and -2.2 V waves are different for the two materials. On stainless steel the -1.5 V wave contributes only about 20 % of the charge for "total" reduction. On iron the proportion is much higher , nearly 50 % under some circumstances.

Additional contributions to the total charge passed in reduction may result from reduction of solution species. Ferrous ions derived from previous reduction of oxide films, or hydroxide impurities in the melt, for example, would both be reduced in the potential range studied[100][70]. A particularly strong influence could be anticipated at low current densities when a large proportion of the total charge for reduction might be associated with these solution species reactions. Such effects would therefore be very dependent on the melt history : ferrous ion content, for example, would be determined by how many electrodes had been immersed in the melt and for how long, and so on. This could be a cause of the current

density dependence of the reduction observed at low currents.

3.4.4. The -1.8 V wave on iron and stainless steel

This is a much less well-defined wave than the others. It is often apparent only on inspection of the differentiated data. Only at low current densities on iron is it clearly distinguishable. On stainless steel it is apparent only when all oxide has been removed, such as in second and subsequent reductions on the same electrode. It is possible that the previous, -1.5 V, wave obscures it under many circumstances.

There appear to be two possible sources of this wave: the reduction of ferrous ions in solution :

$$Fe^{2+} + 2e \rightarrow Fe \quad \text{.....(3.8)}$$

or the reduction of hydroxide ions, present as impurities in the melt (see chapter 2):

$$OH^- + e \rightarrow O^{2-} + 1/2\ H_2 \quad \text{.....(3.9)}$$

This is supported by the observation that the charge associated with the wave depends on current density (see table 3.1, but note that the nature of the wave probably makes the precision of the values determined rather less than for the other features). At high currents the transition time for the wave will be short, such that it will merge into, and become indistinguishable from, adjacent waves. Consequently it is only at low currents that the feature is clearly observable.

The standard reduction potential of reaction (3.8) is -0.445 V vs $Ag/Ag^+(1m)$ while that of reaction (3.9) is -1.57 V[100], [73]. This perhaps suggests that reaction (3.9) is the more likely explanation.

If reaction (3.8) were important, then it might be inferred that some reduction of Fe_2O_3 to Fe^{2+} in solution occurs, i.e. that there is some contribution from reaction (3.7) in the overall reduction process. It is not possible to draw definitive conclusions from these results. The formation (or not) of Fe^{2+} in solution during reduction should preferably be investigated to shed further light on this. The importance of the ferrous ion reduction can be expected to be enhanced for long immersion times because of the proposed mechanism of non-electrolytic dissolution of the film as described by reaction (3.5).

3.4.5. The -2.2 V wave on iron and steel

It is not possible to explain this wave in terms of the reduction of solution species, because there are significant differences in behaviour between the different electrode surfaces. The magnitude of the charge associated with the wave also depends on the pre-treatment of the electrode : it is much smaller on the etched stainless steel surface than on the unetched electrode.

The proximity of this wave to the lithium discharge potential suggested the possibility of alloy formation of lithium with the substrate metal. This process would be limited by diffusion of lithium into the steel. To test this hypothesis, the current was reversed immediately after the cathodic pulse and the potential-time response to the anodic current also recorded. An arrest in the potential-time curve is observed in the case of stainless steel (figure 3.14), but only on the second and subsequent cycles of reduction followed by oxidation. No such arrest was observed for iron, even after several cycles. Thus while the presence of an

arrest during current reversal in the case of stainless steel is good support for the hypothesis of lithium alloy formation, the different behaviour of iron and the absence of this feature following the first reduction on stainless steel, still need to be accounted for.

The first reduction on stainless steel differs from subsequent ones with respect to another characteristic also. The -2.2 V wave is very much less well-defined during the first reduction. An explanation which might account for the anomalous behaviour of the first reduction is that alloy formation begins before the removal of surface ferric oxide is complete. Alloyed lithium, and pure lithium metal, can then undergo chemical reaction with remaining surface oxide, i.e. act as a chemical reducing agent. Lithium is thus consumed and not available for dissolution in any current reversal step. Subsequent reduction on the same surface, now free of any ferric oxide coverage, allows alloy formation without concurrent oxide reduction so that the lithium alloy remains for dissolution when anodic current is passed. The presence at the metal/melt interface of a chromium-enriched substrate (after oxide removal) may be a facilitating factor in alloy formation.

The different effects observed on iron and stainless steel can be explained in terms of the necessary rearrangement of the electrode surface following oxide reduction in each case. Consider that lithium alloy formation may only occur with the Fe_2O_3 type lattice structure. Following reduction of ferric ions to Fe metal there is a finite time delay before the newly formed iron atoms rearrange themselves to become indistinguishable from the iron lattice of the

substrate material. During the period of this rearrangement the possibility of lithium ingress (i.e. alloy formation) exists. Therefore the -2.2 V wave appears following the ferric ion reduction wave in the first reduction. However in subsequent reductions, after lattice rearrangement has taken place, no alloy formation can occur and the wave is absent. However, the observation of the effect of potentiostatic pre-reduction tends to go against this argument.

On stainless steel much more lattice rearrangement is required for the newly formed iron to be accommodated by the substrate structure. This takes longer, and subsequent reductions on stainless steel show the alloy formation wave at -2.2 V. The chromium oxide component of the oxide film is also likely to be important. There is no clear evidence that this oxide is reduced electrochemically. It may therefore represent a permanent structure in which lithium atoms can be accommodated, so that, irrespective of the time available for lattice rearrangement, there is always some lithium alloy formation.

The importance of the amount of oxide on the substrate surface in determining the extent of alloy formation and hence the amount of charge associated with this wave is consistent with the observed difference between etched and unetched stainless steel surfaces. The former can be expected to have a relatively thin oxide film, and its -2.2V wave has typically 0.005 coulombs/cm^2 associated with it. The latter would have much greater oxide coverage, and has a correspondingly larger charge associated with the wave, about 0.03 coulombs/cm^2. Probably both Cr_2O_3 and Fe_2O_3 can accommodate lithium atoms to a similar extent, as their lattice structure is the same. However, while stainless steel has a permanent lithium "sink" in the form of its chromium oxide, iron can only sustain lithium "alloy"

formation while it retains some ferric oxide coverage, i.e. during the first reduction of an electrode.

If the chromium oxide were reduced to chromium metal (either electrochemically or by reaction with lithium metal) then a chromium rich surface would be the result. The actual alloy composition of the surface can be expected to have an effect on the extent of alloy formation and indeed on the potential at which it takes place: enhanced chromium content might facilitate alloy formation, for example. The same argument concerning time for rearrangement involving solid state diffusion of the metal atoms would apply as was discussed above.

The physical state of the surface may also be an important factor : mechanically roughened, etched and the as-received surfaces may show significant differences in the extent of alloy formation, irrespective of the effects of associated differences in the nature of oxide coverage.

3.5. Conclusions

1. It is possible to cathodically reduce oxides on both iron and stainless steel in lithium/potassium chloride at 450 C. There is some solubility of iron oxide in this melt but cathodic reduction produces a "cleaner" surface. The characteristics of galvanostatic reduction are consistent with reduction of Fe_2O_3. There is also evidence for lithium alloy formation at more negative potentials.

Further conclusions concerning the nature of the reduction reactions are limited by the nature of the investigation : in particular the uncertain nature of the composition of the oxide films undergoing

reduction and the effect of low concentrations of ferrous ions in solution in the melt.

2. Inclusion of an anodic etching procedure is beneficial for the pre-treatment of electrodes in order to ensure a relatively oxide-free surface.

3. The potentials at which oxide reduction takes place are more negative than many metal deposition reactions. Metal deposition reactions will therefore, under most circumstances, take place in preference to oxide reduction. It can therefore be expected that substrate pre-treatment, by virtue of its effect on the oxide film, will influence observations of electrocrystallisation processes.

TABLE 3.1 POTENTIAL/CHARGE DATA FOR IRON

EXPERIMENTAL CONDITIONS*	CHARGE, COULOMBS/CM2**				POTENTIAL, V. VS AG/AGCL**					
	QA	(QB-QA)	(QC-QB) or (QD-QB)	(QD-QC)	QE	EA	EB	EC	ED	EE
vs. current density										
0.77 mA.cm^{-2}	0.0054	0.0206	0.042	0.037		-0.82	-1.33	-1.8	-2.04	
1.17 mA.cm^{-2}	0.0047	0.0173	0.036	0.042	0.12	-0.82	-1.31	-1.8	-2.17	-2.38
1.67 mA.cm^{-2}	0.0025	0.0125	0.017	0.025	0.08	-0.92	-1.35	-1.82	-2.18	-2.38
8.82 mA.cm^{-2}	0.0017	0.0133	0.01	0.02	0.053	-0.95	-1.45	-1.85	-2.25	-2.38
15.5 mA.cm^{-2}	0.0016	0.0139	0.009	0.018	0.048	-0.93	-1.45	-1.9	-2.26	-2.39
38.7 mA.cm^{-2}	0.0012	0.0115	0.0201		0.04	-1.01	-1.56	(-1.85)	-2.25	-2.38
79.4 mA.cm^{-2}	0.00125	0.0136	0.005	0.015	0.045	-0.97	-1.53	(-1.88)	-2.23	-2.38
116.2 mA.cm^{-2}	0.0017	0.0148	0.0055	0.02	0.051	-0.98	-1.55	(-1.87)	-2.26	-2.38
162.8 mA.cm^{-2}	0.0012	0.0136	0.0022	0.0155	0.034	-0.97	-1.62	(-1.88)	-2.27	-2.38
226.8 mA.cm^{-2}	0.0012	0.0136	0.0192		0.039	-0.93	-1.6	(-1.9)	-2.25	-2.38
384.6 mA.cm^{-2}	0.0008	0.0135	0.0178		0.035	-0.93	-1.64		-2.26	-2.3
Repeated reductions, 90 mA.cm^{-2}										
1st reduction	0.002	0.015	0.004	0.014	0.046	-0.95	-1.56	(-1.9)	-2.25	-2.38
2nd reduction		0.0025			0.01			(-1.88)		-2.38
After reduction @ -1.8 V.	0.001	0.003	0.016		0.023		-1.74		-2.3	-2.38
After partial reduction @ 1 mA.cm^{-2}		0.0025	0.0035		0.01		(-1.8)		-2.27	-2.38
Time above melt, (seconds) 80 mA.cm^{-2}										
0	0.001	0.0128	(0.0062)	0.0148	0.039	-0.93	-1.48	(-1.9)	-2.26	-2.33
15	0.001	0.0121	0.0058	0.012	0.036	-0.92	-1.5	(-1.9)	-2.25	-2.32
30	0.002	0.0156	(0.0042)	0.012	0.037	-1.0	-1.49	(-1.9)	-2.25	-2.32
60	0.002	0.018	(0.01)	0.013	0.047	-0.89	-1.47	(-1.92)	-2.27	-2.35
322	0.002	0.02	(0.006)	0.015	0.042	-0.93	-1.53	(-1.9)	-2.26	-2.38
526	0.002	0.0215	(0.008)	0.0095	0.042	-0.96	-1.53	(-1.9)	-2.28	-2.38
3120	0.002	0.036	(0.012)	0.04	0.1	-0.93	-1.43		-2.3	-2.39
Time immersed before reduction (minutes), 80 mA.cm^{-2}										
10	0.0007	0.0113	(0.006)	0.0165	0.041	-1.0	-1.5	(-1.83)	-2.26	-2.31
17	0.0007	0.0103	(0.005)	0.015	0.038	-0.97	-1.54	(-1.9)	-2.28	-2.32
26	0.0008	0.008	(0.0037)	0.0175	0.038	-1.0	-1.59	(1.93)	-2.28	-2.35
120		0.0082	0.0163		0.028		-1.66		-2.28	-2.36

* Unless otherwise specified, the immersion time before reduction was about 10 seconds, the electrode being immersed immediately on introduction into the cell (i.e. not held above melt surface for any length of time. The only pre-treatment employed for iron was a simple ultrasonic degrease in trichloroethane.

** See Key diagrams for the significance of the Q and E parameters.

TABLE 3.2 POTENTIAL/CHARGE DATA FOR STAINLESS STEEL

EXPERIMENTAL CONDITIONS*	CHARGE, COULOMBS/CM2**			POTENTIAL, V, VS AG/AGCL**		
	QA	(QB-QA)	QC	EA	EB	EC
Degreased only						
0.81 mA.cm^{-2}	0.01	0.087	0.13	-1.25	-2.07	-2.3
1.55 mA.cm^{-2}	0.0075	0.042	0.062	-1.39	-2.18	-2.38
15.9 mA.cm^{-2}	0.0040	0.028	0.038	-1.36	-2.24	-2.38
36.7 mA.cm^{-2}	0.004	0.024	0.032	-1.45	(-2.18) -2.28	-2.38
50.5 mA.cm^{-2}	0.0042	0.022	0.03	-1.45	(-2.18) -2.3	-2.39
81.4 mA.cm^{-2}	0.0035	0.023	0.03	-1.4	-2.25	-2.38
167.1 mA.cm^{-2}	0.0038	0.02	0.029	-1.45	(-2.18) -2.25	-2.36
317.5 mA.cm^{-2}	0.0032	0.0173	0.026	-1.42	(-2.16) -2.25	-2.33
433.1 mA.cm^{-2}	0.004	0.0181	0.027	-1.58	(-2.15) -2.26	-2.33
Etched						
3.5 mA.cm^{-2}	0.001	0.0067	0.018	-1.27	-2.01	-2.38
7.9 mA.cm^{-2}	0.0008	0.0035	0.007	-1.3	-2.08	-2.38
16.3 mA.cm^{-2}	0.0007	0.003	0.006	-1.35	-2.09	-2.38
38.7 mA.cm^{-2}	0.00042	0.0026	0.0049	-1.35	-2.1	-2.39
77.4 mA.cm^{-2}	0.0008	0.0029	0.0049	-1.5	-2.15	-2.38
81.6 mA.cm^{-2}	0.0007	0.0029	0.0052	-1.4	-2.15	-2.38
90.6 mA.cm^{-2}		0.0032	0.0045		-2.15	-2.38
125.2 mA.cm^{-2}	0.0005	0.0025	0.0039	-1.47	-2.08	-2.38
181.2 mA.cm^{-2}		0.0039	0.005		-2.13	-2.37
333.9 mA.cm^{-2}		0.0039	0.0059		-2.15	-2.38
500.8 mA.cm^{-2}		0.0032	0.0049		-2.2	-2.38
Degreased only, 70 mA.cm^{-2}						
1st reduction	0.0035	0.0217	0.029	-1.34	-2.26	-2.38
2nd reduction	0.0038	0.0252	0.03	-1.77	-2.25	-2.38
3rd reduction	0.0032	0.0159	0.02	-1.76	-2.27	-2.38
4th reduction	0.002	0.0118	0.015	-1.82	-2.3	-2.38
after partial reduction @ 1 mA.cm^{-2}		0.0092	0.012		-2.17	-2.35
Time above melt, seconds: 75 mA.cm^{-2}						
0	0.004	0.024	0.031	-1.5	(-2.15) -2.26	-2.35
10	0.005	0.019	0.026	-1.5	(-2.13) -2.23	-2.35
20	0.0055	0.0195	0.0275	-1.55	(-2.14) -2.25	-2.35
40	0.0055	0.02	0.029	-1.52	(-2.16) -2.25	-2.35
138	0.0055	0.022	0.031	-1.48	(-2.17) -2.25	-2.38
300	0.006	0.023	0.033	-1.48	-2.21	-2.37
600	0.0078	0.024	0.034	-1.5	-2.23	-2.39
1467	0.017	0.029	0.05	-1.5	-2.21	-2.39
2112	0.017	0.036	0.058	-1.46	-2.23	-2.39
Time immersed, seconds 70 mA.cm^{-2}						
10	0.004	0.022	0.029	-1.43	(-2.15) -2.25	-2.38
30	0.004	0.023	0.033	-1.48	(-2.17) -2.28	-2.38
60	0.004	0.024	0.032	-1.47	(-2.18) -2.28	-2.36
180	0.0048	0.0317	0.039	-1.56	-2.26	-2.38
360	0.006	0.039	0.048	-1.7	-2.26	-2.36

* Unless otherwise specified, the immersion time before reduction was about 10 seconds, the electrode being immersed immediately on introduction into the cell (i.e. not held above the melt surface for any length of time).

** See Key diagrams for the significance of the Q and E parameters.

FIGURE 3.1
KEY TO TABLES 3.1 AND 3.2

SCHEMATIC DIAGRAM SHOWING REDUCTION WAVES FOR IRON

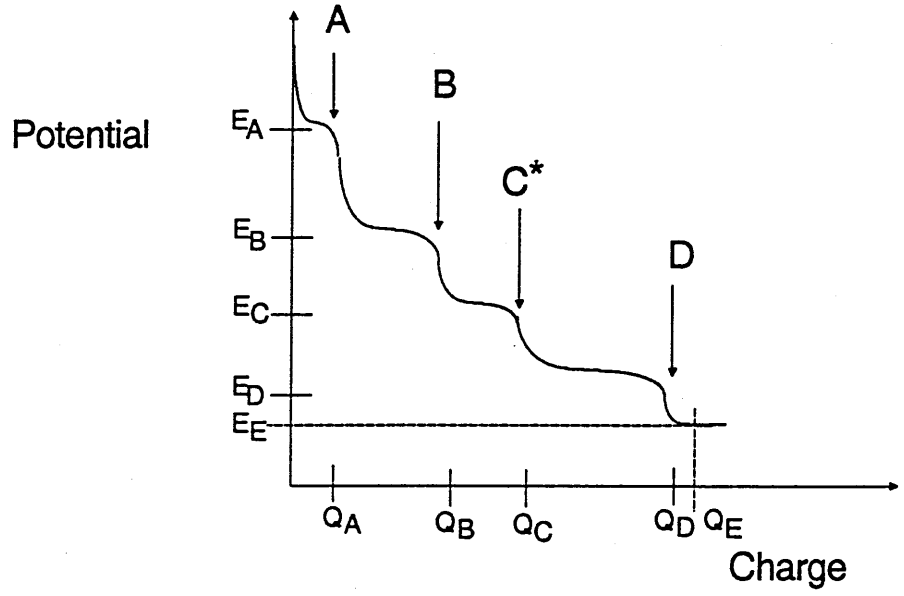

* Wave C not always present.

SCHEMATIC DIAGRAM SHOWING REDUCTION WAVES FOR STAINLESS STEEL

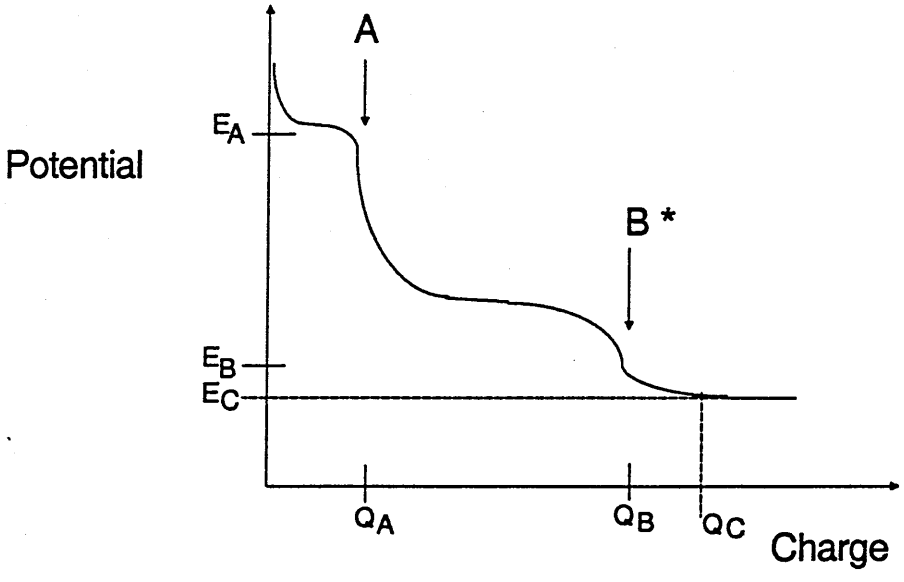

* Wave B sometimes appears split in the differentiated potential-charge data.

FIGURE 3.2

REDUCTION AT VARIOUS ELECTRODE MATERIALS

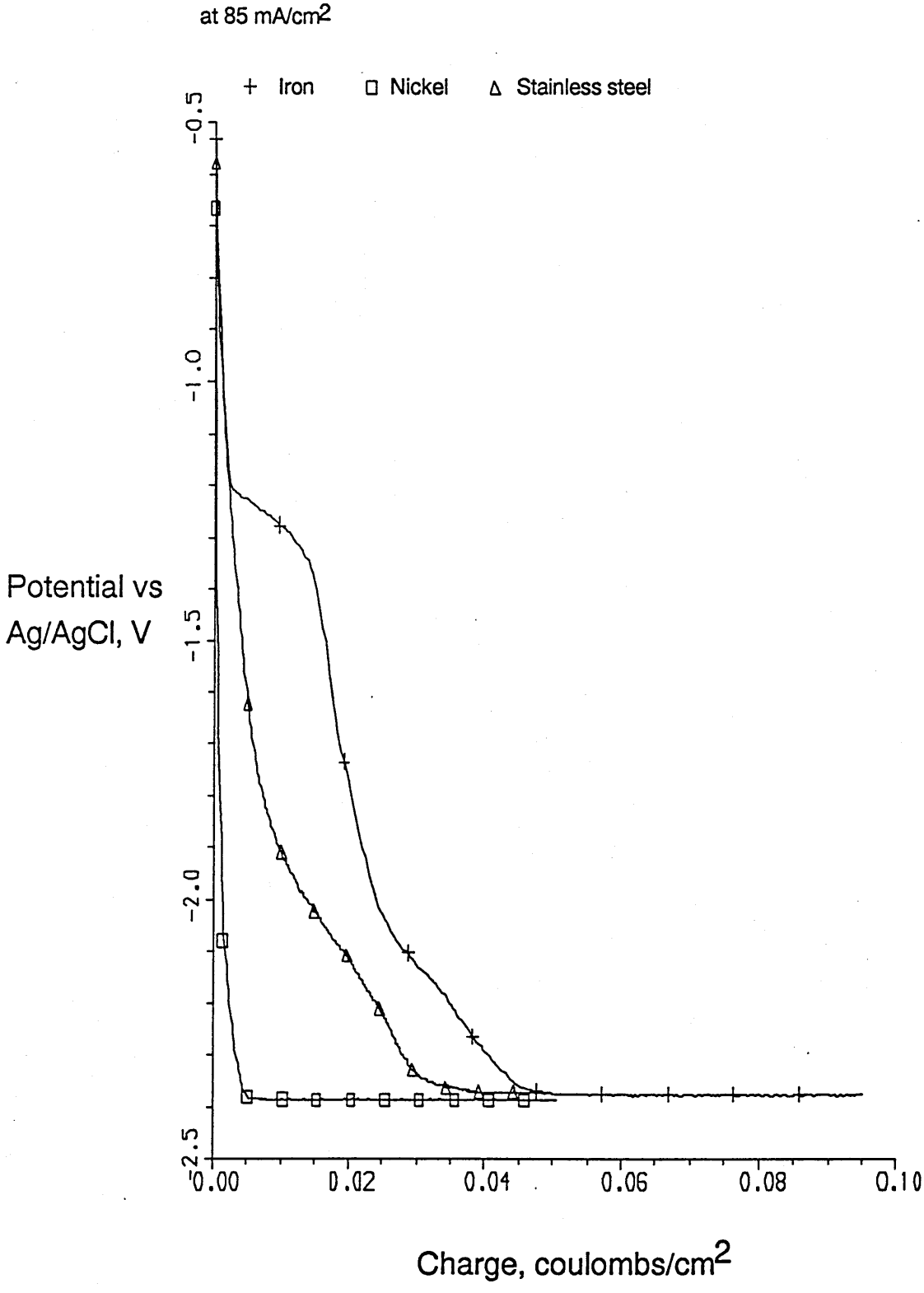

FIGURE 3.3
ORIGINAL AND DIFFERENTIATED DATA (as for iron in figure 3.2)

a) vs. charge

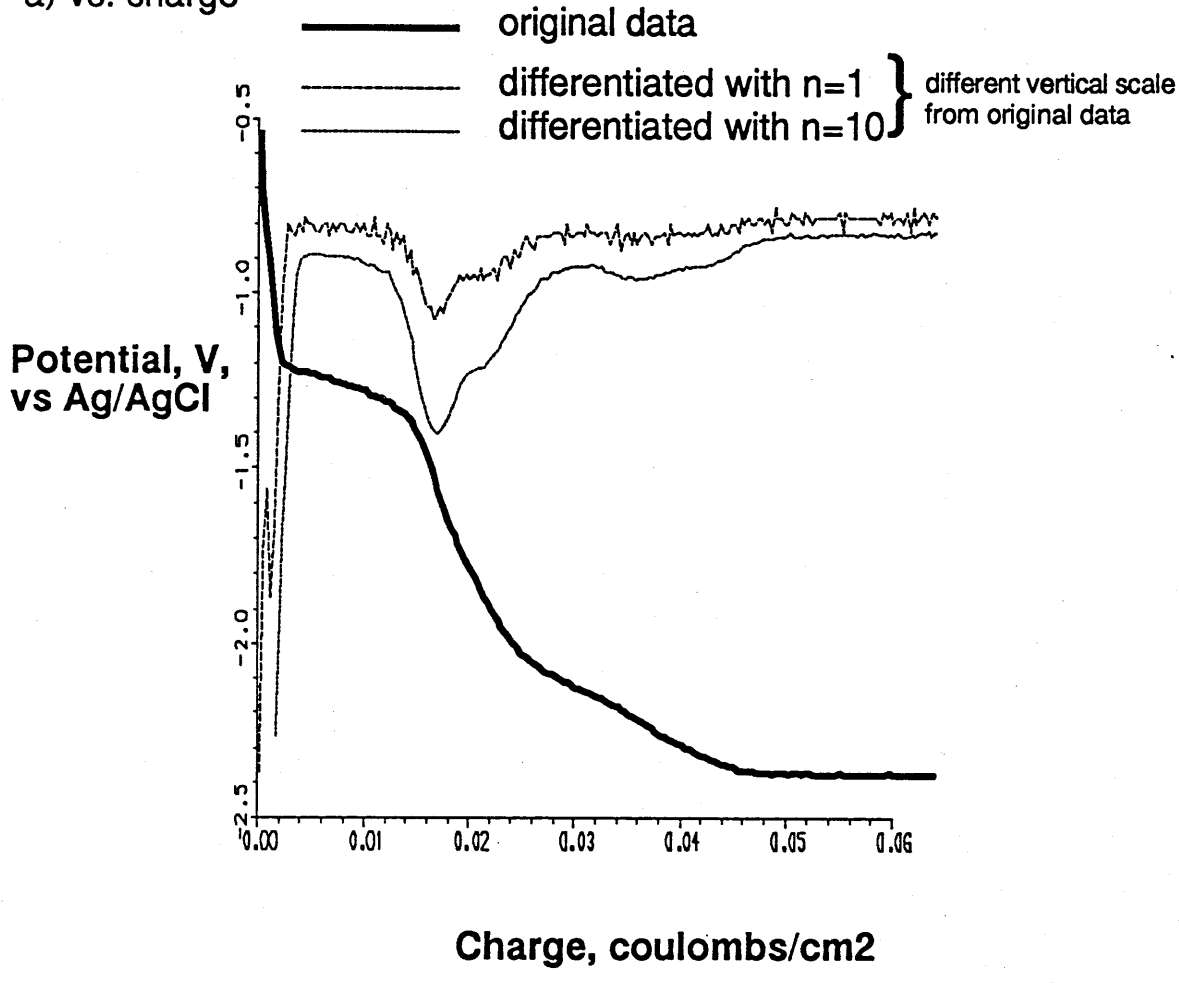

b) vs. potential

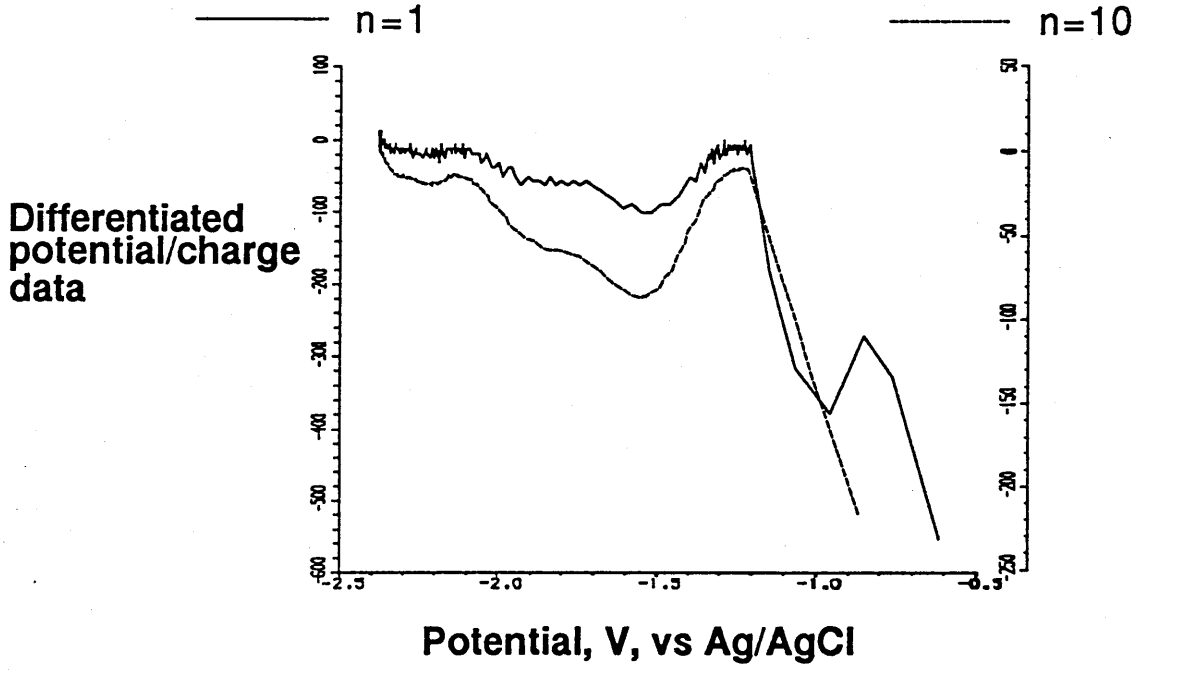

FIGURE 3.4

EFFECT OF CURRENT DENSITY ON IRON REDUCTION

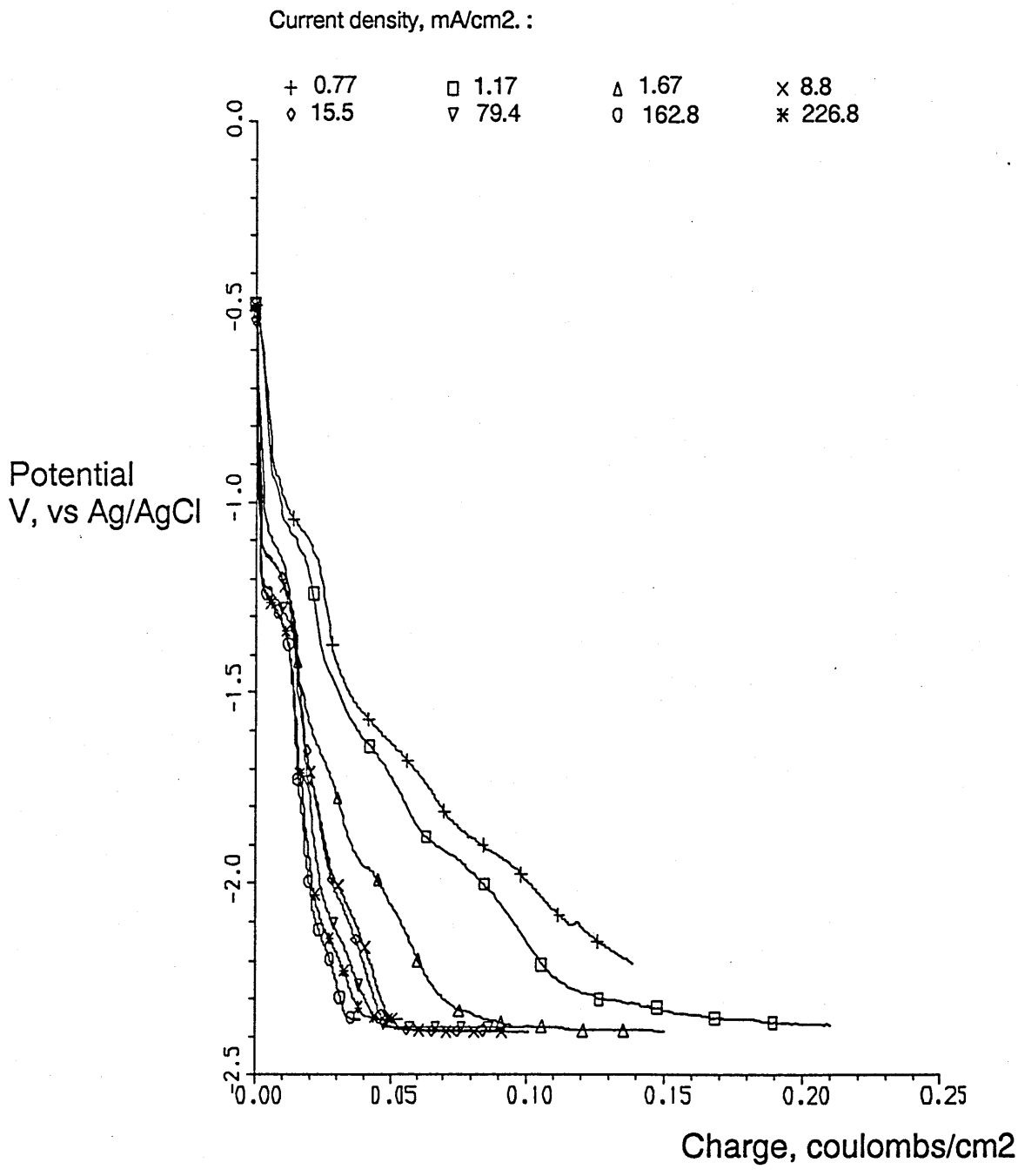

FIGURE 3.5

EFFECT OF CURRENT DENSITY ON REDUCTION OF STAINLESS STEEL (DE-GREASED ONLY)

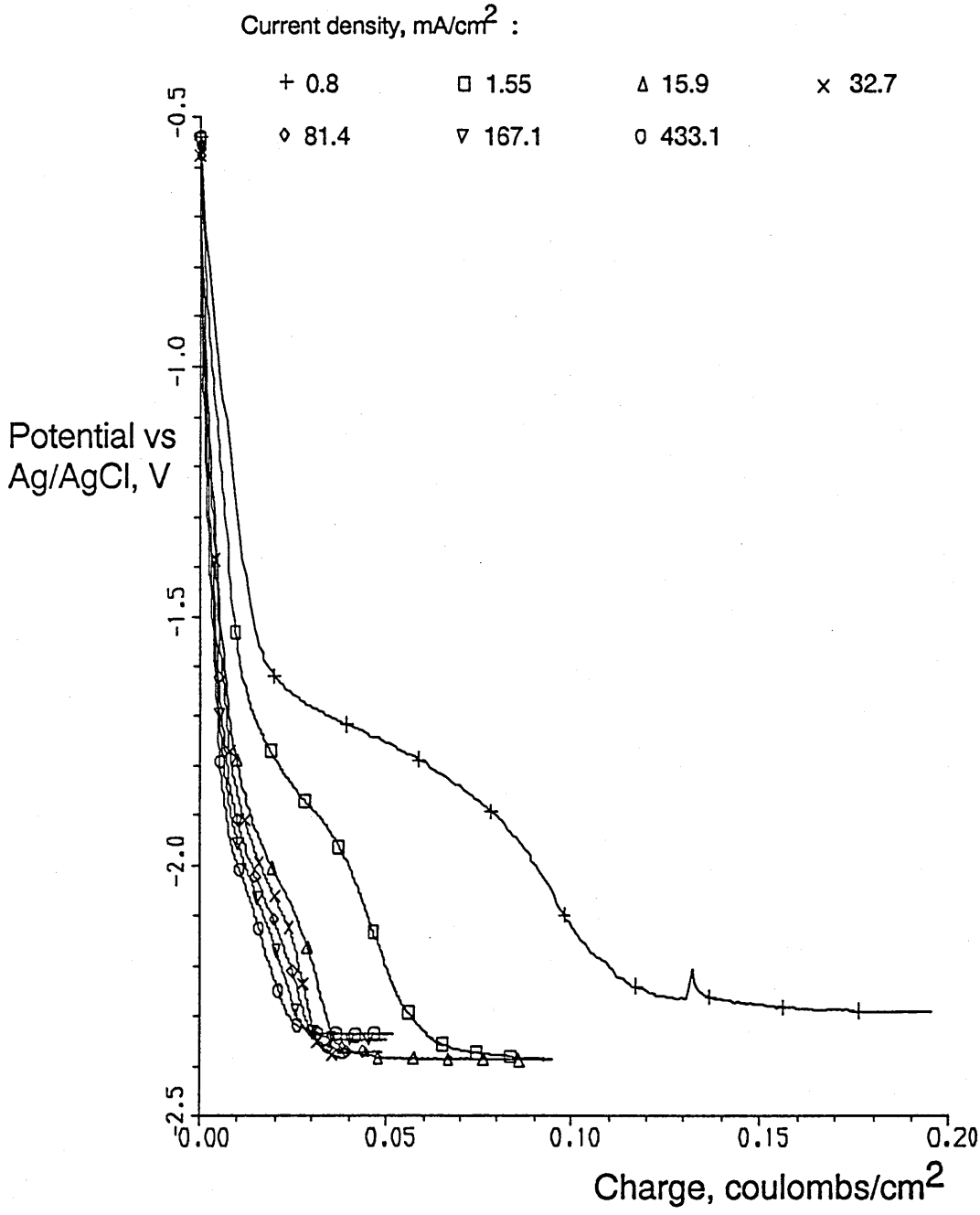

FIGURE 3.6

EFFECT OF CURRENT DENSITY ON REDUCTION OF STAINLESS STEEL (ANODICALLY ETCHED)

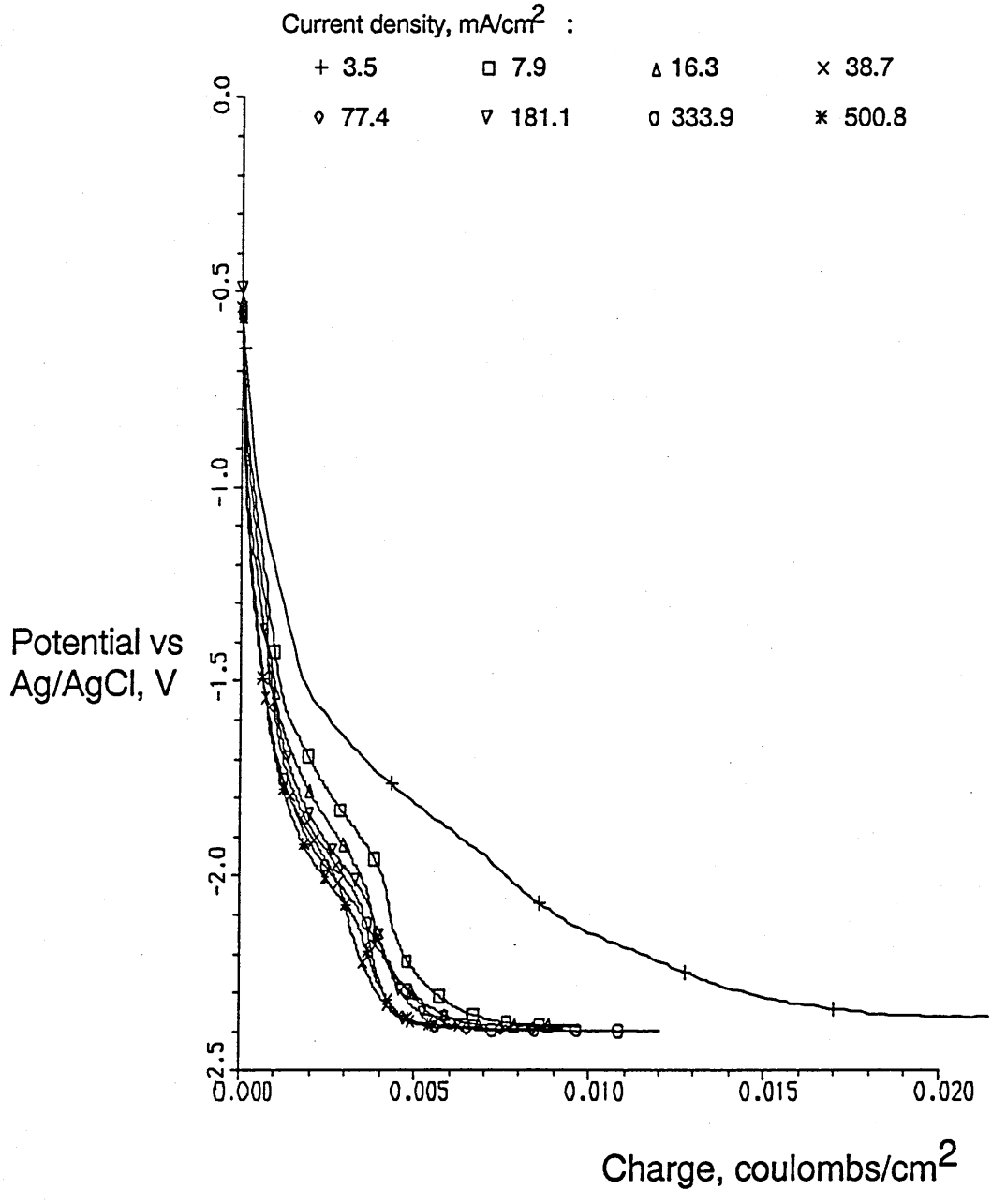

FIGURE 3.7

REPEATED REDUCTION OF STAINLESS STEEL

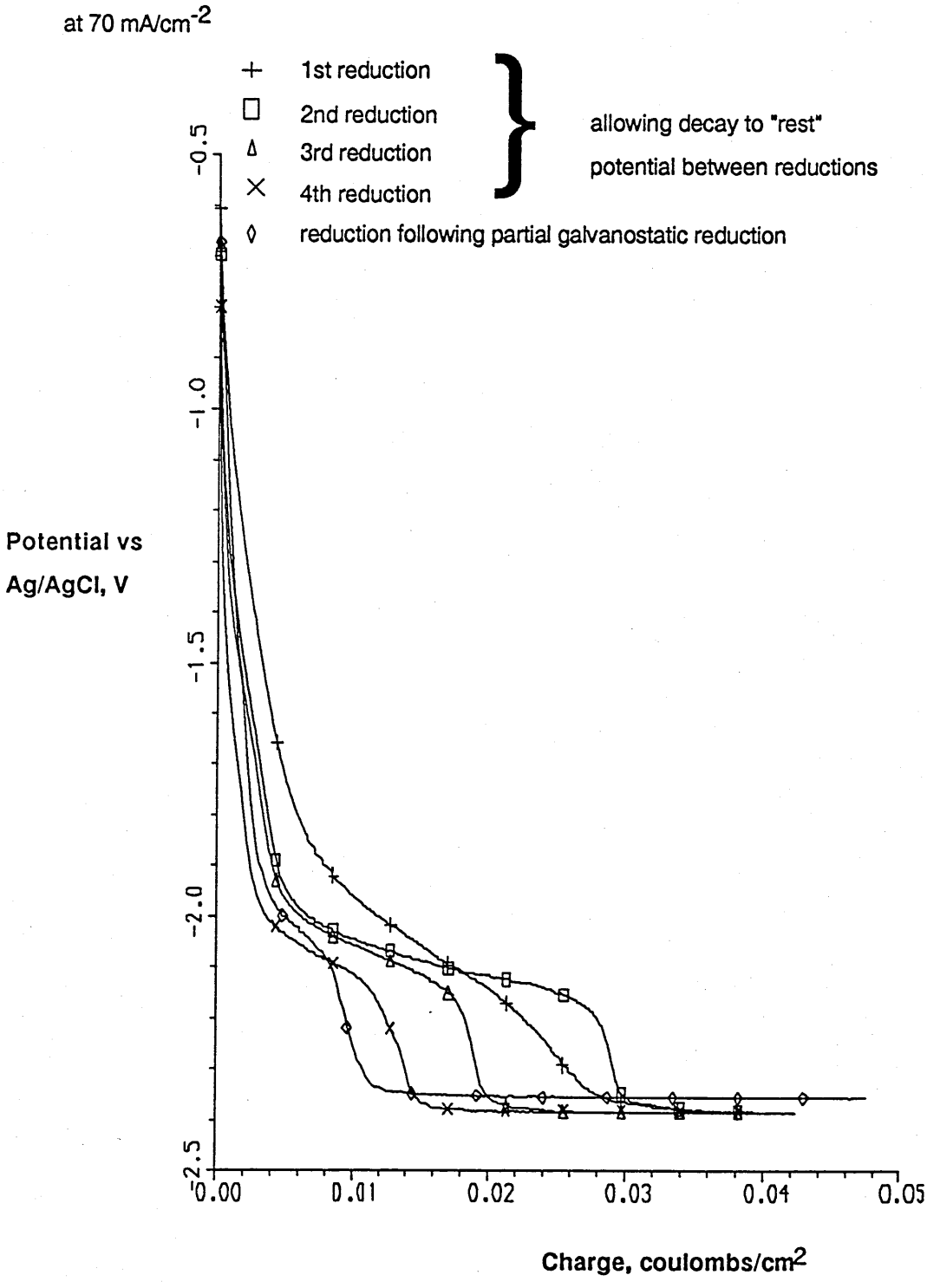

FIGURE 3.8

REPEATED REDUCTIONS OF IRON

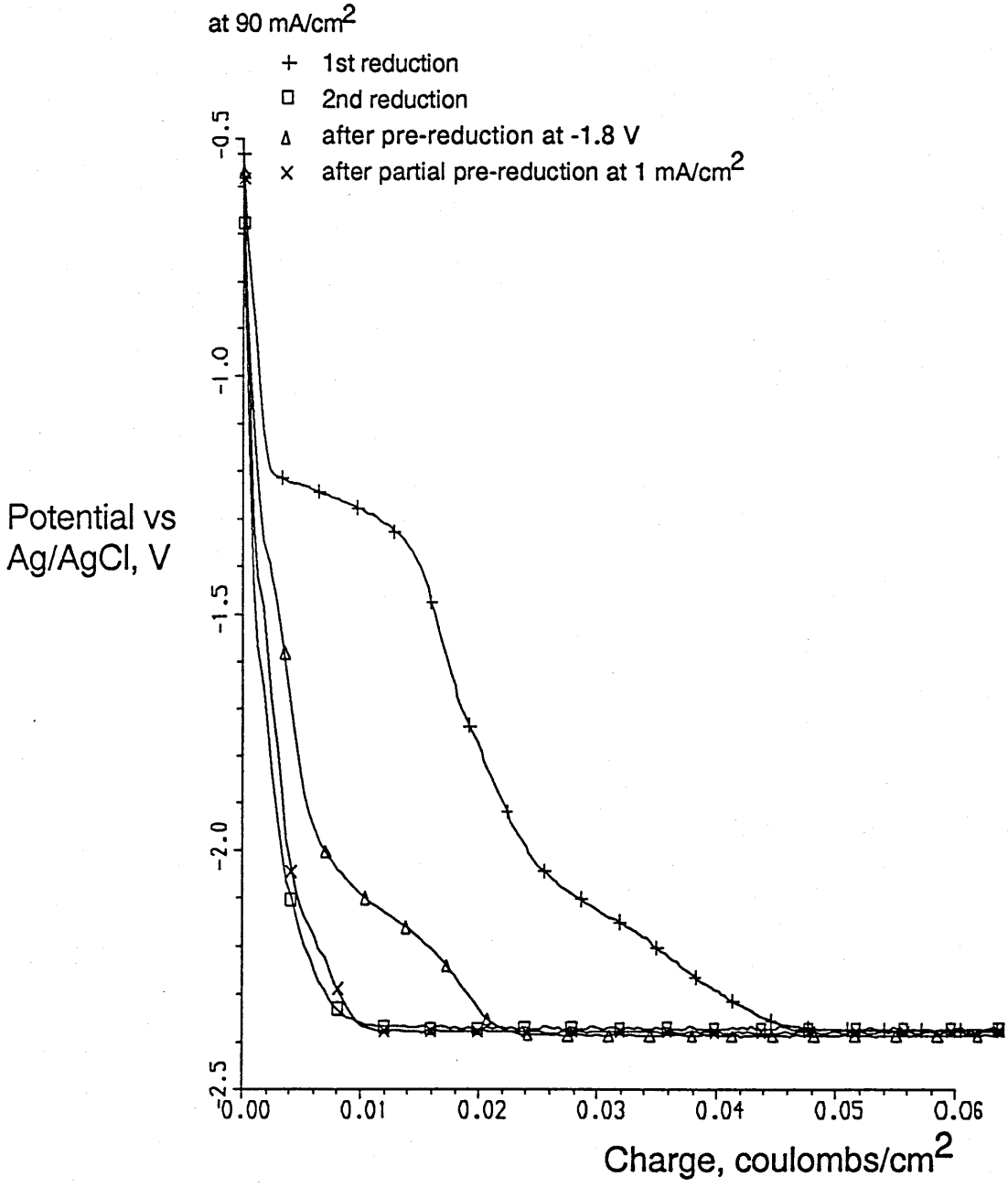

FIGURE 3.9

REDUCTION OF IRON AFTER HOLDING ABOVE MELT

at 80 mA/cm ^{2}

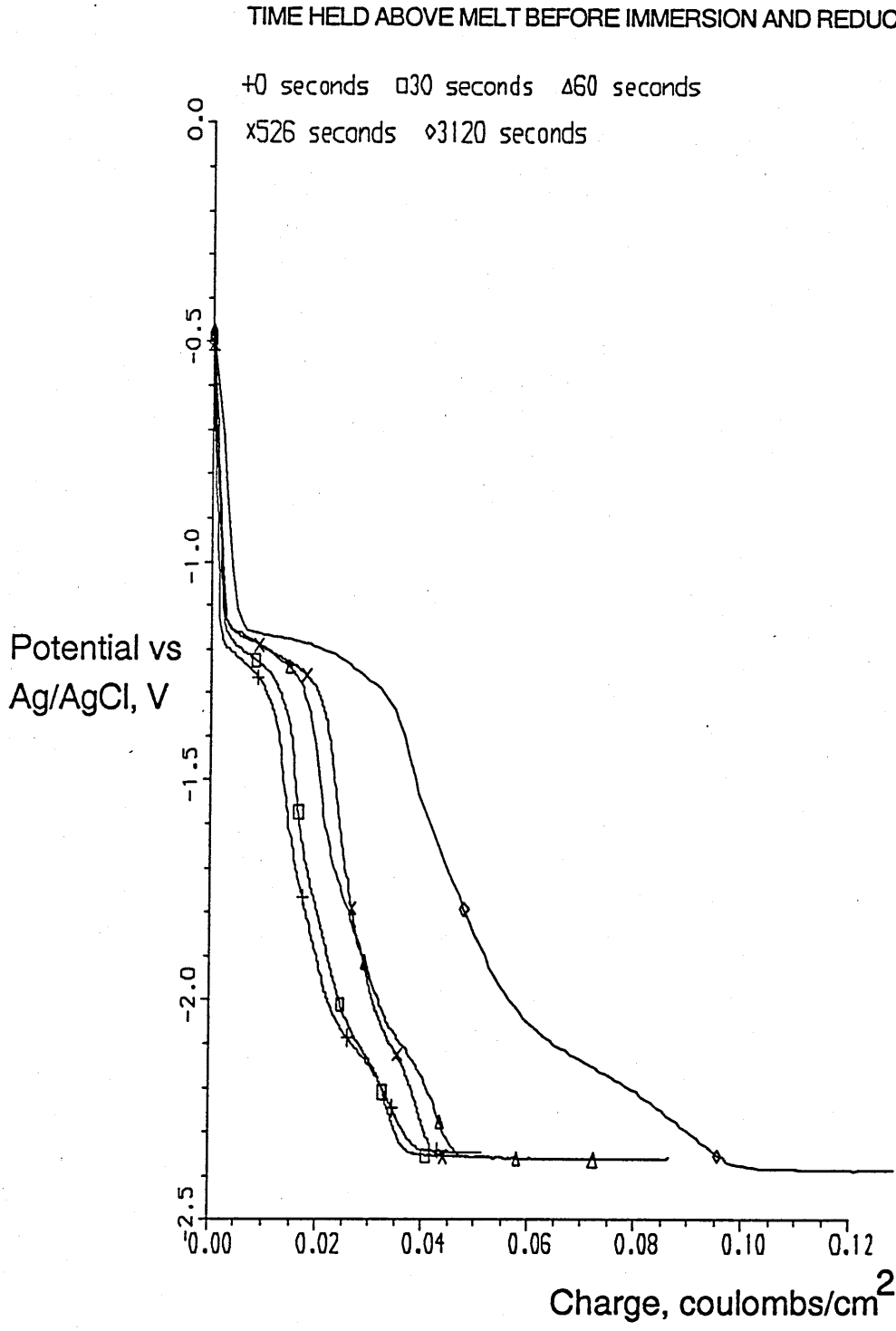

FIGURE 3.10

REDUCTION OF STAINLESS STEEL AFTER HOLDING ABOVE MELT SURFACE

at 75 mA/cm^2

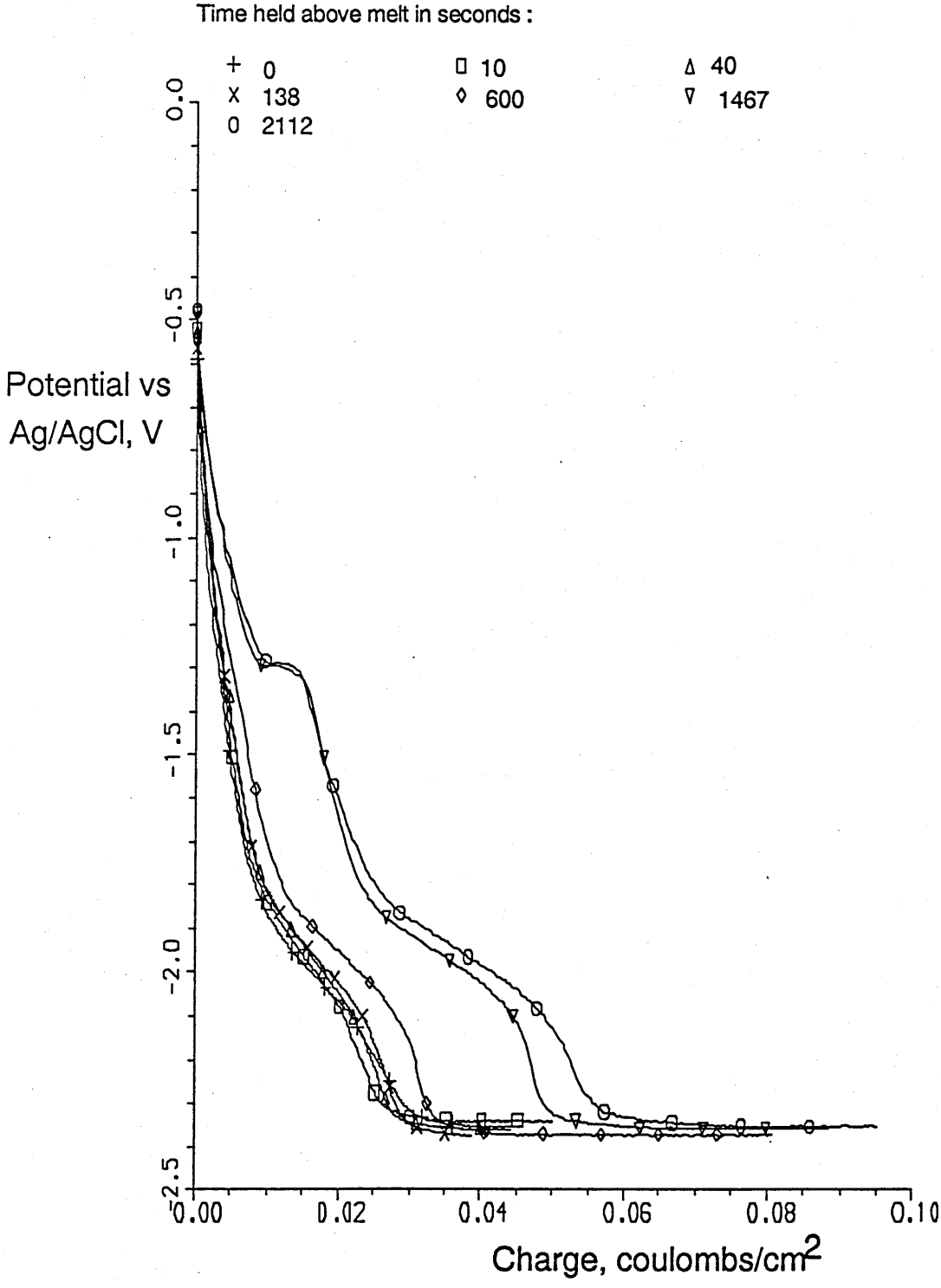

FIGURE 3.11

EFFECT OF TIME IRON IMMERSED BEFORE REDUCTION

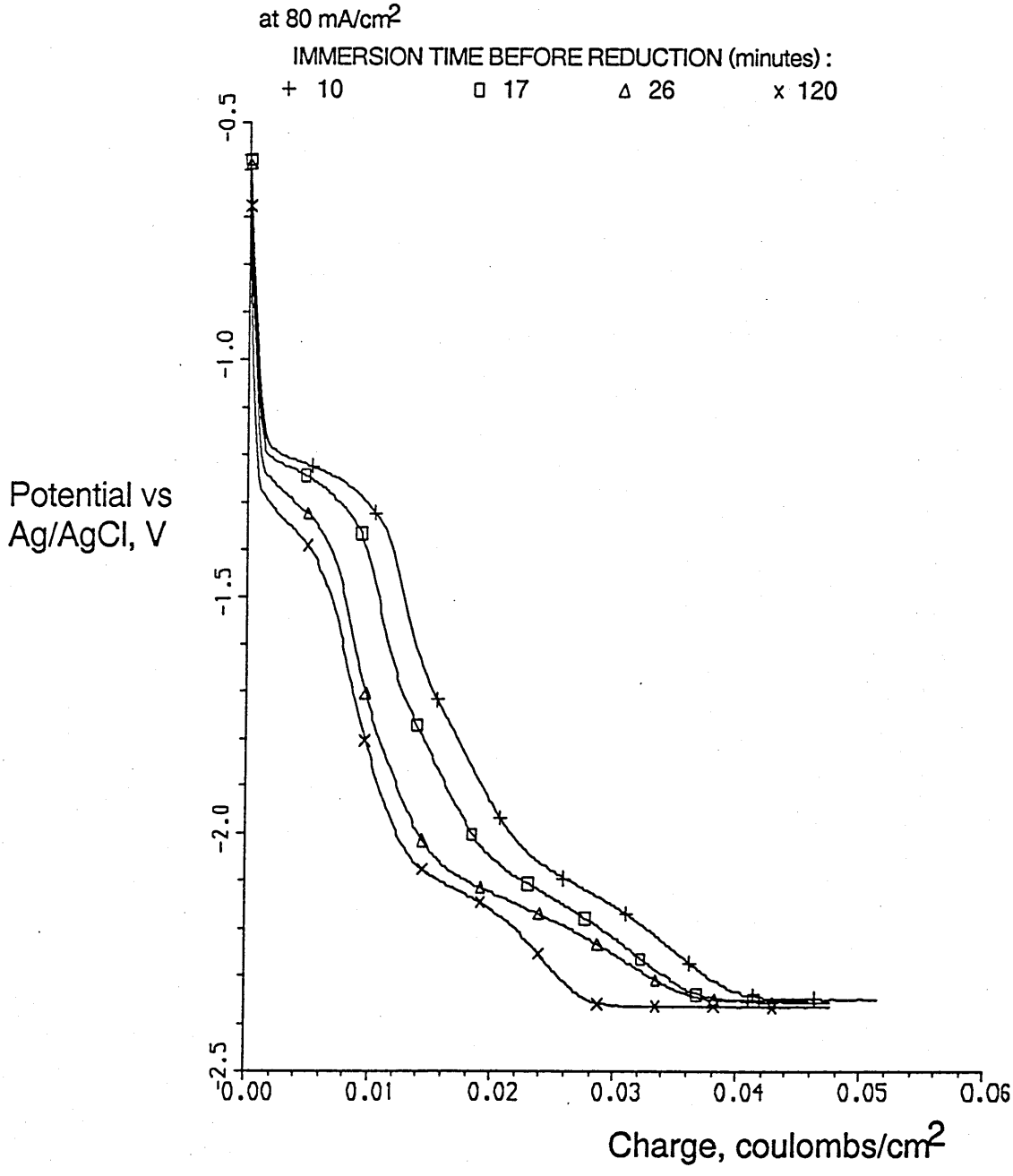

FIGURE 3.12

EFFECT OF TIME STAINLESS STEEL IMMERSED IN MELT BEFORE REDUCTION

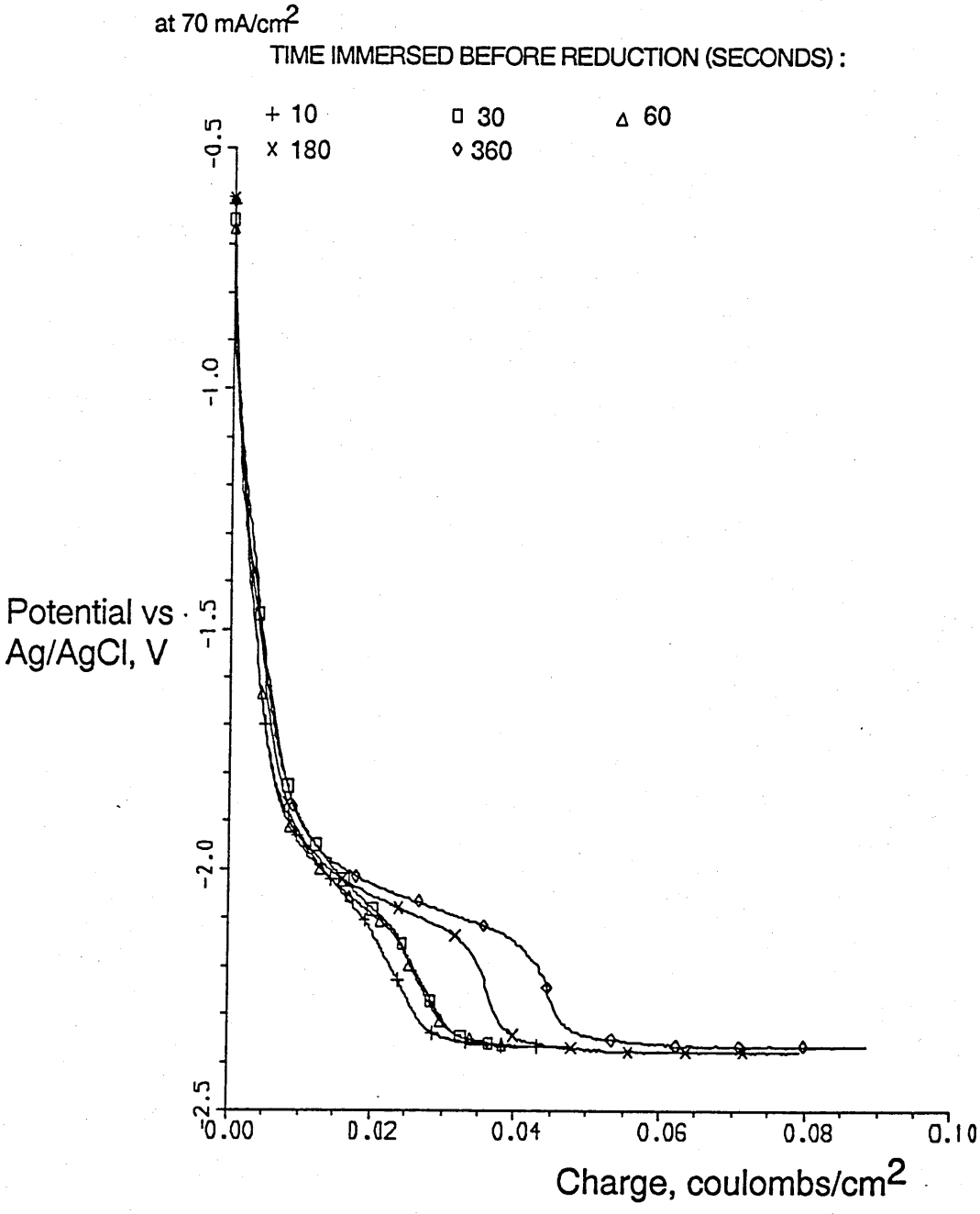

FIGURE 3.13

EFFECT OF PRE-TREATMENT (STAINLESS STEEL)

on reduction at 80 mA/cm^2

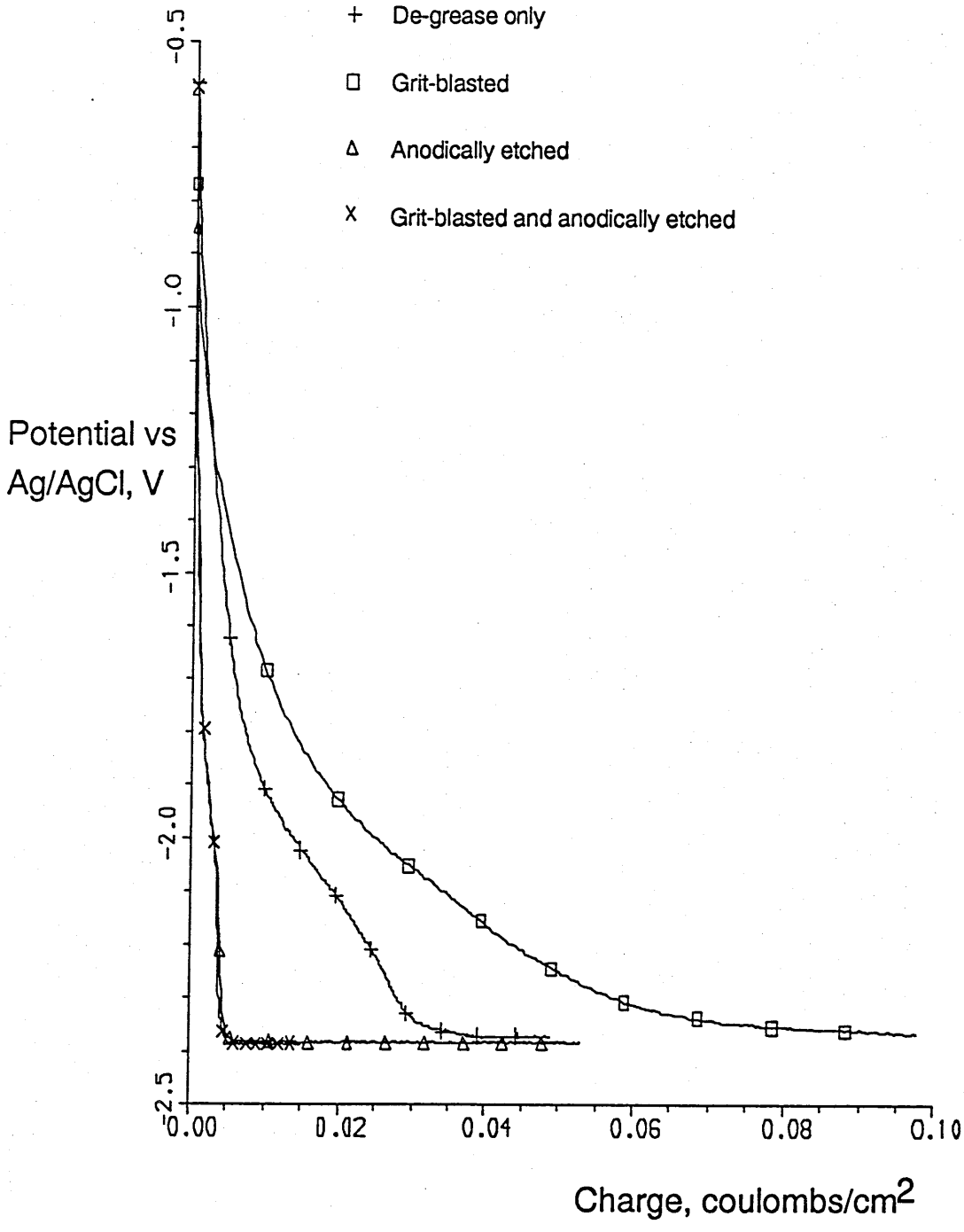

FIGURE 3.14
REDUCTION AND CURRENT REVERSAL

(a) stainless steel

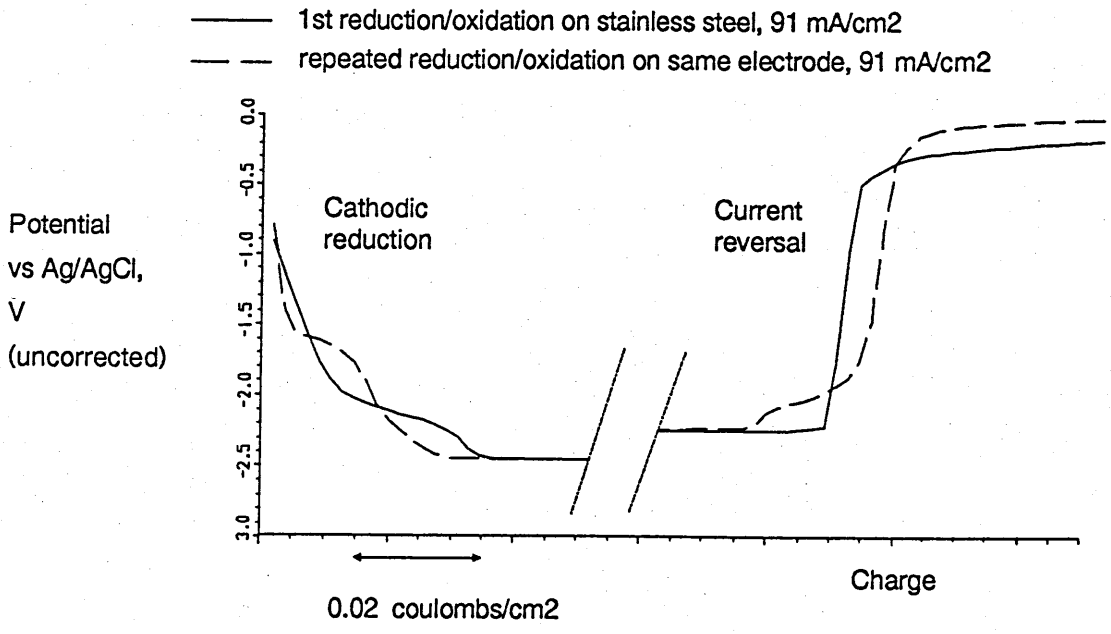

(b) iron

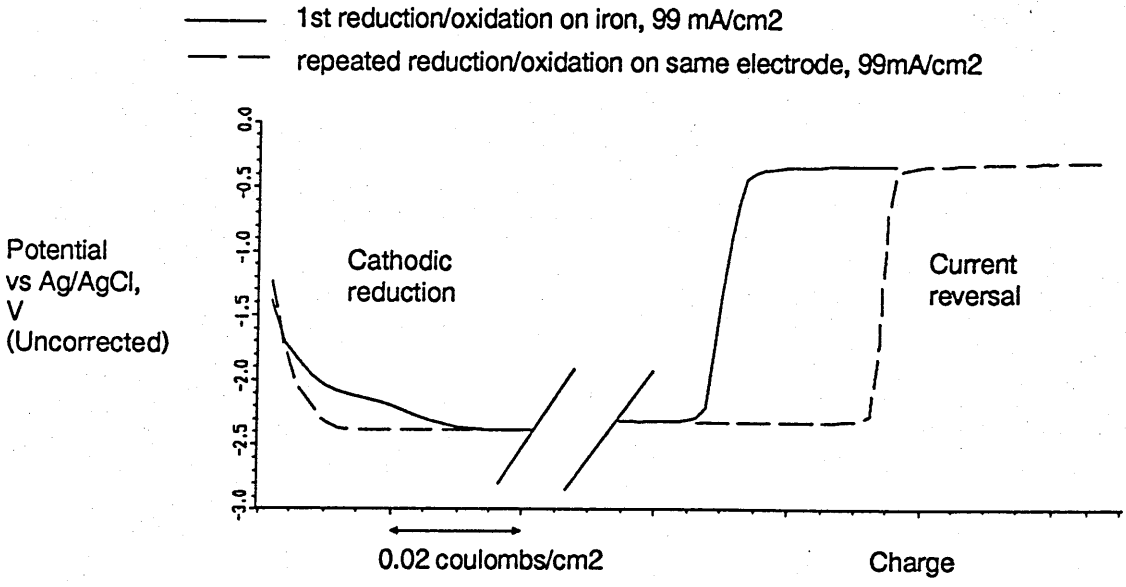

CHAPTER 4

THE ELECTROREDUCTION CHARACTERISTICS OF TITANIUM IN CHLORIDE MELTS

4.1. Electrocrystallisation

Such reactions as metal deposition in which a new solid phase is formed on the electrode are termed electrocrystallisation processes. Electrocrystallisation involves several steps, any one of which may dominate in the overall process kinetics[105]:

(1) diffusion of reactant ions from solution to the electrode surface;

(2) electron transfer;

(3) formation of ad-atoms on the surface by loss of solvation sheath;

(4) surface diffusion of ad-atoms;

(5) clustering of ad-atoms to form nuclei on a foreign substrate;

(6) incorporation of ad-atoms in lattice structure;

(7) continued deposit growth with characteristic morphology and crystal structure.

The sequence is shown schematically in figure 4.1. The most easily observable stage is of course the last one, in which the bulk deposit develops. However the initial stages of deposition including nucleation are likely to be of critical importance in determining the nature of the bulk deposit on a foreign substrate. The importance of surface preparation before electroplating[108] is one practical manifestation of this.

4.2. Experimental

Several techniques were used to investigate the reduction process. These are described below.

4.2.1. Cyclic voltammetry

This technique is frequently used for preliminary investigation of an electrochemical system[105]. The "electrochemical spectrum" is readily determined by imposing a potential ramp on the working electrode between two potential limits and measuring the current response. Results are plotted as current versus potential, and electrochemical activity shows up as a series of peaks at the characteristic potentials of the electrode reactions. These peaks arise as follows. As the potential changes the surface concentration of the reacting species falls. This sets up a concentration gradient across the diffusion layer next to the electrode surface which gives rise to a current. Under steady-state conditions this is limited when the surface concentration falls to zero. If the sweep rate is sufficiently high, however, the diffusion layer does not have time to relax, and larger concentration gradients than would be present under steady-state conditions are experienced, with correspondingly increased currents. Once the surface concentration of the reacting species reaches zero the concentration gradient diminishes as a result of diffusion effects, and current falls. By altering sweep limits and observing peak appearance or absence, and by comparing first with subsequent sweeps, significant mechanistic information concerning the electrochemical activity under investigation can be derived. Analysis of sweep rate dependence can give kinetic information.

However, cyclic voltammetry is not generally a good technique by which to study electrodeposition reactions, because of the continually changing electrode surface as deposition, and, on the oxidation cycle, dissolution take place. Sometimes, however, the technique can be useful diagnostically if voltammogram shapes characteristic of nucleation processes are determined[105]. On the forward (reduction) sweep a potential negative of the usual reversible electrode potential must be attained before nucleation on the foreign substrate takes place. When the sweep is reversed, the current crosses the forward trace, and the reverse peak is sharp and symmetrical, representing stripping of the deposit formed during the forward half of the cycle. The nucleation overpotential may be determined from the difference between the crossover point and the point at which deposition begins on the forward sweep. Figure 4.2 shows a schematic diagram of a cyclic voltammogram for a deposition process.

4.2.2. Chronoamperometry

4.2.2.1. Soluble reactants and products

Consider an electrode reaction in which O is reduced to R which can be described by the following equation where initially only O is present in solution:

$$O + ne^- \underset{k^O}{\overset{k^R}{=}} R \quad \text{.....(4.1)}$$

Where k^R and k^O are the rate constants for the electrochemical reduction and oxidation reactions respectively. If the potential of an electrode is stepped from a value where no electrode reaction takes place to a value at which species O is reduced, at a rate

governed by the rate of diffusion of species O from the bulk solution to the electrode surface, then the current, I, can be shown to vary as a function of time, t, according to the Cottrell equation[105]:

$$I = \frac{nFD^{1/2}c_o^b}{\pi^{1/2}t^{1/2}} \qquad \text{.....(4.2)}$$

where F is the Faraday constant, D is the diffusion coefficient, c_o^b is the concentration of O in the bulk of the solution. A plot of I against $t^{-1/2}$ would therefore be linear and pass through the origin. This is a useful diagnostic test for diffusion control, allowing the diffusion coefficient, D, to be determined. Timescales of between 1 ms (limited by the charging characteristics of the cell) and 10 s (limited by natural convection effects) are usually appropriate.

If the applied potential is smaller, then the change in the surface concentration of the reactant species may be small, and diffusion of species O may not be significant in determining the rate of the reaction. The current in such a case is given by[105]:

$$I = nFk^R c_o^b \qquad \text{.....(4.3)}$$

This is independent of time, current depending on the rate constant of the reaction, and therefore the reaction is described as kinetically controlled.

Between these two extremes, mixed kinetic and diffusion control is possible. This gives rise to a current-time relationship similar to the diffusion controlled case but with a less steep decline in current. Figure 4.3 shows typical responses for these 3 situations.

Under mixed control, it can be shown that the reaction is entirely

kinetically controlled at t=0. Therefore, in principle, rate constant information can be derived if the current at t=0 can be found. However the determination of $I_{t=0}$ is not straightforward because of the finite rise times of instrumentation and because of the double-layer charging current. When a potential step is imposed, a certain amount of charge is necessary to constitute the electrochemical double-layer capacitance. The current which flows as a result rapidly decays with time, and is typically negligible after a few hundred microseconds.

Under mixed control at short times a plot of I vs. $t^{1/2}$ should give a straight line of intercept $I_{t=0}$ where

$$I_{t=0} = -nFk^{R}c_{O}^{b} \quad \ldots\ldots\ldots\ldots\ldots\ldots\ldots\ldots\ldots\ldots(4.4)$$

from which k^R can be determined. This approximation is useful only where $I/I_{t=0} > 0.8$, i.e. close to the top of the current-time curve.

4.2.2.2. Phase formation

Where phase formation is involved in the reaction then very different I-t transients may be observed from those types depicted in figure 4.3. The precise relationship between current and time depends on the type of nucleation process which is occurring: whether it is two or three-dimensional, for example[106][107]. A rising portion of an I-t curve is usually taken as confirmation of a nucleation step. Some examples of typical nucleation behaviour as represented by current-time relationships are given in figure 4.4.

Adsorption can be thought of as a particular form of phase change, giving rise to characteristically-shaped I-t curves of the sort

shown in figure 4.4. This could describe a system in which the reaction product adsorbs on the electrode surface. It can be considered as the sum of a diffusion controlled falling transient and a nucleation controlled rising transient.

The precise nature of the time dependence of a rising current transient is a function of the type of nucleation process taking place. This is usually two or three dimensional, and either type of nucleation may be "instantaneous" or "progressive"[105][106][107]. These terms are defined below. Where the rate limiting step is incorporation of the ad-atom into the expanding growth centres, current is dependent on the total area of the growth surfaces of all the nuclei present. This in turn is obviously determined by the individual nucleus geometry.

Two-dimensional nucleation describes the formation of monolayers. The nucleus consists of a disc or cylinder one atom or molecule high. Growth takes place to expand and coalesce the discs, ultimately leading to formation of a complete layer. A new layer then forms on top of the first by nucleation of new growth centres. Typical I-t transient behaviour is shown in figure 4.4. Instantaneous nucleation refers to the situation when all the growth centres exist at the start of deposition. Current is then a linear function of t. Progressive nucleation is the case when the number of growth centres increases with time, and leads to a relationship of the form I proportional to t^2.

Where growth centres are three-dimensional, such as conical in shape, different relationships are derived: current is proportional to t^2 for instantaneous and t^3 for progressive nucleation. If the

rate limiting step in the growth of the nuclei is diffusion then the respective time-dependencies are $t^{1/2}$ for instantaneous and $t^{3/2}$ for progressive. Different geometries (such as hemispheres) give rise to different I-t transients.

It is apparent that simple examination of the time dependence of current in the rising portion of a transient cannot give an unambiguous diagnosis of nucleation mechanism. For example, both progressive two-dimensional and instantaneous three-dimensional nucleation can produce a similar t^2 dependence. Moreover this description ignores complications such as overlap of growth centres. Consequently it is usually unwise to draw conclusions from transient data alone. Microscopic examination (by scanning electron microscope) of nucleated surfaces is often helpful in providing additional evidence for a particular mechanism. Indeed, it may be essential, if double-layer charging or other effects obscure nucleation behaviour at short times in current-time transients.

4.2.3. Chronocoulometry

There are advantages in using charge-time information instead of current-time to determine kinetic information. Double-layer charging effects are minimised, and data over a longer time period can be used. For mixed control if charge, Q, is plotted versus $t^{1/2}$ then the data at long times approaches a straight line given by[105]:

$$Q = \frac{4nFk^R c_o^b (t_L^{1/2} t^{1/2} - t_L)}{\pi} \qquad \ldots\ldots\ldots (4.5)$$

where $t_L^{1/2}$ is the intercept on the x (time) axis. A value for k^R can be derived from the slope of the plot. Under diffusion control, no intercept is observed, and integration of the Cottrell equation

(equation(4.2)) gives:

$$Q = \frac{2nFD^{1/2}c_o^{*}t^{1/2}}{\pi^{1/2}} \qquad \ldots\ldots\ldots\ldots(4.6)$$

to describe the $Q\text{-}t^{1/2}$ relationship from which D may be determined from the slope of the plot.

The adsorption of electroactive species prior to electrochemical reaction can also be detected using chronocoulometry. Plots of Q against $t^{1/2}$ have an intercept on the charge axis as a result of the instantaneous reduction of adsorbed species.

4.2.4. The potential dependence of rate constants

If rate constants are determined (such as from evaluation of equation 4.4 or 4.5) at several different potentials, E, then it is useful to check that a linear relationship exists between log k and E as predicted by the following expression[105]:

$$k^R = k^{\ominus}\exp\frac{-\alpha_c nF(E-E_e^{\ominus})}{RT} \qquad \ldots\ldots\ldots\ldots(4.7)$$

$$\text{Therefore, } \log k^R = \log k^0 - \frac{\alpha_c nF\,(E-E_e^{\ominus})}{2.3RT} \qquad \ldots\ldots\ldots(4.8)$$

where α_c is the cathodic transfer coefficient, $k^{\ominus}$ is the standard rate constant, $E_o^{\ominus}$ is the standard electrode potential, R is the gas constant and T is the temperature (K). If a non-linear plot is obtained, then it is good evidence that the reaction mechanism is more complex than has been assumed in evaluation of the rate constant.

4.2.5. Deposit microstructure

Ambiguities in interpretation of other experimental data, for example the time dependence of current during phase formation in chronoamperometric experiments, may often be resolved by examination of the nature of the electrodeposit produced. Scanning electron microscopy is particularly convenient when used in conjunction with elemental analysis using EDAX. Under most circumstances, particles of about 0.1 - 1.0 microns in diameter or larger are distinguishable from a foreign substrate.

4.3. Preliminary examination of electrochemical characteristics

Figure 4.5 shows a comparison of cyclic voltammograms determined for three different electrode materials in purified lithium chloride - potassium chloride at 400^{0}C using a 100 mv.sec^{-1} sweep rate. Tungsten displays the least electrochemical activity, the only feature of its behaviour being the solvent breakdown at the lithium discharge potential at about -2.41 V vs Ag/AgCl(1%). This is close to the theoretical value[50]. Platinum, on the other hand, exhibits much more activity, and in particular a depolarisation of the lithium discharge potential by about 200 mV compared with tungsten, with an additional peak immediately before this. This suggests that there is some specific interaction, such as lithium-platinum alloy formation, between the two metals. The other activity of platinum is attributable to the Pt^{2+}/Pt^{0} couple which has a standard reduction potential of +0.727V vs Ag/AgCl(1m)[50]. Titanium has a pronounced region of reduction activity between -0.5 and -1.5 V vs Ag/AgCl(1%). Lithium discharge takes place at a potential very close to that on tungsten. However, there does appear to be a region of electroactivity immediately prior to this although this is not well-

defined. It may suggest that some specific interaction of lithium and titanium metals is significant. It is clear that lithium discharge takes place at potentials well-negative of the main region of titanium's electro-reduction activity.

Another cyclic voltammogram of titanium in pure LiCl-KCl is shown in figure 4.6. This extends the anodic portion to more positive potentials and shows an anodic limit at +0.4 V vs Ag/AgCl(1%). This is much less positive than the chlorine evolution reaction (standard reduction potential + 1.35 V vs Ag/AgCl(1m)). It is consistent with the oxidation of TiIII to TiIV as volatile $TiCl_4$. To examine the reduction stages further, a series of potential sweeps was carried out using a titanium wire electrode, beginning at -1.8 V vs Ag/AgCl(1%) where there was essentially no current flowing. The potential was swept in a positive direction up to an anodic limit and then reversed back to -1.8 V. Figures 4.7, 4.8 and 4.9 show the results of such sweeps. The first sweep always exhibits much lower oxidation currents than the second and subsequent sweeps: an example of this behaviour is shown in figure 4.7. This phenomenon is thought to be a result of oxide layers on the electrode being broken down initially to produce a clean titanium surface for subsequent sweeps. It is also noteworthy that the first oxidation peak has a very sharp termination, characteristic of limitation by passivation of the electrode. This could be the case if $TiCl_2$ precipitates as a result of build up of Ti^{2+} ions via the Ti --> Ti^{2+} oxidation. The Ti^{2+}-->Ti^0 reduction peak in the reverse half at about -1.1 to -1.2 V is clear. This sometimes appears as a double peak (see figure 4.5 for example). At slightly less cathodic potentials where a plateau is visible in figure 4.1 TiIII-->TiII reduction takes place.

Cyclic voltammetry using an inert (tungsten) electrode in a solution of titanium ions in the lithium chloride - potassium chloride melt was also carried out. This displays the characteristic shape of a nucleation process (see figure 4.10) in the first sweep. A nucleation overpotential of about 100 mV is indicated.

4.4. Electro-reduction of titanium ions

In order to examine the reduction characteristics more closely, potential steps were applied to wire electrodes immersed in LiCl-KCl-$TiCl_3$-$TiCl_2$ melts and the current-time (chronoamperometric) responses recorded and analysed.

4.4.1. Experimental

The melts were prepared as described in section 2. Different concentrations of titanium in solution in the melt were used. The melts were reduced as described in section 2 to maximise the concentration of TiII, but analysis revealed that there was always a small proportion of TiIII present. This is because of the equilibria set up in the melts between the various oxidation states as discussed in section 1. Stainless steel wires were pre-treated as described in section 3 using grit-blasting, anodic etching and degreasing. Following immersion in the melt, in-situ conditioning (see below) was carried out prior to application of a potential step using the Wenking potentiostat and Hitek waveform generator. The current-time response was recorded using the Nicolet oscilloscope and stored on floppy disk. If required the current-time data was integrated to give charge-time data using a Fortran program running on the Prime computer. Before application of the next potential

step, the electrode was made anodic at +0.6 V vs Ti for 1 minute (to anodically dissolve any titanium metal electrodeposited during the cathodic transient), then held at open circuit for at least 1 minute before imposition of the conditioning cycle prior to the next pulse. Potential was measured against either the Ag/AgCl(1%) reference electrode or against a titanium rod held in the melt.

4.4.2. Effect of in-situ conditioning

Great pains were taken to pre-treat the electrodes in a reproducible manner before immersion in the melt. The work carried out to this end is described in chapter 3. However there were still problems of irreproducibility when determining current-time responses to potential steps imposed on the electrodes in the melt. It became clear that this was due to electrode history immediately prior to imposition of the pulse. In particular it was found necessary to impose an anodic potential before imposing the cathodic potential step for which the current-time transient was required, even for fresh electrodes which had not received any previous cathodic polarisation. Various anodic potentials were investigated (typical results are shown in figure 4.11). An anodic potential of greater than +0.1V vs Ti was required. Without this step, transients were always falling currents, whereas with the anodic conditioning, rising transients were observed at certain potentials. Usually a 1 minute period at +0.6 V was used for in situ conditioning.

Examination of the current-time response to the anodic potential showed behaviour similar to stripping of deposit after cathodic deposition, even when no cathodic potential had been imposed, as with a fresh electrode left at open circuit immersed in a titanium-

containing melt (see figure 4.12). Scanning electron microscope examinations were made of electrodes to attempt to characterise the effect more precisely. Figure 4.13 shows the relatively "dirty" surface resulting after a stainless steel electrode was left immersed in a melt at open circuit for 5 minutes, following washing in dilute hydrochloric acid in an ultrasonic bath, rinsing and drying. The particulate material apparent on the surface was analysed by SEM/EDAX and found to be titanium-rich. The second micrograph shows an electrode prepared and treated in a similar manner, except that it was held at +0.6V vs Ti during the immersion in the melt. The surface is much cleaner, completely devoid of the titanium-rich particles. It can be concluded, therefore, that the anodic potential treatment serves to strip titanium (probably present as metal) from the steel surface.

Further, it was found necessary to condition a fresh electrode with a period of cathodic polarisation (typically -0.4 V vs Ti for 4 seconds) as well as the anodic conditioning of +0.3 V for 1 minute. The need for cathodic conditioning was attributed to the reduction of oxide on the electrode surface as discussed in chapter 3.

The potential (values given are overpotentials) step sequence used to determine the transients was therefore:

-0.4V (fresh electrode only);

+0.6V for 1 minute;

0V for 1 minute;

cathodic potential for transient determination;

+0.6V for 1 minute (or less depending on length of cathodic transient applied) to strip the deposit made during the cathodic period;

open circuit for 3 minutes.

4.4.3. Potentiostatic transient results

4.4.3.1. Low titanium concentrations

At the lowest titanium concentrations investigated, 0.13% by weight (4.47×10^{-5} mol.cm^{-3}), falling i-t transients were determined for the full potential range (to overpotentials of about 600 mV). A series of transients determined at 400°C are given in figure 4.14. If this data is plotted as charge versus $t^{1/2}$ (figure 4.15) then a linear dependence of charge on $t^{1/2}$ is observed at all but short times. The value of the intercept on the x-axis was determined for each curve and the values substituted into equation 4.5. Values for the reduction rate constant of between 0.005 and 0.2 cm.s^{-1} were obtained. Data determined at 450°C was of similar general appearance. Figure 4.16 shows values of log k_R plotted as a function of overpotential. An approximately linear relationship is observed as predicted from equation 4.7.

4.4.3.2. Intermediate titanium concentrations

A typical series of current-time transients for a higher titanium concentration is given in figure 4.17 for 0.65 wt.% titanium (2.24×10^{-4} mol.cm^{-3}) at 450°C. Their appearance is quite different from the results at low concentrations. Particularly at the higher overpotentials, a shoulder on the falling transient is observed, similar to the behaviour expected in adsorption (see figure 4.4). It is not therefore possible to treat the data in the same way as described above. The Q-$t^{1/2}$ relationships plotted in figure 4.18

show no linear region, but as there is no intercept on the charge axis, reaction of an adsorbed species can be ruled out. The shape of the transients can be explained by considering that there is mixed nucleation and diffusion control of the reduction reaction. As there is no distinguishable rising portion of the transients, analysis to determine the nature of the nucleation process cannot be carried out.

Behaviour at a slightly higher concentration (3.68×10^{-4} $mol.cm^{-3}$) but at $400^{o}C$ was similar (see figure 4.19). The current-time response to reversal of potential to +0.6V at the end of each cathodic pulse was also recorded. Figure 4.20 shows examples of these responses. It is noteworthy that only after cathodic polarisation at overpotentials of more than 200 mV was the characteristically-shaped anodic stripping response obtained. This in turn suggests that only at those overpotentials was a titanium deposit laid down on the electrode surface available for stripping during the anodic polarisation period. This may be because the deposit was not in compact, adherent form, but powdery and loose, and therefore not retained on the electrode surface ready for anodic stripping. Alternatively, it might be argued that the electrode reaction represented by the cathodic transients at low overpotentials was not titanium electrodeposition at all. Titanium III reduction to titanium II is a possible alternative, although the potential values used and the relative proportions determined by analysis of the melts makes this unlikely.

4.4.3.3. High titanium concentrations

At titanium concentrations of about 3 wt.% (1.03×10^{-3} $mol.cm^{-3}$)

and above, the rising i-t response characteristic of a nucleation process is observed at overpotentials of about 150-200 mV and above. This is shown in the transient series determined at 450^{o}C illustrated in figure 4.21. At higher overpotentials a double peak is observable. It is significant that the current does not fall to zero before the rising portion of the transient begins. This suggests that there is a simultaneous diffusion controlled process occurring. This could be the diffusion of ad-atoms on the electrode surface, for example. This makes it difficult to analyse the rising portion of the curve in order to characterise the nucleation process. The current-time response is unlikely at any point along its length to approximate to that of a nucleation-controlled reaction alone. However, attempts were made to draw some conclusions, albeit tentative. Figure 4.22 shows the rising portions of the current-time curves for overpotentials in the range 200-400 mV. Plots of log i vs log t were made for this data in order to investigate the nature of the time dependence. Slopes determined were approximately 0.1.

4.4.4. Potential transients and deposit analyses

In order to clarify the conclusions to be drawn from analysis of the potential transients described above, experiments were carried out on stainless steel flag electrodes pre-treated in the same way as the wires. Deposition times of 12, 60 and 180 seconds were used for each of 6 overpotentials ranging from 100 to 1000mV. The current-time responses were recorded in the usual way, and the deposits produced were examined under the Scanning Electron Microscope (SEM).

The current-time transients obtained were generally similar to those

determined using wire electrodes (see figures 4.23, 4.24 and 4.25). Moreover, the results for different deposition times illustrated in figures 4.23-4.25 were self-consistent, demonstrating good reproducibility. At the lowest overpotentials, falling transients were obtained. At slightly higher overpotentials current became almost constant, rising almost imperceptibly at the longest times. At 200-300 mV a distinct shoulder on the falling transient appears at short times. At 600 and 1000 mV a rising portion of the transient is obvious immediately after the shoulder. The SEM examinations revealed only sparse coverage of the electrode surface at the lowest overpotential, 100 mV, even after 180 seconds (2.0 coulombs.cm^{-2}) deposition (figure 4.26). After 12 seconds small (0.1 micron) titanium particles are detectable sparsely distributed over an "orange-peel"-like indistinct surface structure. After 60 seconds the appearance of the particles was similar but the "orange-peel" look of the surface has disappeared. After 180 seconds the titanium was mostly concentrated in a very sparse distribution of large particles of about 5-7 microns in size, overlying a "clean" substrate. Some small 0.1-0.2 micron particles were also present.

At 150 mV the transition with time from an indistinct surface with small emerging particles of 0.1-0.2 microns in size (figure 4.27a), to a clean surface scattered with flattened layered particles 3 microns across (figure 4.27b) to almost complete coverage of the electrode surface (figure 4.27c) with titanium deposit is apparent. The broadly 2-dimensional nature of the growth is perceptible. As the titanium spreads across the substrate the contours of the substrate (imposed by its pre-treatment grit-blast and etch procedures) are obscured. It is also noteworthy that when larger

nuclei have formed, such as in figure 4.27b, there are also much smaller titanium particles present. This suggests progressive rather than instantaneous nucleation kinetics. Behaviour at 200 mV is similar to that at 150 mV.

At 300 mV a slight change in the nature of the growth is apparent. After 12 seconds some of the usual small 0.1-0.2 micron particles are visible, but there are also "trails" of very fine particles (figure 4.28a). Figure 4.28b shows subsequent growth is less distinct than previously, having a generally "smeared" appearance, although constituting more complete coverage of the substrate. After 180 seconds (figure 4.28c) growth appears much more nodular than that at lower overpotentials.

At 600 mV the features first apparent at 300 mV are more pronounced. Fine particulate growth follows the substrate surface contours and large areas have the appearance of discrete sub-micron sized particles rather than a continuous deposit (although no substrate "shows through") after 60 or 180 seconds (figure 4.29). At 1000mV these features are even more marked.

If the rising portion of the current-time curve for the 600 mV/180 second run is examined by plotting data between 20 and 100 seconds as log current vs log time then a slope of 0.43 is obtained (figure 4.30). This indicates that $I \propto t^{0.43}$, approximating to $I \propto t^{0.5}$. This might suggest that nucleation of the 3-dimensional, instantaneous, diffusion-controlled type is taking place. However, on examination of the corresponding deposits, it is readily recognised that during this time period, very substantial deposit growth has already occurred. This rising I-t curve is likely,

therefore, to represent not nucleation on a foreign substrate, but rather continued growth of a roughening surface.

4.5. Discussion

4.5.1. The importance of substrate preparation

It soon became apparent in preliminary electrodeposition experiments that pre-treatment of the electrode surface before immersion in the melt was a significant factor. This is discussed in both chapters 3 and 5. Even with consistent and rigorous pre-treatment, however, the determination of reproducible cathodic reduction data required careful control of electrode "conditioning" in situ in the melt. There are two components of the necessary in situ conditioning:

(1) Anodic polarisation

This appears to be required because of the "open-circuit deposition" phenomenon, whereby particles of titanium become attached to the surface during the electrode's immersion in the melt with no applied current or potential. These particles then act as nuclei for titanium deposit growth during subsequent cathodic polarisation. Under these conditions, no electrochemical nucleation characteristics are apparent in current-time transients. When anodic potentials are applied immediately before the cathodic step, however, these titanium particles are removed from the electrode. A clean surface is therefore presented at the moment the cathodic potential is applied and the appropriate current-time characteristics are recorded. The cause of the original deposition of the titanium particles is not clear. Underpotential deposition

processes[109] may be significant although no specific electrochemical evidence for this has been found. Possibly some interaction of titanium ions in solution with oxide on the surface of the electrode is responsible. Alternatively interaction of titanium metal (present in finely divided form in the melt as a result of disproportionation reactions) with the electrode surface results in the observed deposit.

Another effect of the anodic potential may be etching of the substrate stainless steel. There is no evidence of iron dissolution, but it is possible that the chromium content of the steel might be anodically dissolved at +0.6V. Chromium dissolution from the alloy would be likely to be a self-limiting process, ceasing once chromium in surface layers had been removed. Otherwise, chromium would have to diffuse in the solid at as fast a rate as the electrochemical dissolution takes place. The fact that similar conditioning effects were observed at the less anodic potential of +0.3V, where chromium dissolution is less likely although not impossible[50], does not entirely rule out this hypothesis.

(2) Cathodic reduction

While anodic polarisation alone is certainly an important factor in improving reproducibility of reduction data, on a fresh electrode the use of a cathodic step before the anodic reduction is also necessary. It is likely that this cathodic step (at relatively high overpotentials) reduces oxides on the steel electrode surface, thereby contributing to the production of a cleaner substrate. Concurrent titanium deposition is not a

problem because of the removal of titanium metal during the following anodic dissolution step.

4.5.2. Diffusion coefficient values

If the data of figure 4.14 are re-plotted as i vs $t^{-1/2}$ then at long times the plots are linear, as predicted by equation 4.2. The slope of the i-$t^{-1/2}$ plot allows the diffusion coefficient for Ti^{2+} to be calculated. At 400^{o}C this was determined as 1.8 x 10^{-5} cm^2s^{-1}; at 450^{o}C the value is 3.5 x 10^{-5} cm^2s^{-1}. These values are consistent with the values in the literature in the range 10^{-6} to 10^{-4} cm^2s^{-1} listed in chapter 1.

4.5.3. Rate constant values

Rate constants determined from charge-time data as described in 4.4.3.1. lie in the range 0.005 to 0.2 $cm.s^{-1}$ for overpotentials of between 30 and 590 mV. Extrapolation back to zero overpotential gives a value of about 0.006 at 400^{o}C. Using a value for the slope of log k_R vs E of 3.13 allows a value for α_c of 0.2 to be calculated. The value of k_R at zero overpotential corresponds to an exchange current density (when $E=E_o^e$), calculated using equation 4.3., of about 0.05 $A.cm^{-2}$. This is relatively high and may suggest that the linear extrapolation is not a valid approach. Distortion of the current-time characteristics as a result of nucleation and growth phenomena may be responsible for these inconsistencies and cause the exchange current and α_c values quoted above to be invalid.

Popov et al determined a value for k^R for TiII reduction in LiCl-KCl at 450^{o}C of 2.08 x 10^{-6} $cm.s^{-1}$ [143]. The associated value for $\alpha_c n$ was 0.46. Haarberg et al reported a value for k^R for the same

reaction of 1.7×10^{-4} $cm.s^{-1}$ [100]. These are significantly different both from each other and from the results reported here.

4.5.4. Nucleation characteristics

The characteristic rising current transient indicating nucleation of a new phase on the electrode surface is observed only at concentrations of about 2.5 wt.% titanium and above. It is also necessary that the stainless steel electrode surface be carefully prepared and conditioned so as to produce a clean surface prior to the cathodic polarisation. Even under these, the most favourable, conditions, the nucleation phenomenon is difficult to analyse from the current-time data. The current does not fall close to zero immediately before it rises to a peak value, so that the observed relationship of current to time is unlikely to be due to the nucleation stage alone. This is borne out by attempts to determine the order of the time dependence of the current. Values of about 0.1 have been determined, compared with the following values predicted by theory[105]-[107][168]:

Type of nucleation	n in ($I \propto t^n$)
2 dimensional, instantaneous	1
2 dimensional, progressive	2
3 dimensional, instantaneous	2
3 dimensional, progressive	3
3 dimensional, instantaneous, diffusion-limited	0.5
3 dimensional, progressive, diffusion-limited	1.5

These relationships are accurate representations only where no significant overlap of growth centres takes place. Obviously, in

many real systems, this is a significant factor. Treatments have also been developed to allow for the overlapping diffusion fields of an array of growth centres[169][170].

In some of the transients particularly at higher overpotentials (such as at 620 mV in figure 4.21) a second maximum can be seen in the current-time relationship. This is often taken as evidence of layer formation in 2-dimensional nucleation[171]. It is conceivable that this represents the onset of a second nucleation or phase formation process. A possibility is the discharge of lithium metal, or an alloy of that metal with titanium. Another possibility is the nucleation of a fresh layer of titanium on the first one. Other mechanisms than 2 dimensional growth of the electrodeposit may cause this, for example, the interaction of trace oxygen in the melt with initial titanium deposited may cause re-nucleation to be necessary for subsequent deposition. It should also be noted that calculations for hemispherical 3 dimensional nucleation formed by progressive nucleation also give rise to multiple maxima in the current-time curve[170].

Examination of electrodeposits produced at short times sheds some light on the processes taking place. The results at 100 and 150 mV are similar. After 12 seconds deposition the electrode surface has a "fuzzy" appearance, with an even distribution of titanium particles of up to 1 micron in size. However, after 60 seconds the general appearance is distinctly different: discrete titanium particles (up to 1 micron at 100 mV, up to 3 microns at 150 mV) overlie an otherwise very clean, bare surface. The titanium particles present after 12 seconds appear to have aggregated into many fewer growth

centres. After 180 seconds much more extensive growth and surface coverage is apparent at 150 mV. Layer structure can be seen. At 300 mV very tiny particles and incipient steps or ridges can be seen as "trails" on the clean substrate surface. Continued growth leads to a "smeared" appearance completely covering the substrate after 60 seconds. Later, more 3-dimensional nodular growth develops. At 600 mV after 12 seconds the substrate is completely covered with very fine structure, not readily resolvable. Subsequent growth shows rough, nodular growth and particle formation, with voids beginning to appear in the structure.

It is clear that at the higher overpotentials coverage of the substrate with the growing electrodeposit is very much better than at the lower overpotentials. This may be because of the smaller critical size (the minimum size for a growth centre to be viable) of nuclei at higher overpotentials. Moreover, the varying sizes of the growth centres suggest that nucleation cannot be considered instantaneous. Although the deposit ultimately develops 3-dimensionally , in the early stages distinct layering is apparent, so that 2 dimensional nucleation may be the appropriate representation. This is consistent with the observation of two maxima in the current-time curves. However the possibility that hemispherical 3-dimensional progressive nucleation is taking place at the higher overpotentials cannot be ruled out because the individual nuclei are too small to characterise.

It has not been possible to determine the $i\text{-}t^n$ relationship diagnostic of this type of nucleation from the reduction data, probably because of the relative dominance of other processes. In general the form of the i-t relationships suggests addition of

diffusion controlled and nucleation controlled processes. At intermediate titanium concentrations and overpotentials this manifests itself as a shoulder on the falling i-t transient.

There have been two notable previous studies of the nature of the nucleation of titanium from molten LiCl-KCl[100][139]. Both these concluded that nucleation was instantaneous, 3-dimensional, followed by growth under mass transport control, from determinations of current dependence on $t^{1/2}$.

It is conceivable that similar results were not obtained here because of differences in substrate material, pre-treatment and conditioning, in view of the importance of these factors discussed above.

4.6. Conclusions

1. The electro-reduction data is consistent with a simple reduction reaction $Ti^{2+} \rightarrow Ti^{0}$ occurring under mixed kinetic and diffusion control.

2. Early stages of growth of the electrodeposit at about 3 wt.% titanium concentrations are controlled by nucleation. However, diffusion controlled processes are still important such that analysis of the nucleation component is not possible.

3. Evidence for 2-dimensional nucleation exists in the form of more than one maxima in the i-t relationship, and in the observation of the morphology of the early stages of deposit growth. However progressive hemispherical 3-dimensional nucleation cannot be ruled out.

4. At low overpotentials, relatively few nuclei develop, and poor coverage of the substrate ensues. At higher overpotentials, typically at least 300 mV, the coverage of the electrode substrate is good.

5. Strong nucleation characteristics, including the consequent good coverage of the substrate surface, require adequate substrate pre-treatment and in-situ conditioning.

FIGURE 4.1

ELECTROCRYSTALLISATION ON A FOREIGN SUBSTRATE

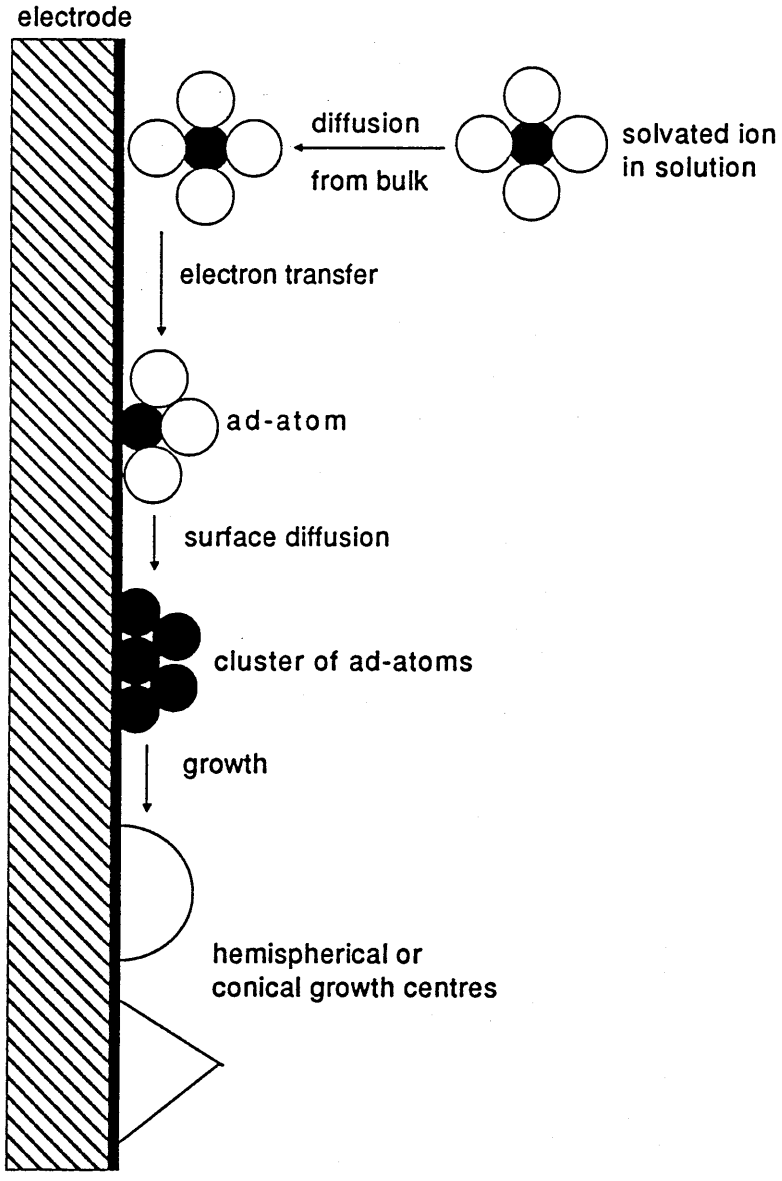

FIGURE 4.2

CYCLIC VOLTAMMOGRAM CHARACTERISTIC OF NUCLEATION

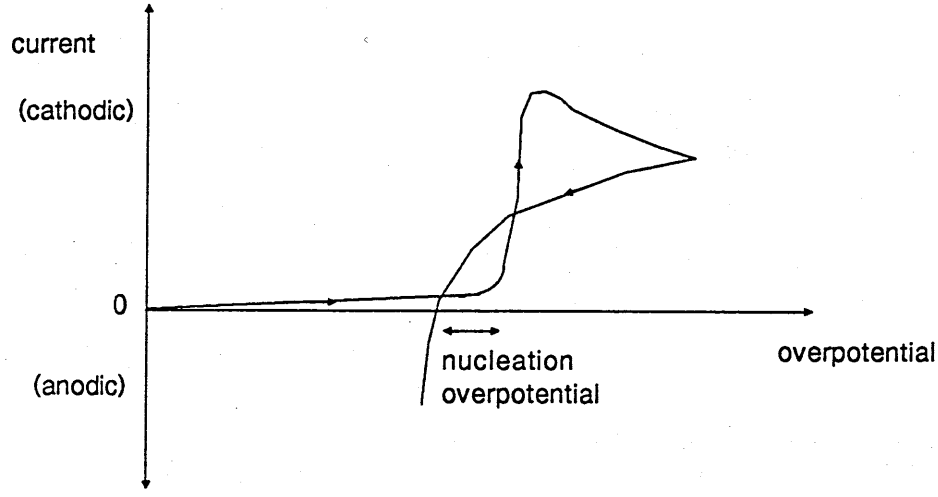

FIGURE 4.3

SCHEMATIC DIAGRAM SHOWING TYPICAL CURRENT-TIME TRANSIENTS IN A POTENTIAL STEP EXPERIMENT

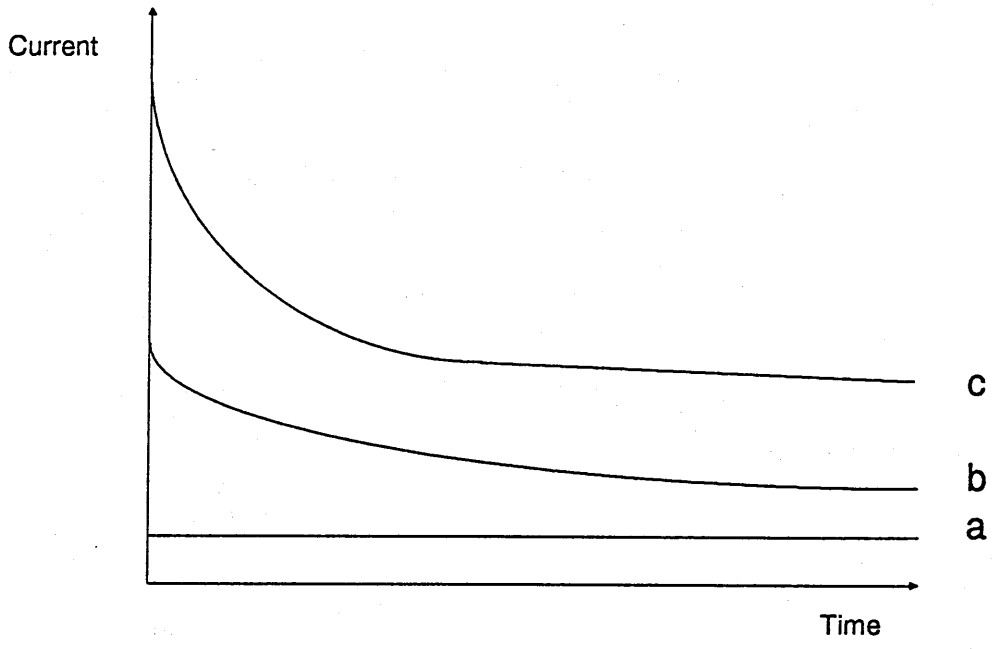

a reaction is kinetically controlled
b reaction is under mixed kinetic and diffusion control
c reaction is diffusion controlled

FIGURE 4.4

TYPES OF NUCLEATION I-t TRANSIENT

a) 2 dimensional, instantaneous

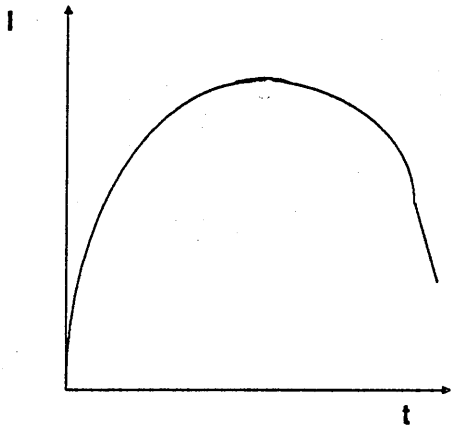

b) 2 dimensional, progressive

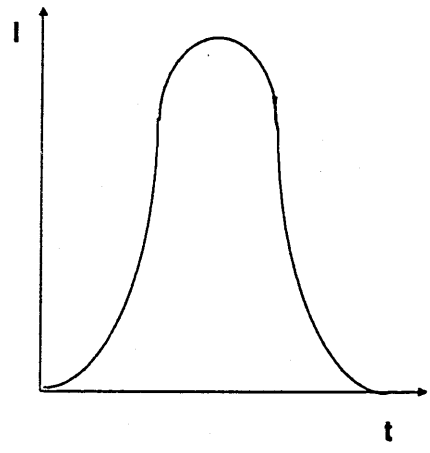

c) 3 dimensional nucleation and growth

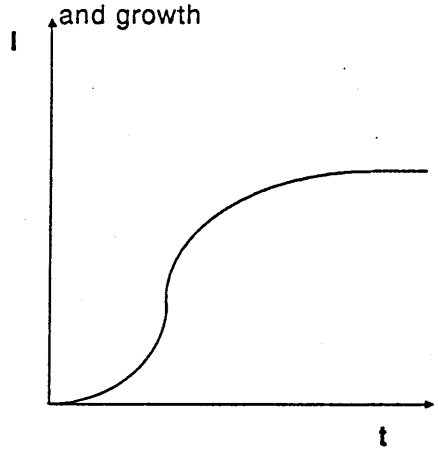

d) successive monolayer formation

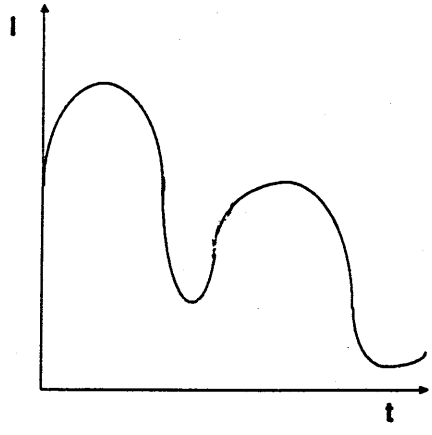

e) product adsorption

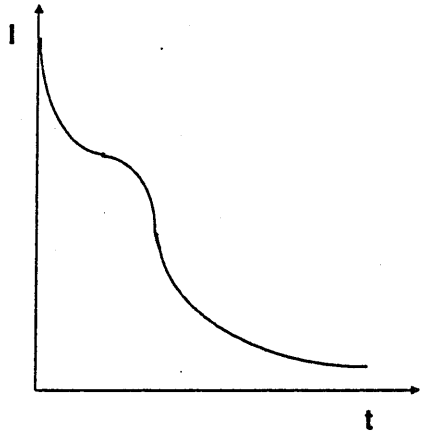

FIGURE 4.5

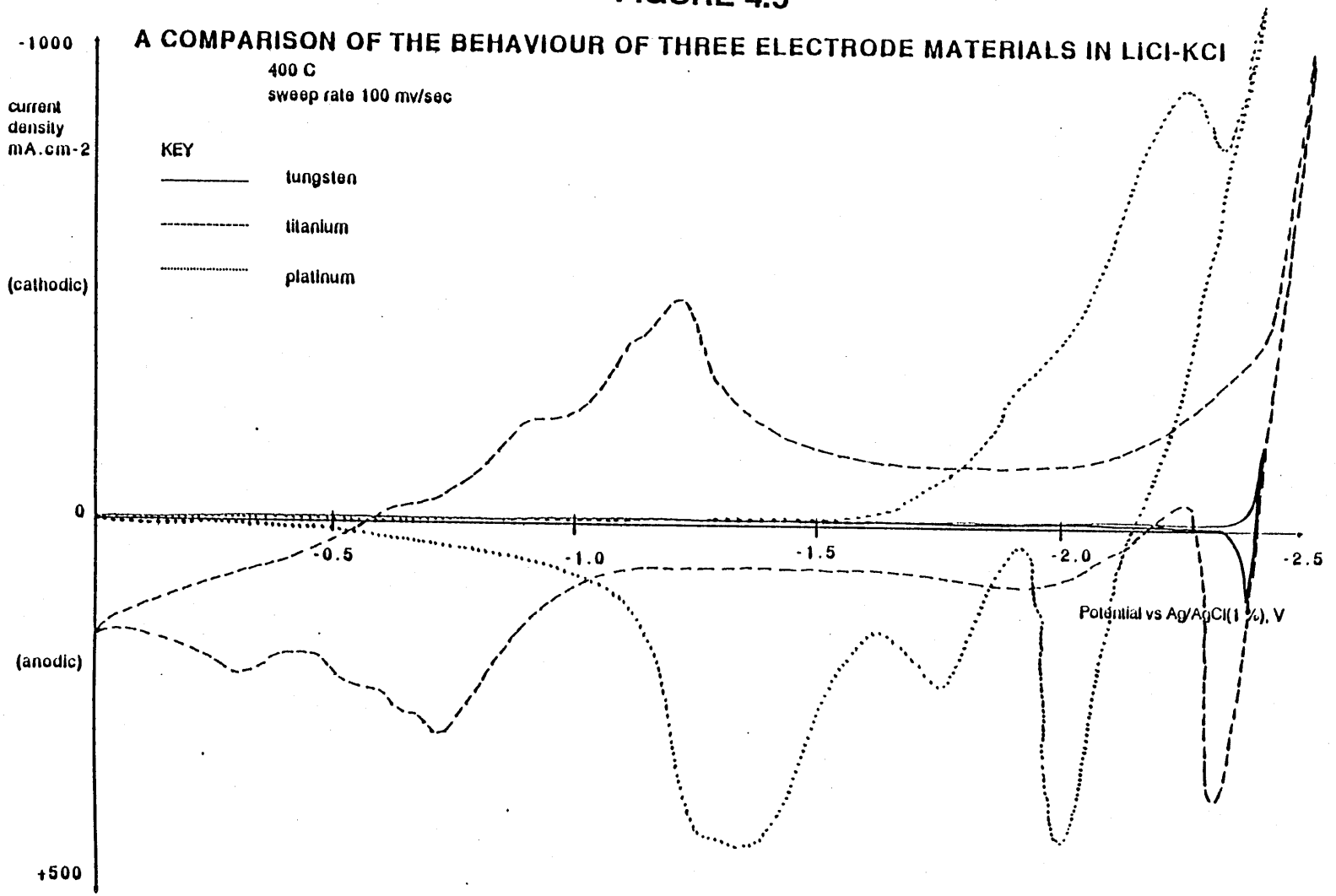
A COMPARISON OF THE BEHAVIOUR OF THREE ELECTRODE MATERIALS IN LICI-KCI
400 C
sweep rate 100 mv/sec
-1000
current
density
mA.cm-2
KEY
tungsten
titanium
platinum
(cathodic)
0
(anodic)
+500
-0.5
-1.0
-1.5
-2.0
-2.5
Potential vs Ag/AgCl(1 %), V

FIGURE 4.6

CYCLIC VOLTAMMOGRAM OF TITANIUM IN LiCl-KCl AT 440 c

sweep rate 100 mv/sec

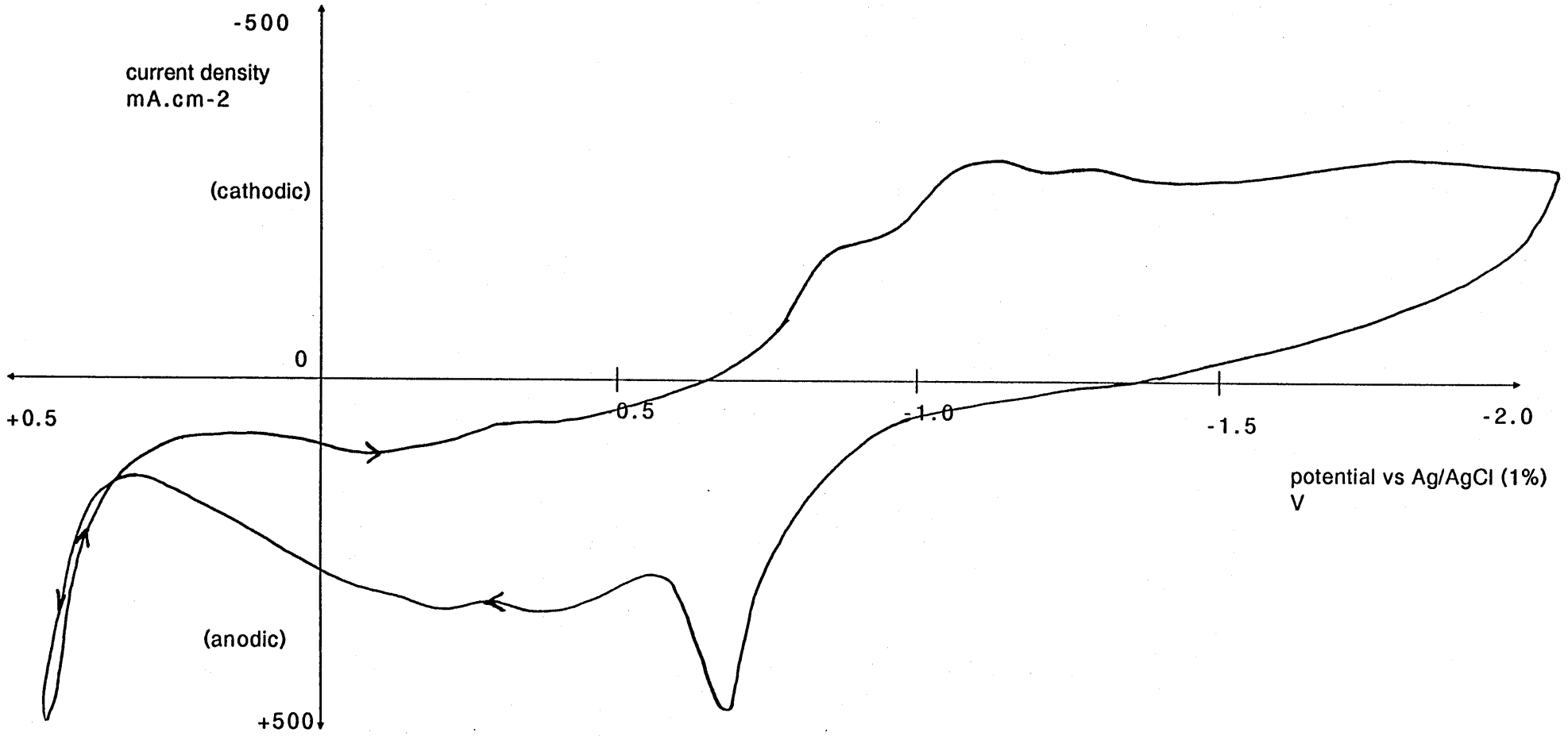

FIGURE 4.7

COMPARISON OF 1ST & 2ND SWEEPS ON TITANIUM WIRE IN LiCl-KCl

sweep rate 10 mV/sec
407 C
sweep begins at -1.8V

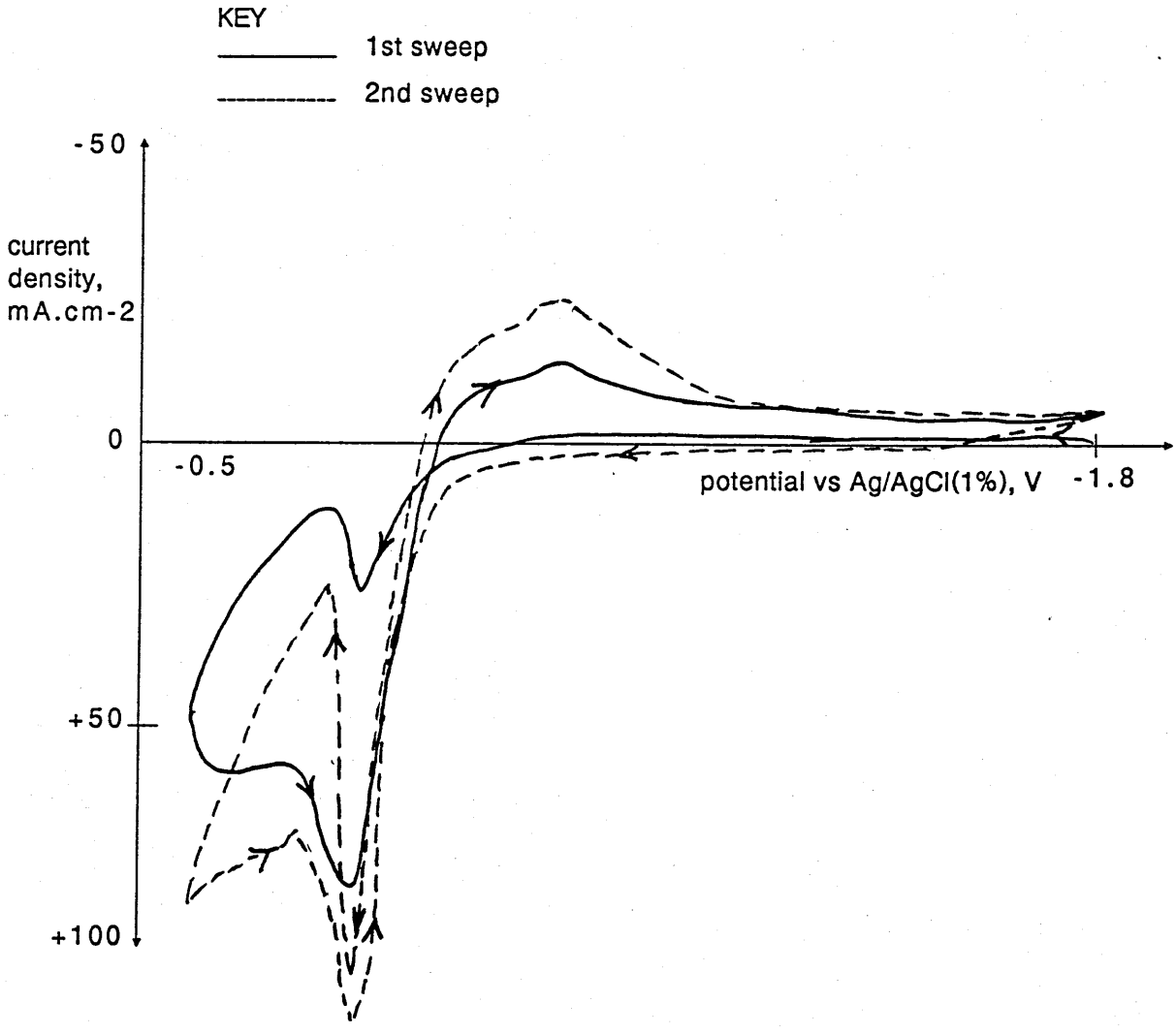

FIGURE 4.8

CYCLIC VOLTAMMOGRAM FOR TITANIUM ELECTRODE IN LiCl-KCl

sweep rate 100 mV/sec
407 C
sweep begins at -1.8V

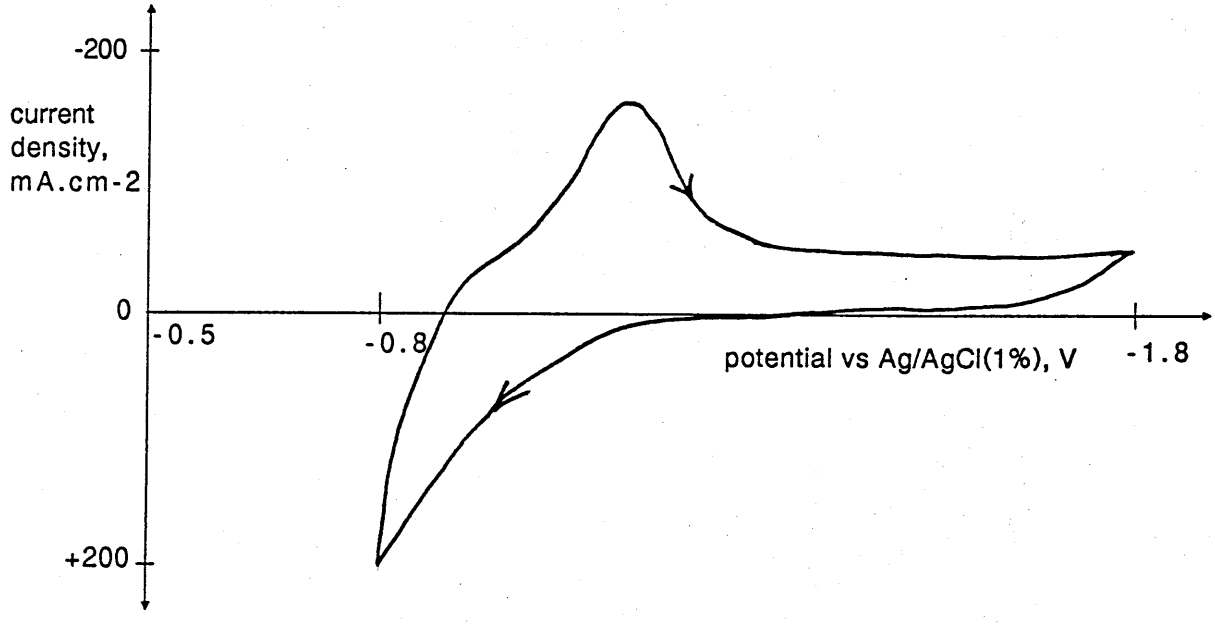

FIGURE 4.9

CYCLIC VOLTAMMOGRAM FOR TITANIUM ELECTRODE IN LiCl-KCl

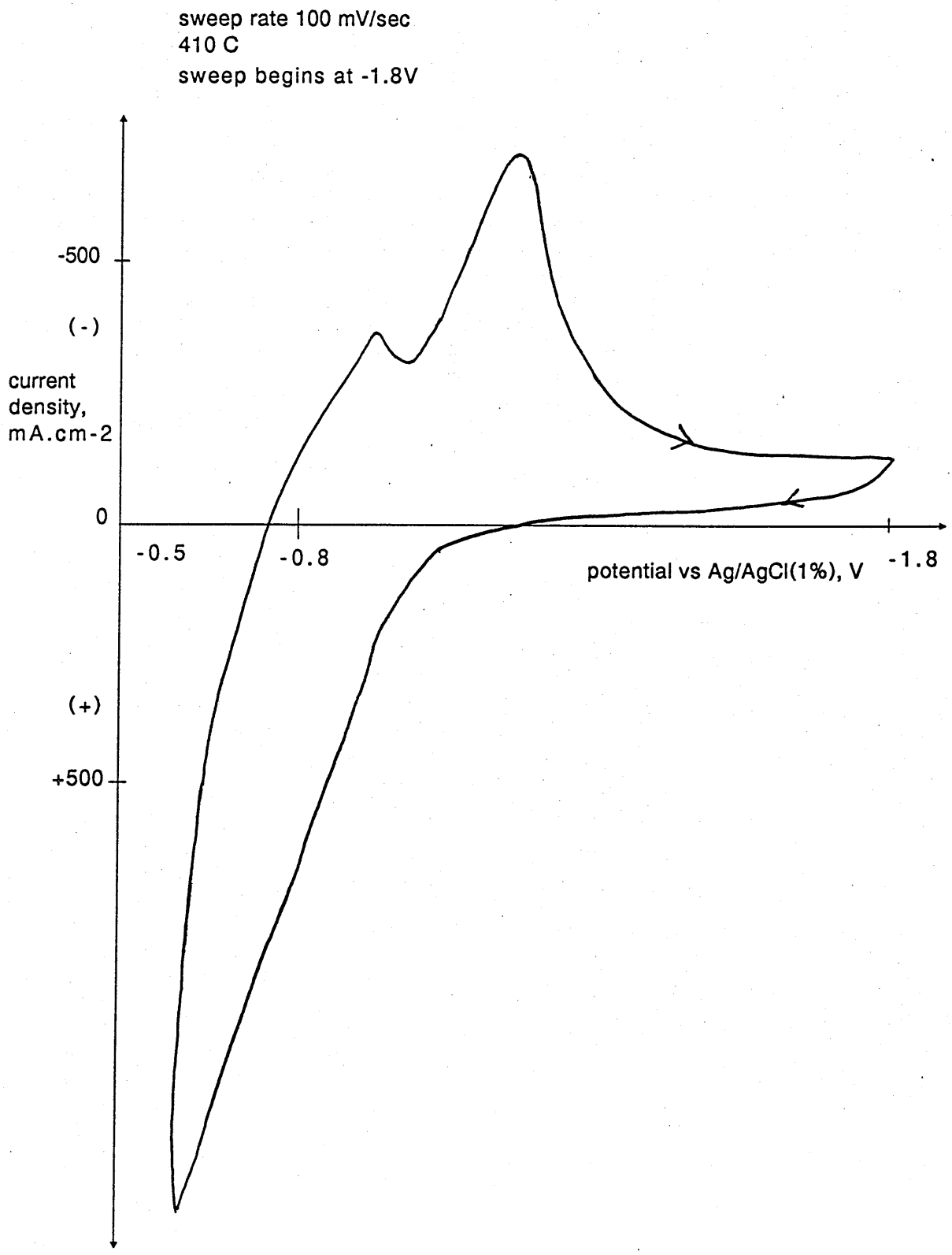

FIGURE 4.10

CYCLIC VOLTAMMOGRAM OF TUNGSTEN ELECTRODE IN LiCl-KCl-$TiCl_3$

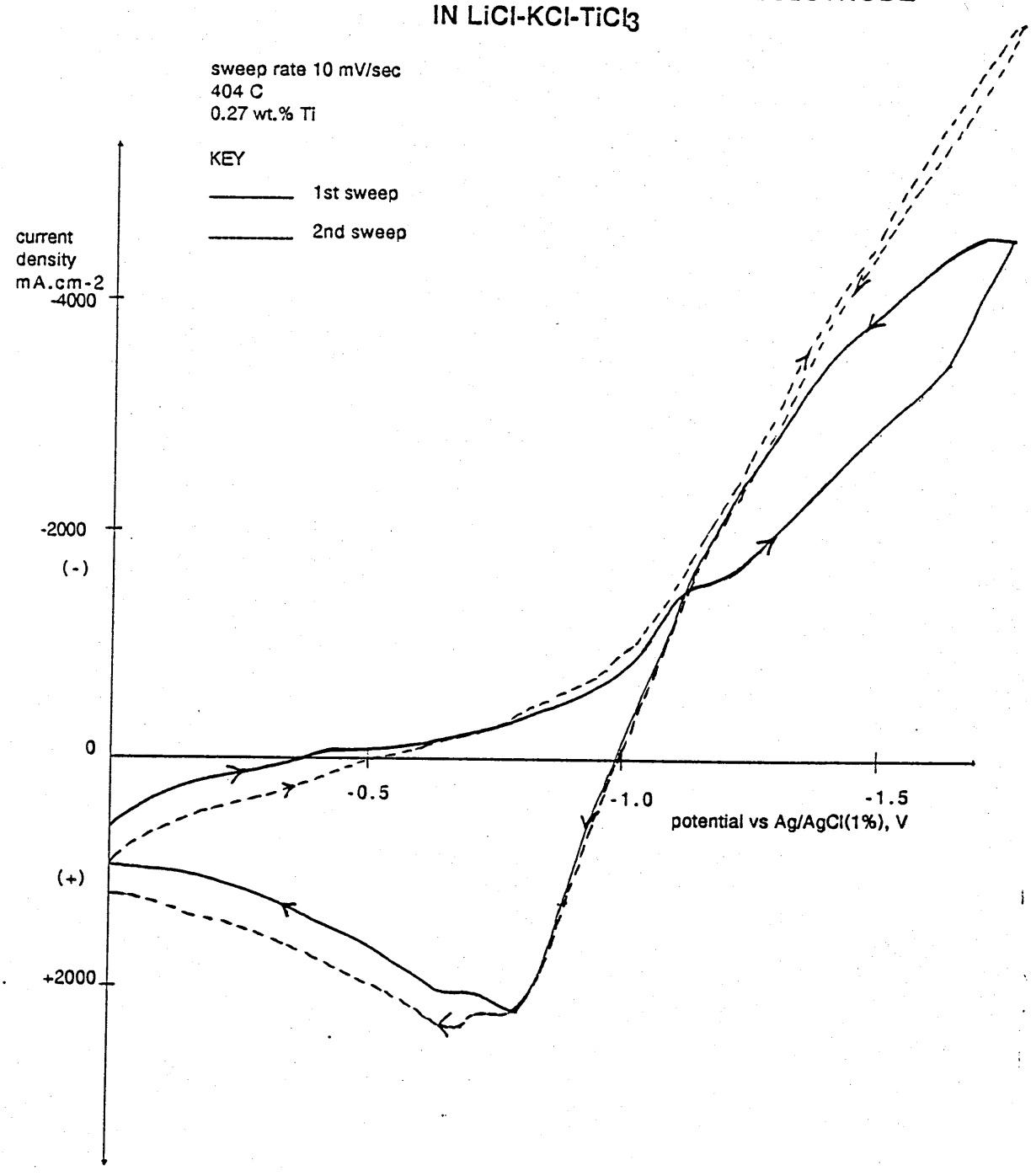

FIGURE 4.11

EFFECT OF ANODIC CONDITIONING ON CATHODIC TRANSIENTS

405 C; [Ti] = 2.5 %

Stainless steel wire electrode, 0.677 cm2 in area (0.5 mm diameter)

Electrode conditioning : +0.6 V vs Ti for 1 minute, then 0 V vs Ti for 2 minutes followed by anodic conditioning as specified below immediately before cathodic step to -0.5 V vs Ti.

The current-time response to this last cathodic step as a function of the anodic conditioning applied is shown in the figure.

Anodic conditioning = 60 seconds at the following potential vs Ti :

+ 0 mV □ +100 mV ∆ +300 mV x +600 mV

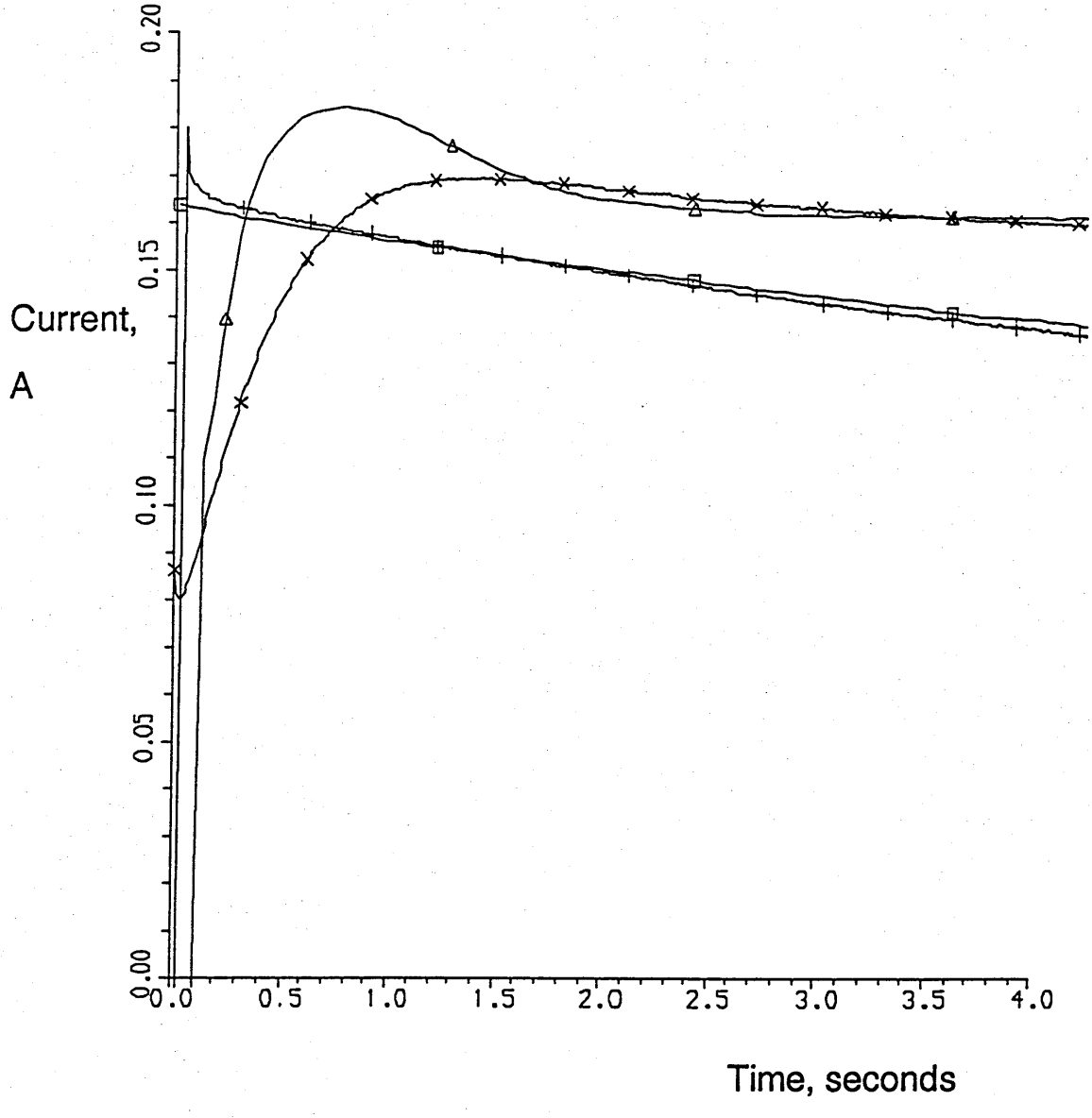

FIGURE 4.12

ANODIC OXIDATION OF FRESH STAINLESS STEEL ELECTRODE IN PLATING MELT

400 C, 2.5 % Ti, stainless steel wire electrode, 0.5 mm diameter
at +0.3 V vs Ti

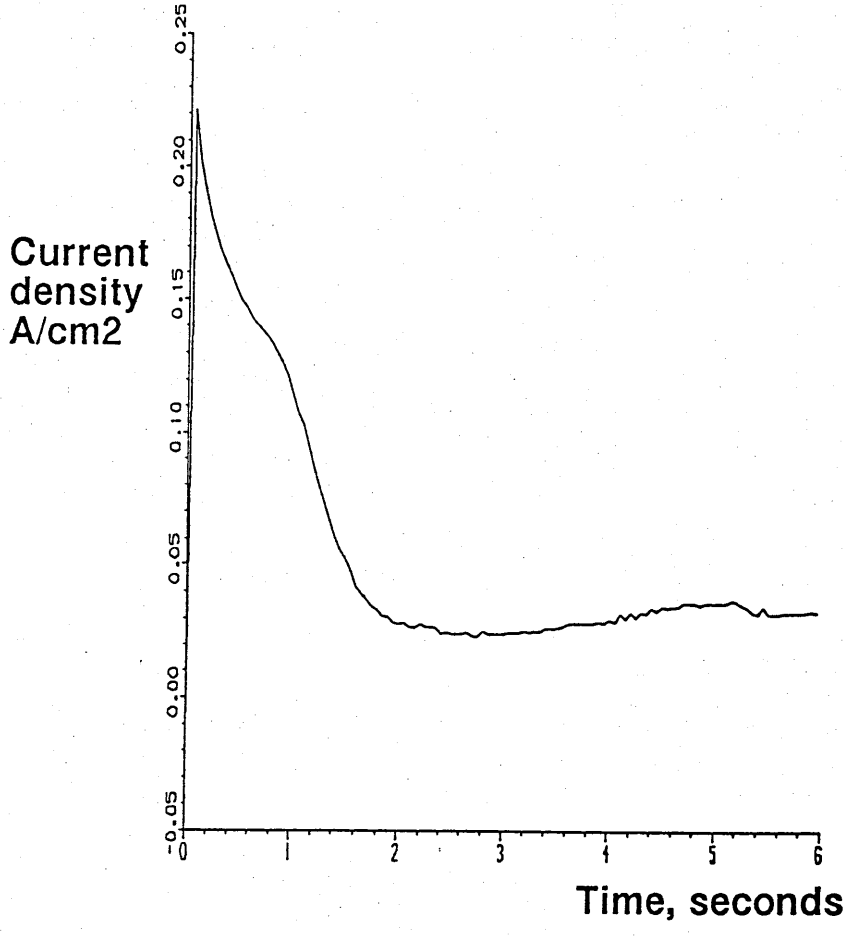

FIGURE 4.13

STAINLESS STEEL AFTER IMMERSION IN MELT

Stainless steel flags, immersed in melt, then washed in dilute HCl in an ultrasonic bath, rinsed and dried.

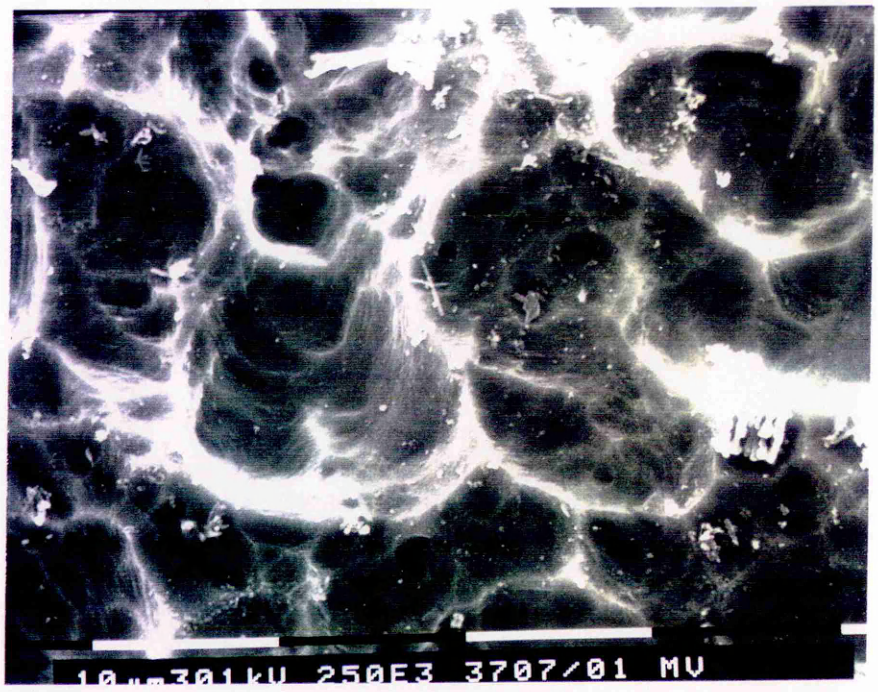

5 minutes, no applied potential

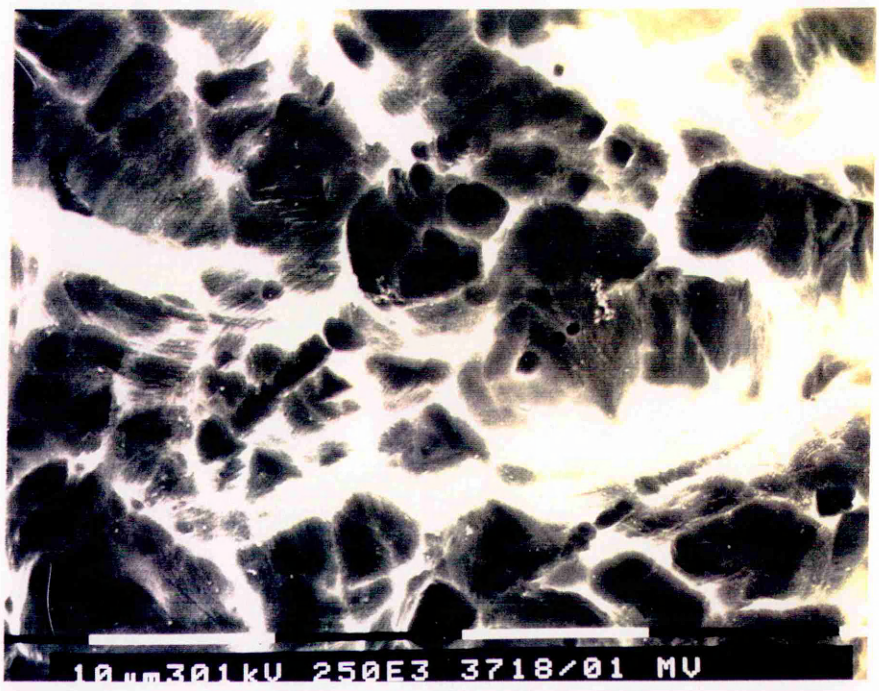

5 minutes at +600 mV vs Ti

FIGURE 4.14

REDUCTION AT CONSTANT POTENTIAL: 400 c, 0.13 % Ti, CURRENT DENSITY vs. TIME

On stainless steel wire, 0.5 mm diameter, 0.285 cm2 in area.

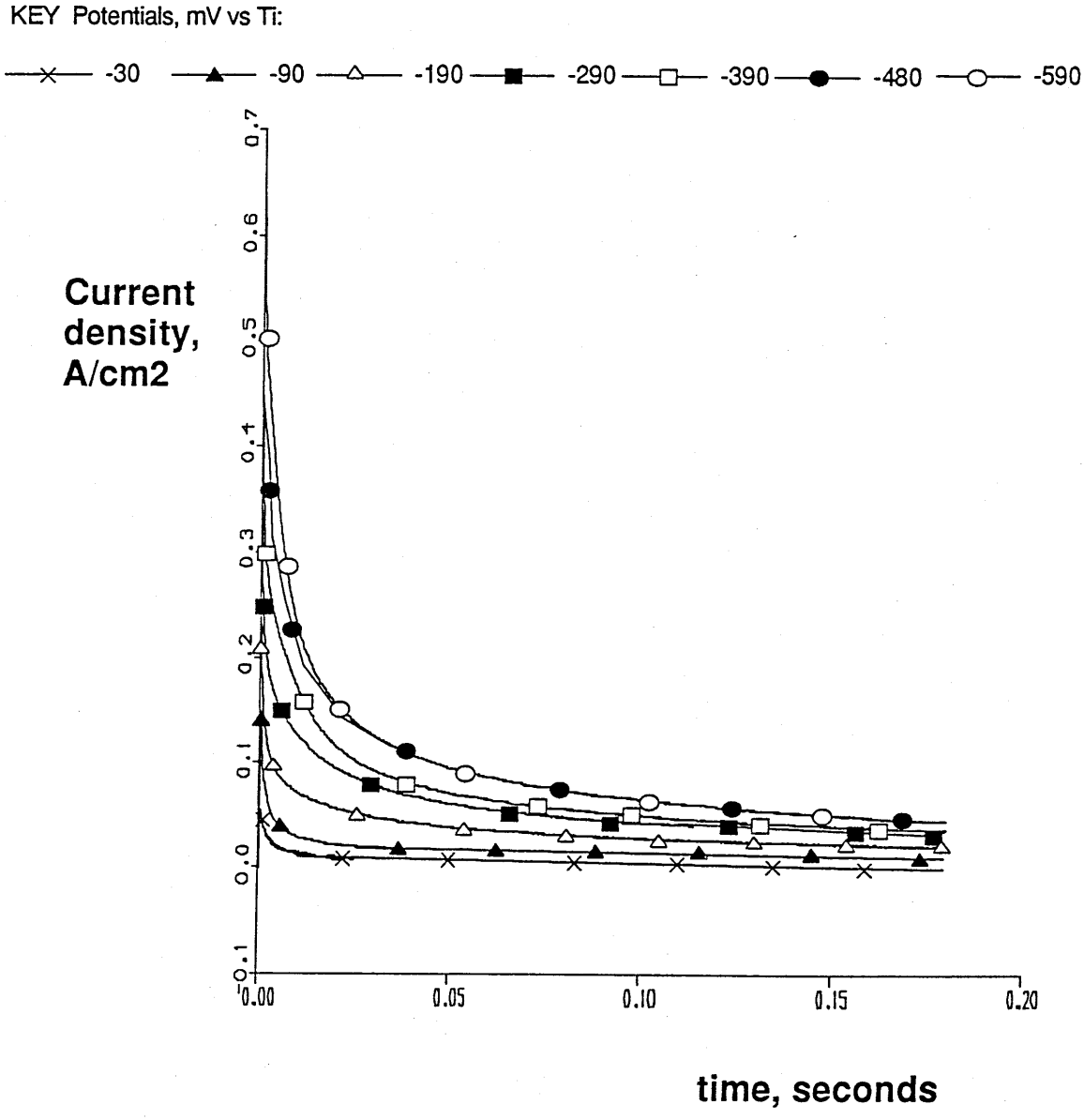

FIGURE 4.15

REDUCTION AT CONSTANT POTENTIAL: 400 C, 0.13 % Ti
CHARGE vs. TIME

on stainless steel wire, o.5 mm diameter, 0.285 cm2 in area

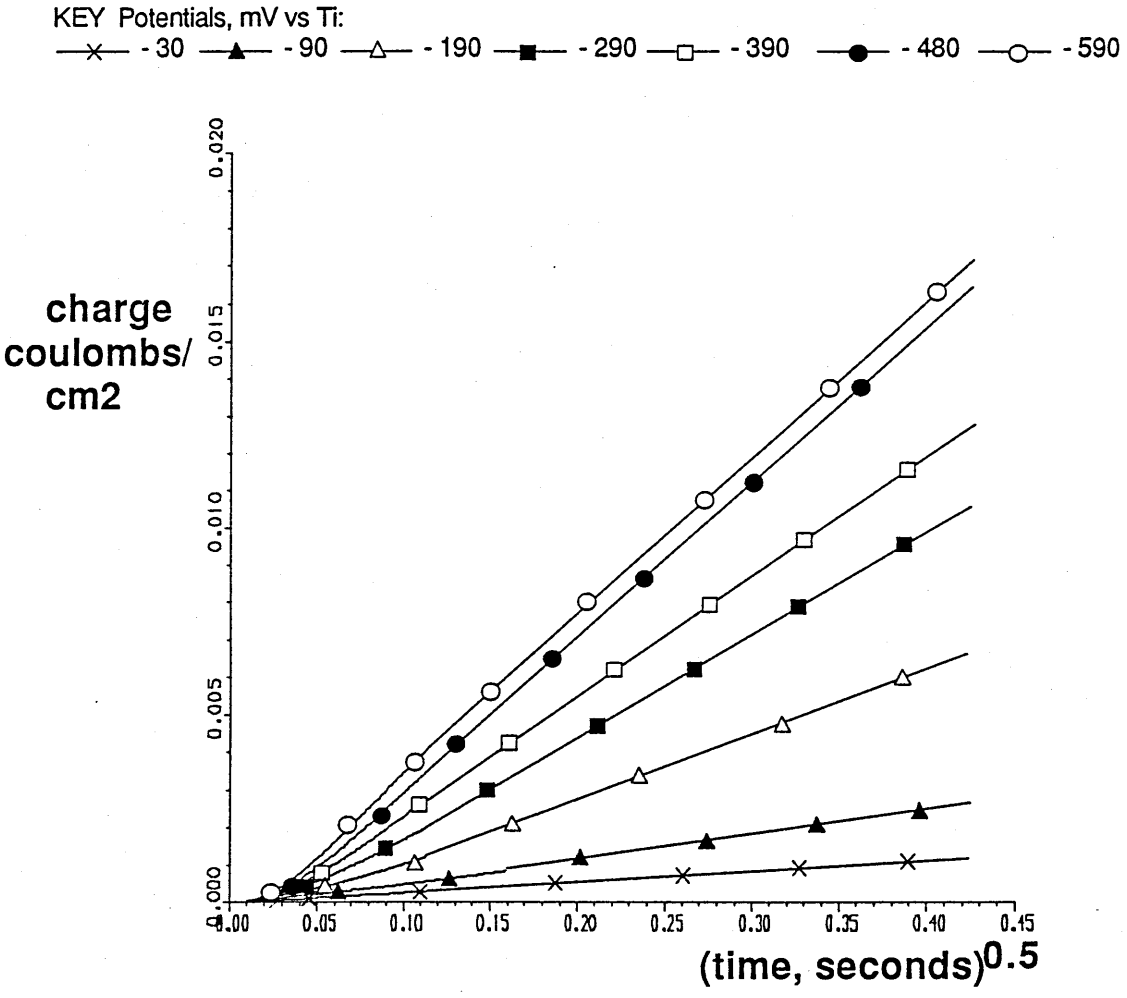

FIGURE 4.16

REDUCTION AT CONSTANT OVERPOTENTIAL, 0.13 % Ti
E vs log k^R

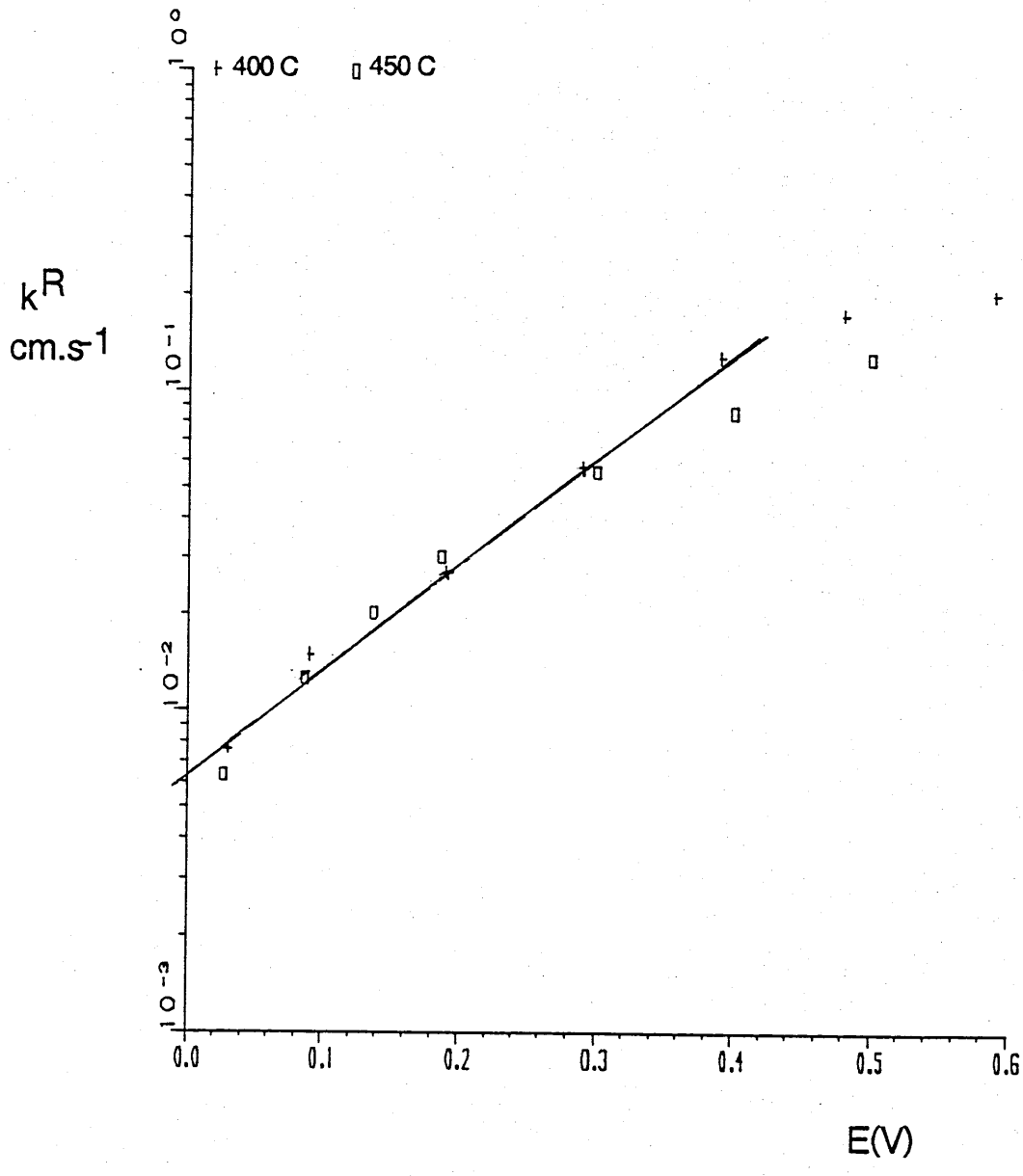

FIGURE 4.17

REDUCTION AT CONSTANT POTENTIAL: 450 C, 0.65 % Ti
CURRENT DENSITY vs. TIME

on stainless steel wire, 0.5 mm dia., 0.35 cm2 in area

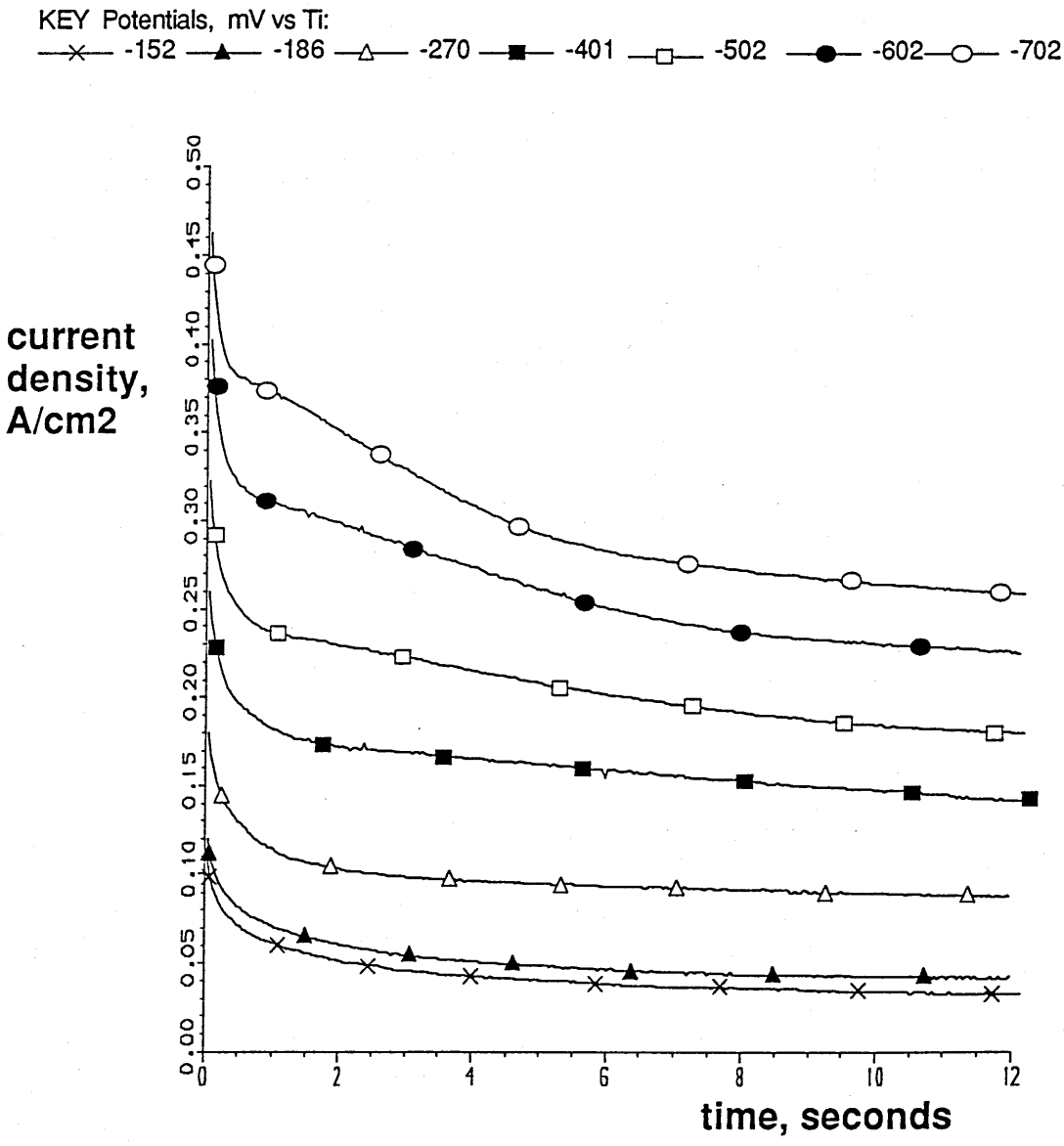

FIGURE 4.18

REDUCTION AT CONSTANT POTENTIAL: 450 C, 0.65 % Ti
CHARGE vs. TIME$^{0.5}$

on stainless steel wire, 0.5 mm dia., 0.35 cm2 in area

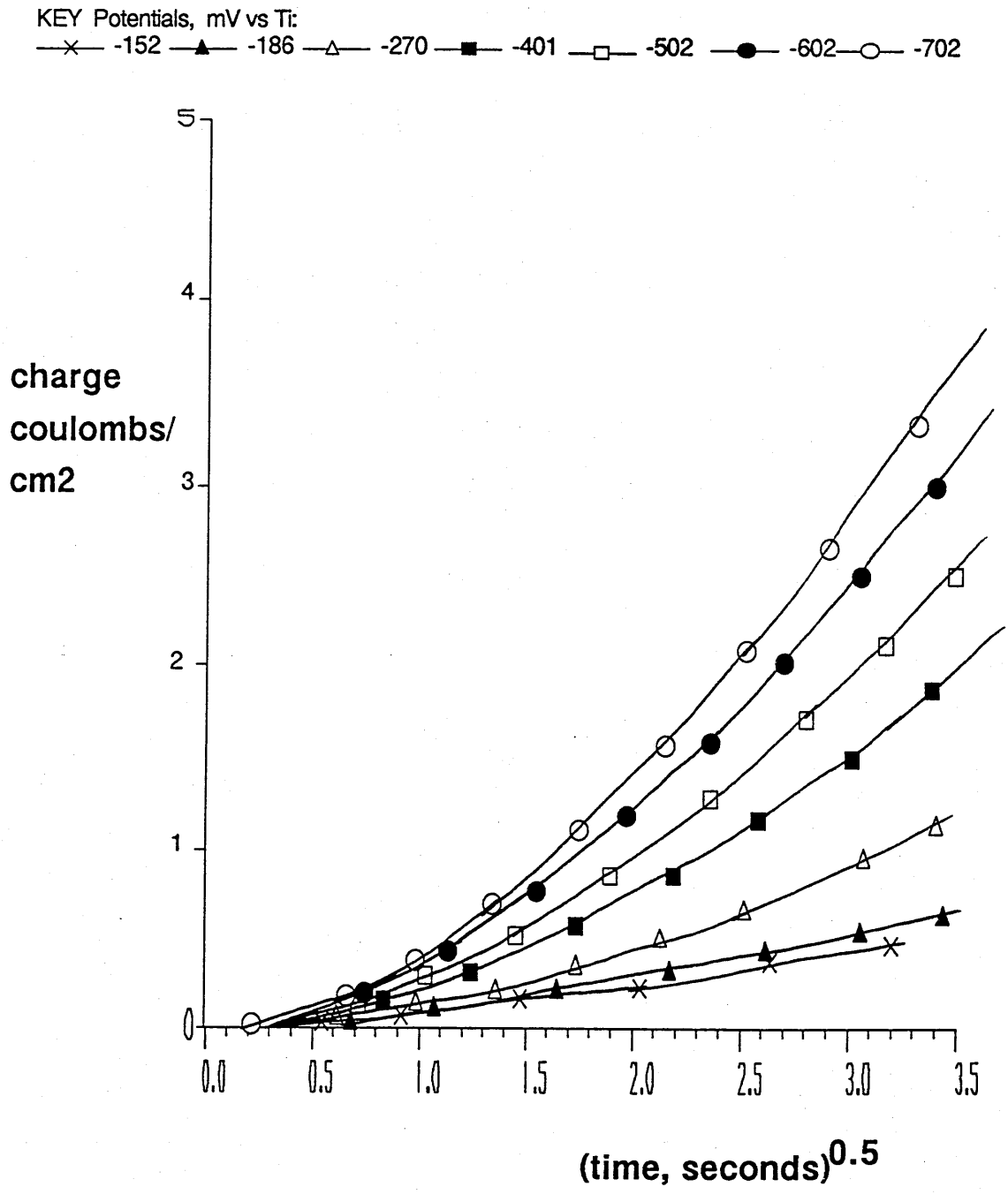

FIGURE 4.19

REDUCTION AT CONSTANT POTENTIAL: 400 C, 1.07% Ti
CURRENT DENSITY vs. TIME

on stainless steel wire, 0.5 mm dia., 0.379 cm2 in area

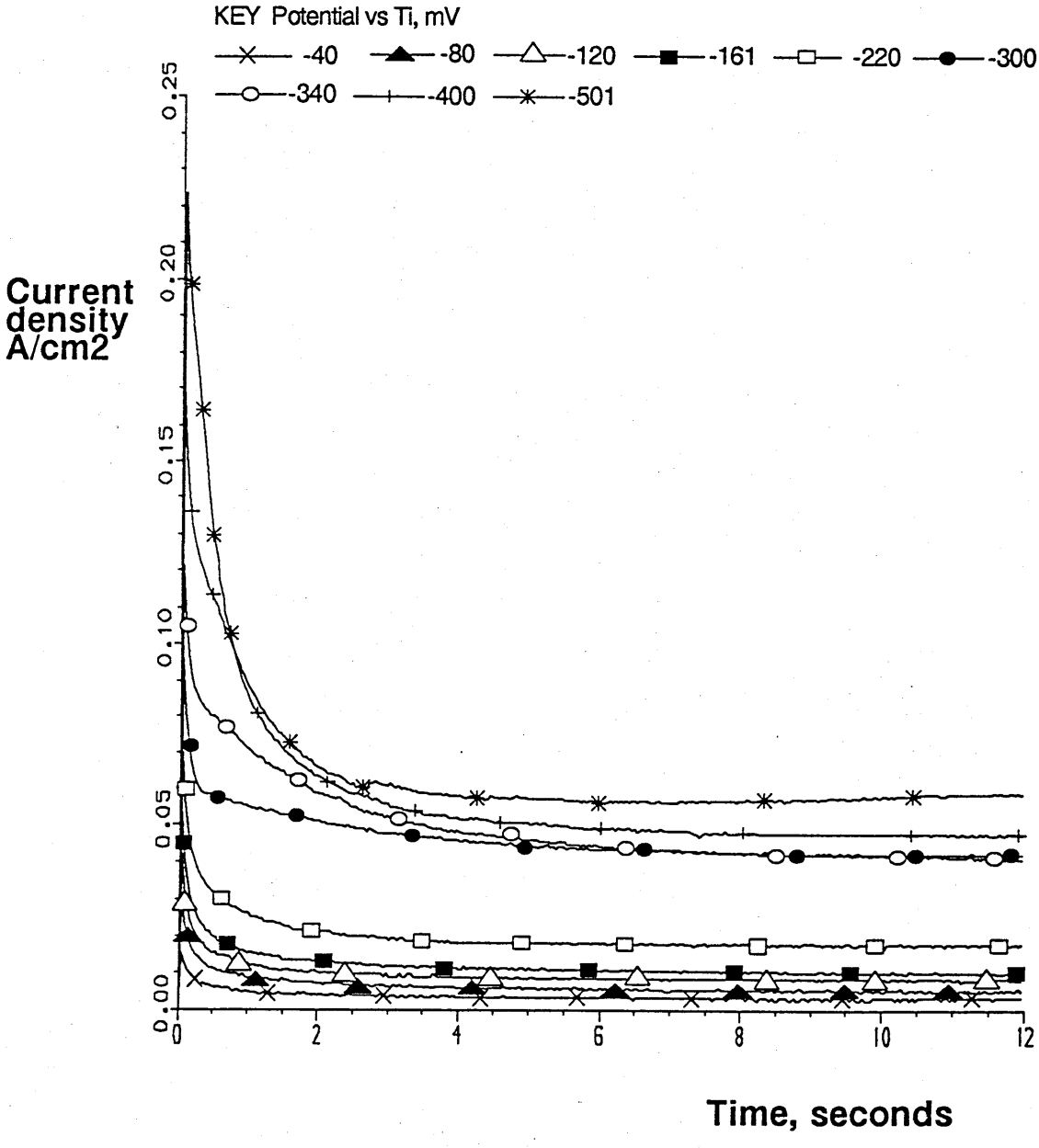

FIGURE 4.20

REDUCTION AT CONSTANT POTENTIAL FOLLOWED BY OXIDATION AT +600 mV vs Ti
400 C, 1.07% Ti
CURRENT DENSITY VS TIME

on stainless steel wires, 0.5 mm dia, 0.38 cm2 in area

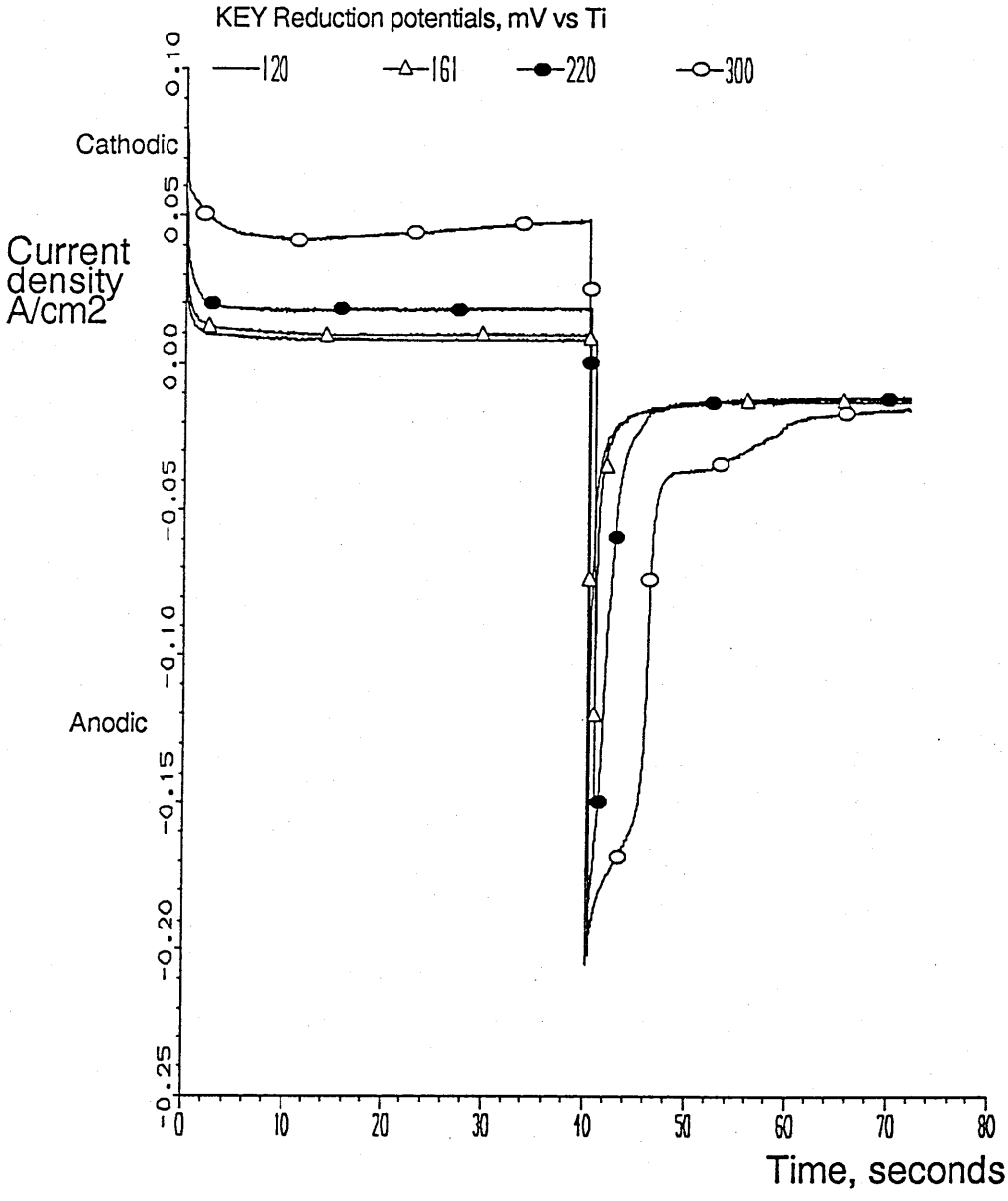

FIGURE 4.21

REDUCTION AT CONSTANT POTENTIAL: 450 C, 3.0 % Ti CURRENT DENSITY vs TIME

on stainless steel wires, 0.5 mm diameter, 0.16 cm2 area

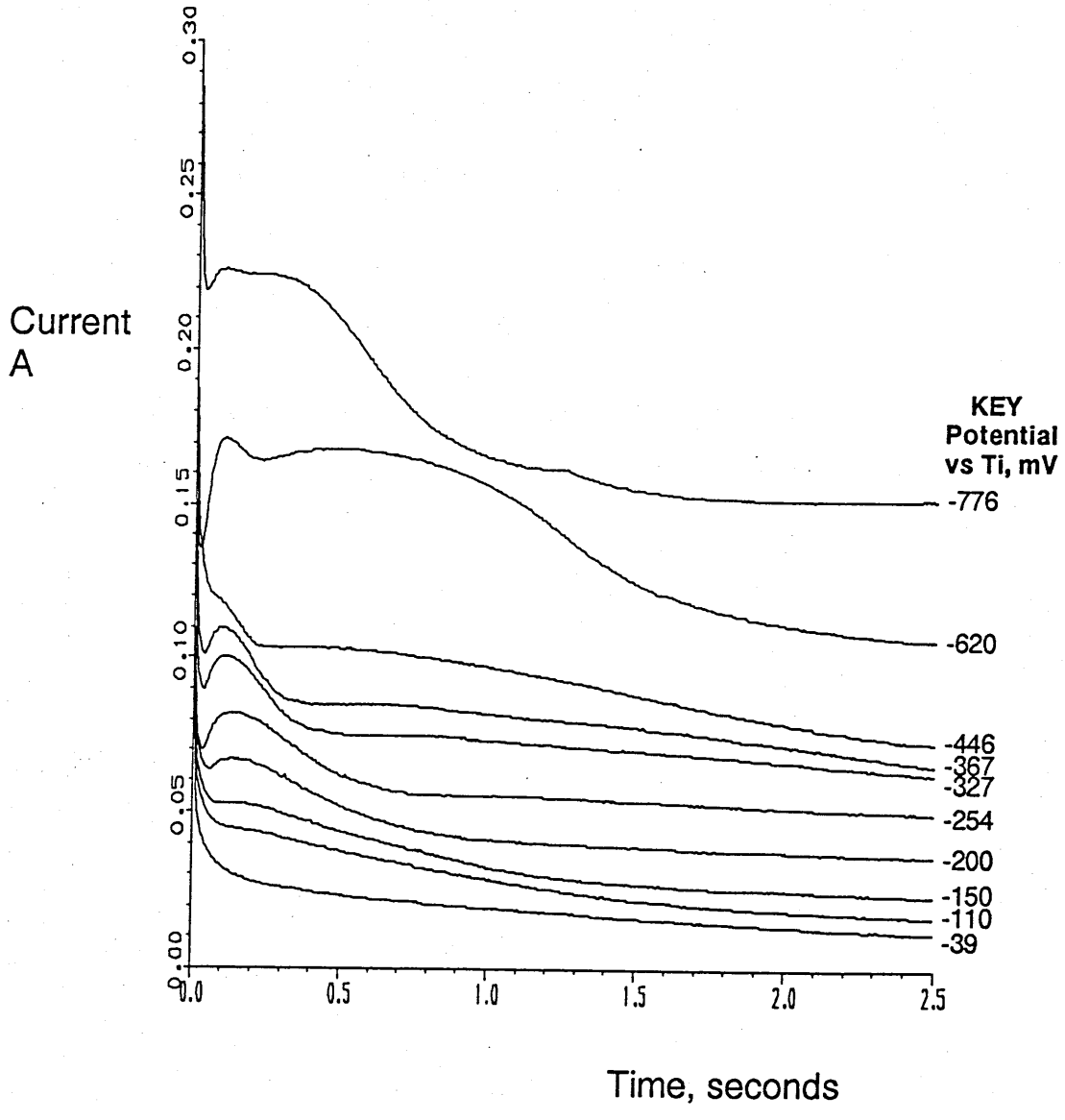

FIGURE 4.22

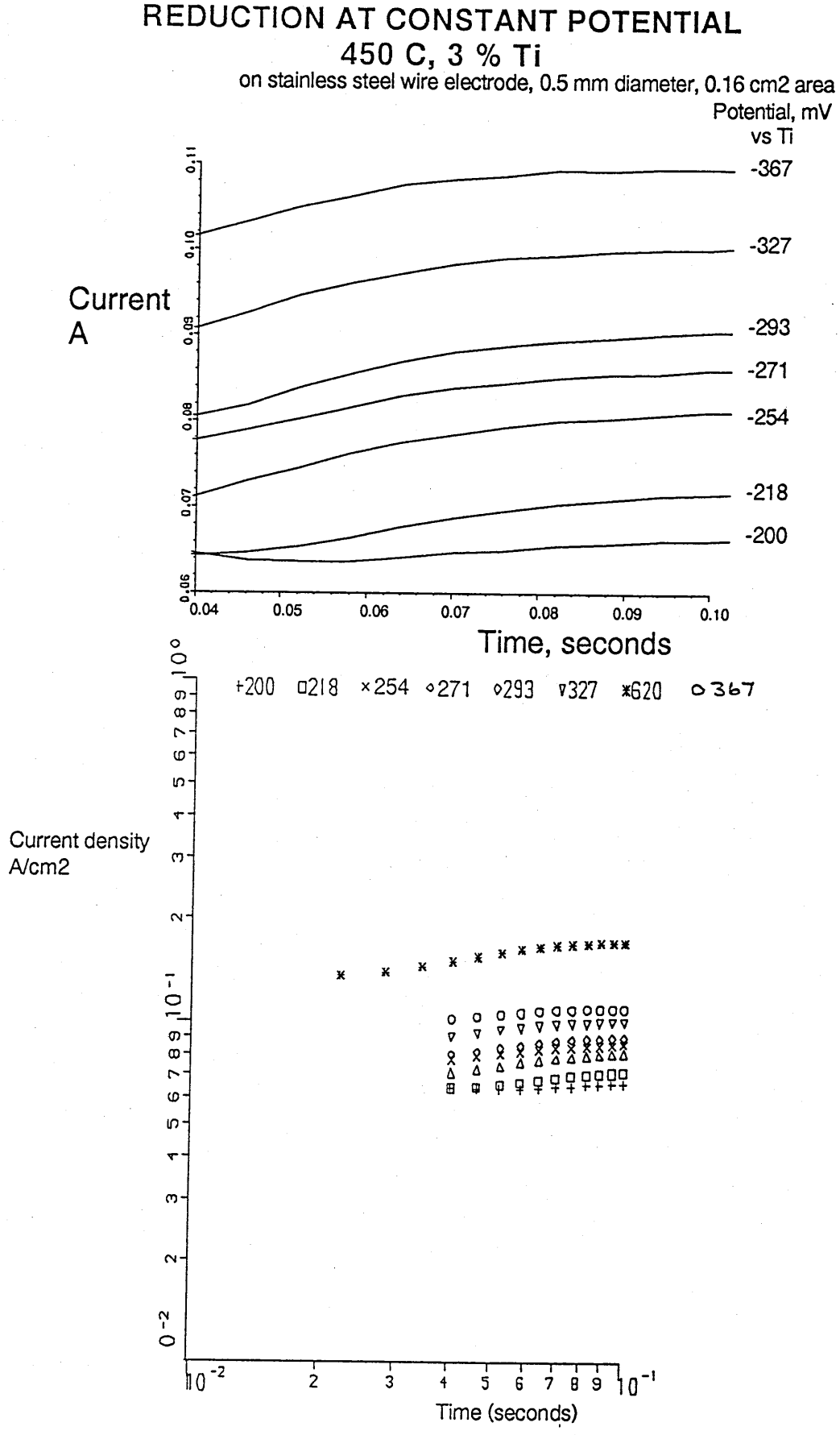
REDUCTION AT CONSTANT POTENTIAL
450 C, 3 % Ti
on stainless steel wire electrode, 0.5 mm diameter, 0.16 cm2 area
Potential, mV
vs Ti
-367
-327
-293
-271
-254
-218
-200
Current
A
0.11
0.10
0.09
0.08
0.07
0.06
0.04
0.05
0.06
0.07
0.08
0.09
0.10
Time, seconds
+200 □218 ×254 ◇271 ◇293 ▽327 ✱620 ○367
Current density
A/cm2
Time (seconds)

FIGURE 4.23

ELECTRODEPOSITION AT CONSTANT POTENTIAL : CURRENT-TIME OVER FIRST 180 SECONDS

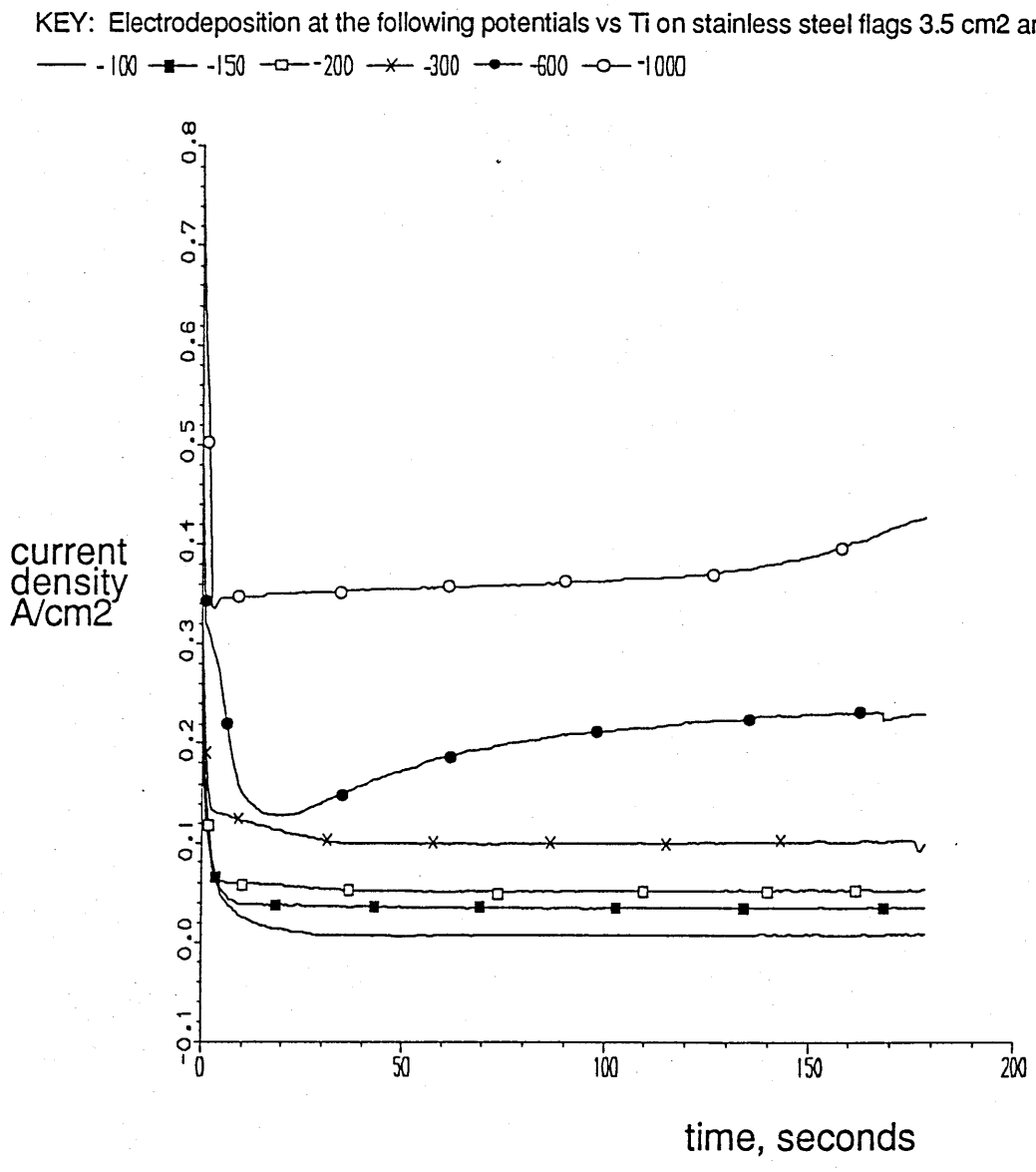

FIGURE 4.24

ELECTRODEPOSITION AT CONSTANT POTENTIAL : CURRENT-TIME OVER FIRST 60 SECONDS

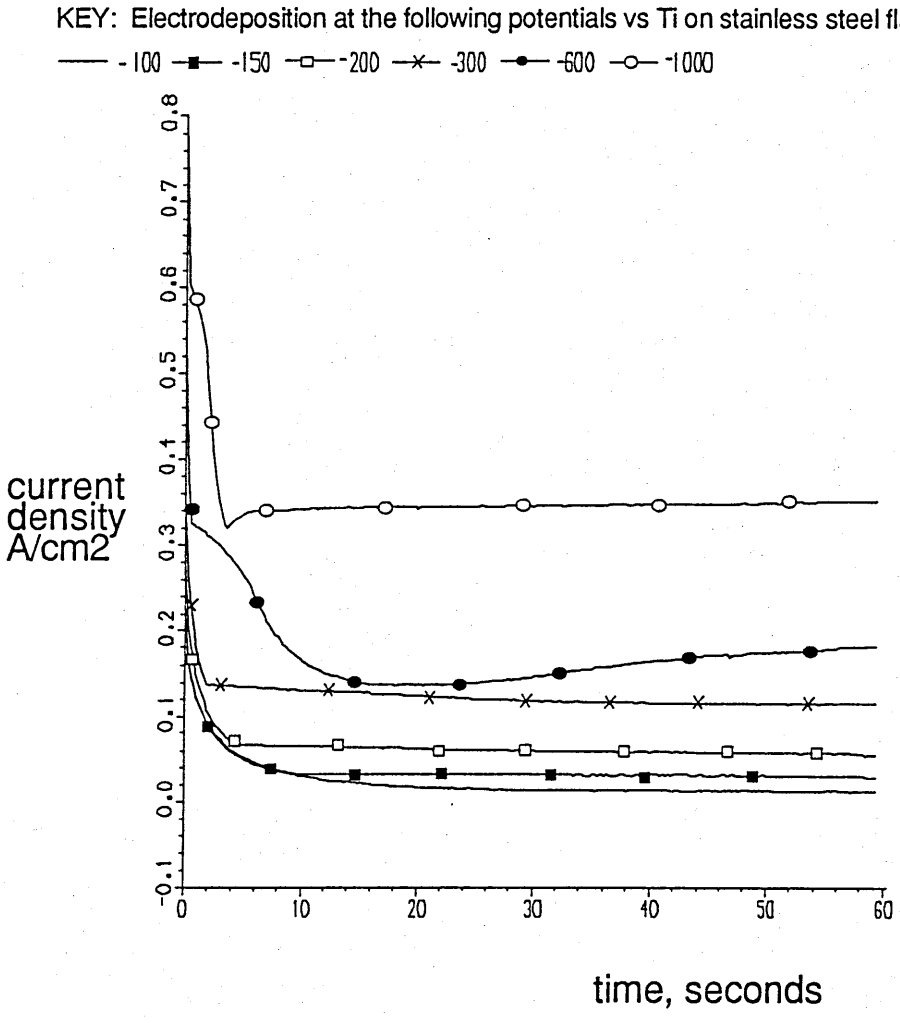

FIGURE 4.25

ELECTRODEPOSITION AT CONSTANT POTENTIAL : CURRENT-TIME OVER FIRST 12 SECONDS

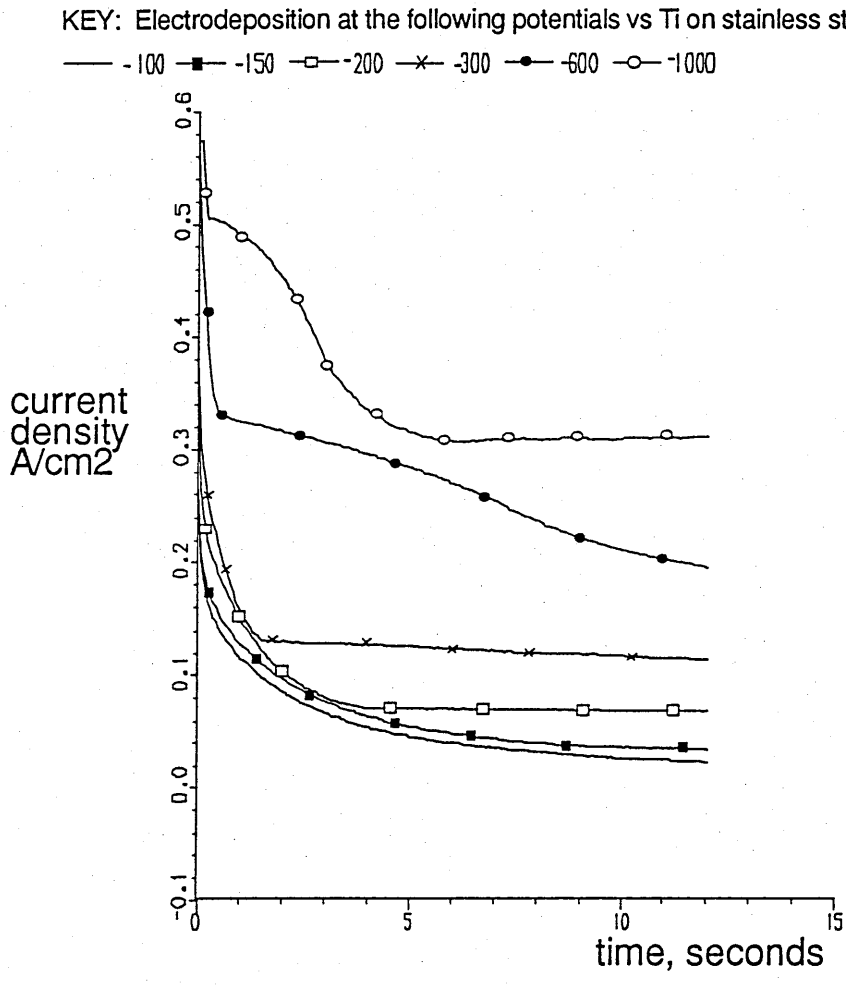

FIGURE 4.20

ELECTRODEPOSITION AT CONSTANT OVERPOTENTIAL OF 100 mV

Substrate in each case is fully pre-treated stainless steel flag.
Deposition conditions: 450 C; 2.23 wt.% Ti (proportion as TiII, 0.83); duration of deposition as shown.

(a) 12 seconds
(0.7 coulombs/cm2)

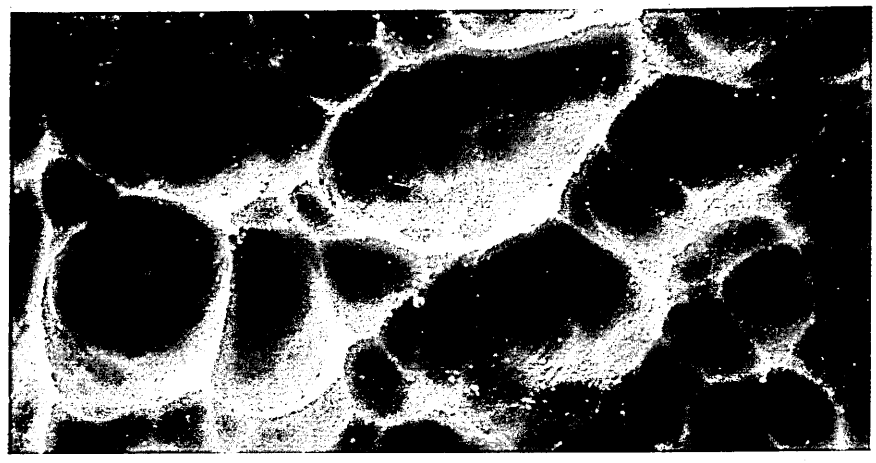

(b) 60 seconds
(1.4 coulombs/cm2)

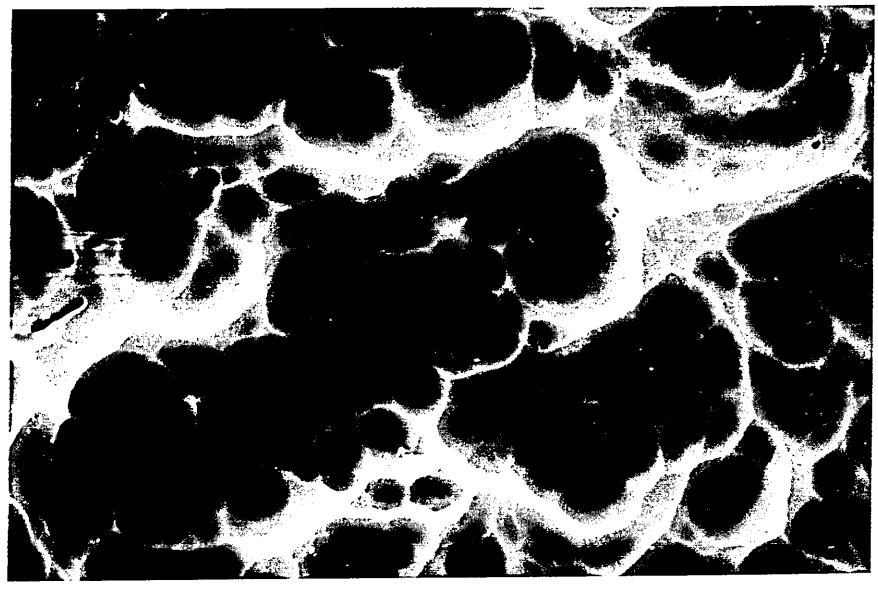

(c) 180 seconds
(2.0 coulombs/cm2)

FIGURE 4.27
ELECTRODEPOSITION
AT CONSTANT OVERPOTENTIAL OF 150 mV

Substrate in each case is fully pre-treated stainless steel flag.
Deposition conditions: 450 C; 2.23 wt.% Ti (proportion as TiII, 0.83); duration of deposition as shown.

(a)12 seconds
(0.8 coulombs/cm2)

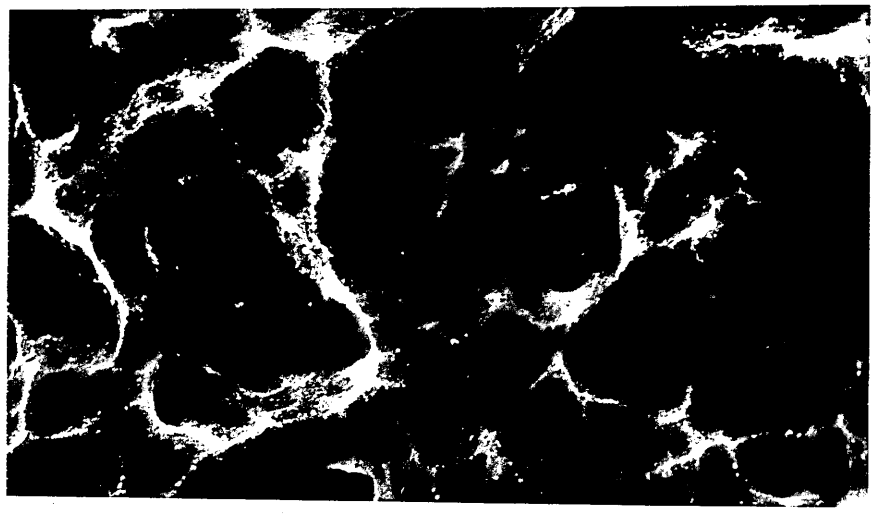

(b) 60 seconds
(2.2 coulombs/cm2)

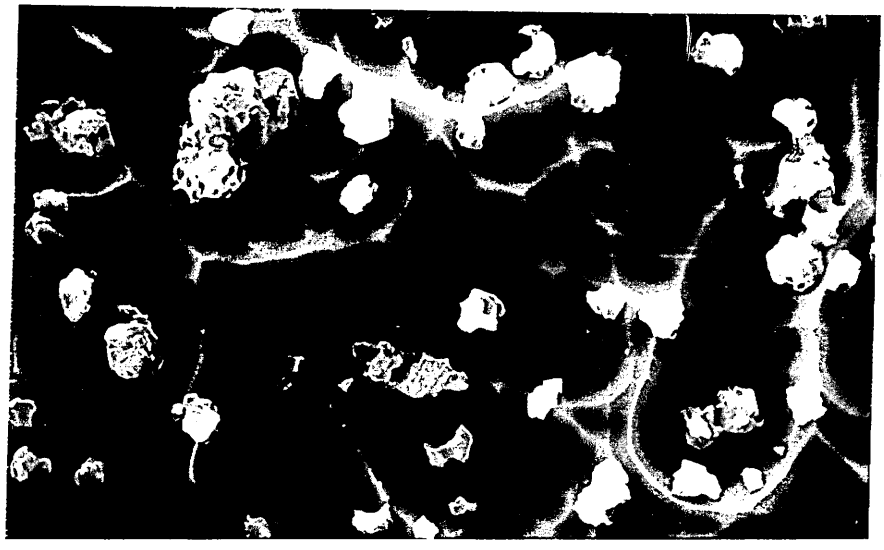

(c) 180 seconds
(6.8 coulombs/cm2)

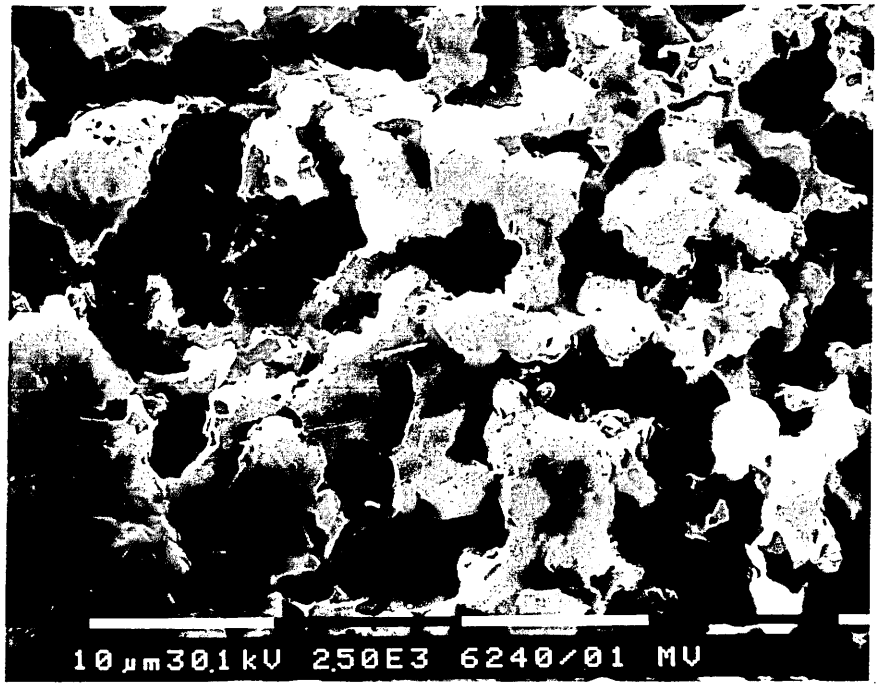

FIGURE 4.28
ELECTRODEPOSITION
AT CONSTANT OVERPOTENTIAL OF 300 mV

Substrate in each case is fully pre-treated stainless steel flag.
Deposition conditions: 450 C; 2.23 wt.% Ti (proportion as Till, 0.83); duration of deposition as shown.

(a) 12 seconds
(1.6 coulombs/cm2)

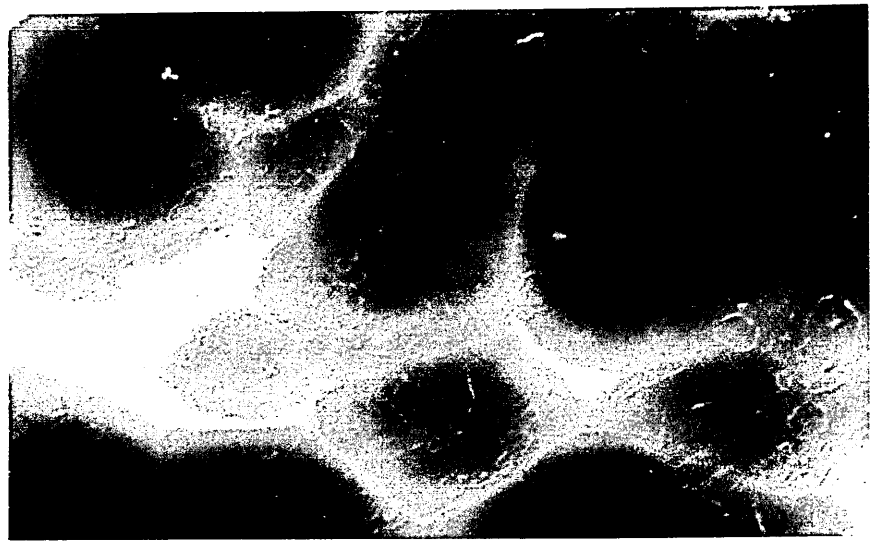

(b) 60 seconds
(7.5 coulombs/cm2)

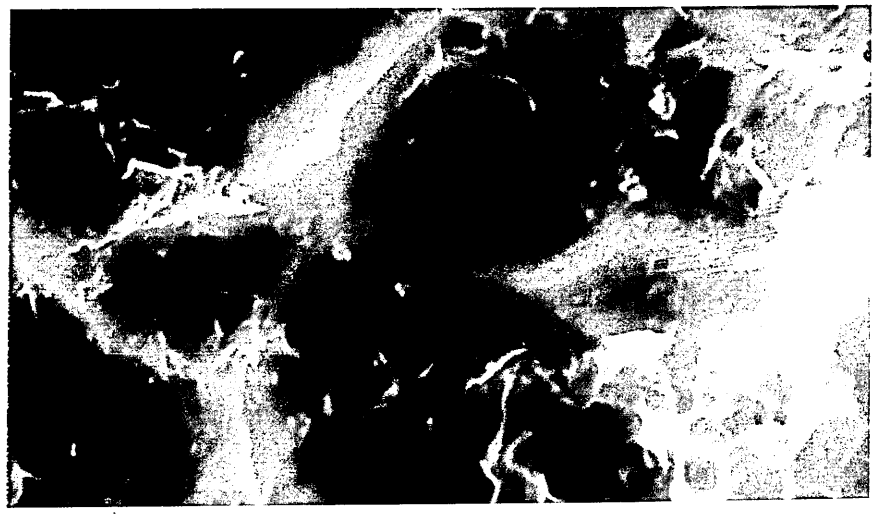

(c) 180 seconds
(18.5 coulombs/cm2)

FIGURE 4.29
ELECTRODEPOSITION
AT CONSTANT OVERPOTENTIAL OF 600 mV

Substrate in each case is fully pre-treated stainless steel flag.
Deposition conditions: 450 C; 2.23 wt.% Ti (proportion as TiII, 0.83); duration of deposition as shown.

(a) 12 seconds
(3.2 coulombs/cm2)

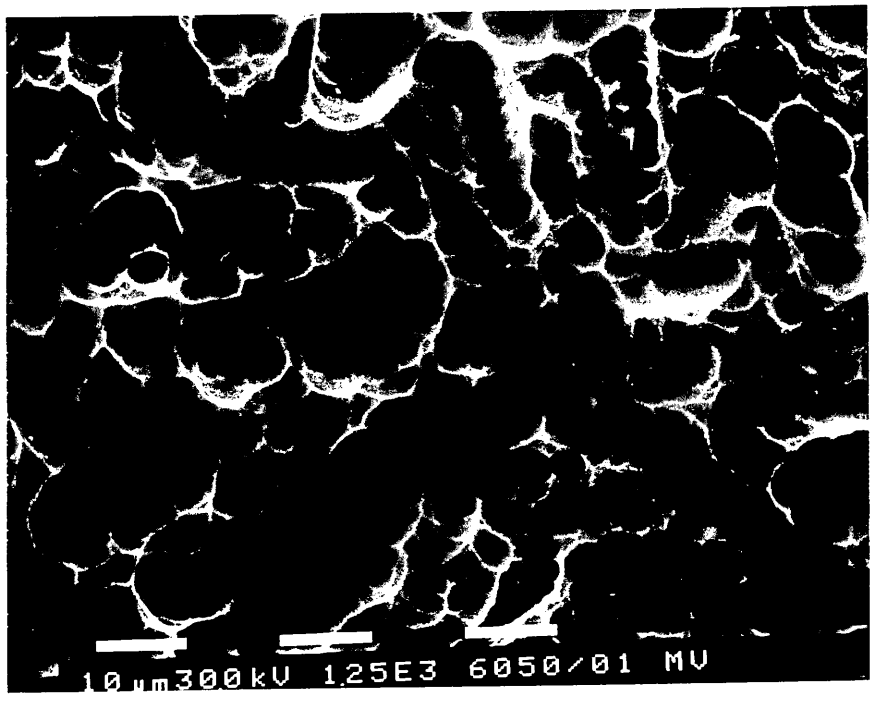

(b) 60 seconds
(11.0 coulombs/cm2)

(c) 180 seconds
(35.0 coulombs/cm2)

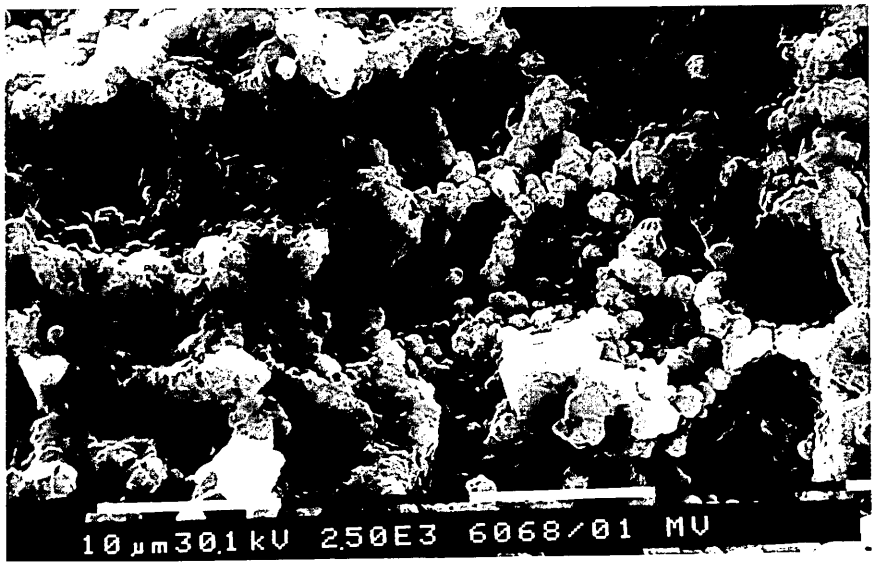

FIGURE 4.30
ELECTRODEPOSITION AT -600 mV

(data from figure 4.23)

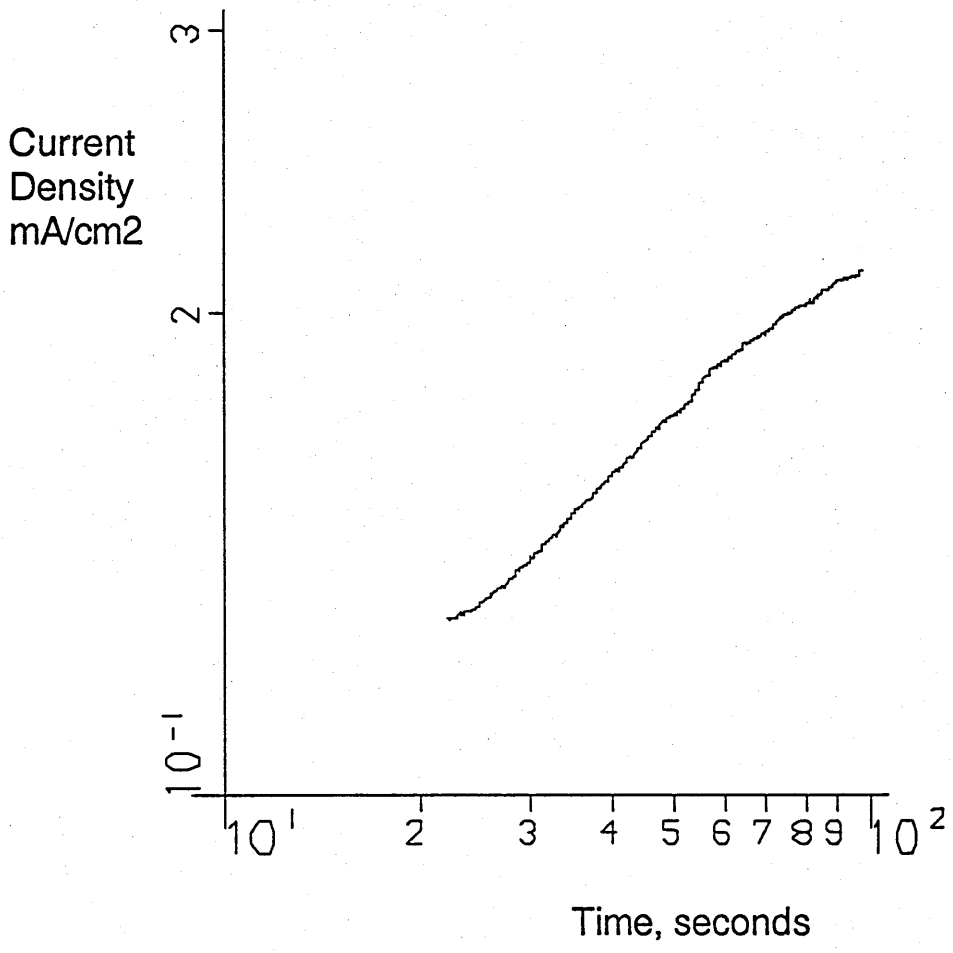

CHAPTER 5

THE PRODUCTION OF ELECTROPLATED COATINGS OF TITANIUM

5.1. Introduction

5.1.1. Characteristics desirable in electroplated coatings

For a coating to perform adequately in preventing corrosion of the substrate, the following characteristics are desirable[111][162][108].

5.1.1.1. Galvanic protection

Often, in corrosion protection, the substrate/coating combination are chosen so that when both materials are in contact with each other and with the corroding medium oxidation of the coating metal takes place in preference to that of the substrate material. This is the case for zinc coatings on iron or steels, for example. If the coating is breached, as a result of mechanical damage such as scratching or deformation of the coated article, then under most conditions, it is the zinc which corrodes in preference to the substrate iron with which it is in contact, as a result of the relative positions of the Fe/Fe^{2+} and Zn/Zn^{2+} couples in the electrochemical series for their particular environment. A titanium coating in contact with most likely substrates, however, would not corrode preferentially[34]. Consequently any hole in the coating, whether present as an original flaw, or caused subsequently by abrasion or other damage, will lead to corrosion of the substrate. Considerable damage can result from even small non-continuities in the coating. Because of this factor the integrity of the coating is of prime importance. This causes thin "flash" coatings to be

unsuitable, as only thicker coating layers can be expected to provide the necessary barrier allowing for surface damage through handling and wear.

5.1.1.2. Continuity and uniformity

That the coating is continuous, free of pores, cracks and other voids, is of particular importance for titanium in view of the above discussion. Uniformity must always be ensured to prevent recesses or other shaped areas suffering as a result of localised thin or porous coatings, while most of the deposit is adequate. Small pores or voids within a thick coating, which do not link up to form a continuous channel through the coating from the outside corroding medium to the substrate, are usually acceptable. If the deposit is highly stressed, then cracks may appear after deposition in order to relieve the stress. Co-evolution of gases such as hydrogen in aqueous plating systems often causes this type of problem. This is most notable in chromium plating where the micro-cracked structure is usual. Assessment of coating uniformity and continuity is most conveniently made by SEM studies of prepared cross-sections. Direct determination of porosity is possible, but performance assessment of the coating in a given corroding medium is a more realistic test. In this study, occasional comparative corrosion tests of coated and uncoated specimens immersed in chloride solutions for extended periods have been carried out, but no systematic assessment using these techniques has been undertaken.

5.1.1.3. Thickness

Where an intrinsically porous structure is produced, then thickness may be built up in order to make it less likely that pores will link

to provide a continuous route for a corroding solution or vapour to reach the substrate. The nature of the growth making up the corroding structure will also influence the minimum thickness necessary to ensure complete coverage of the substrate. Gold or silver electroplates can be used to cover a substrate at extremely small thicknesses, of about 1 micron or even less. Other electroplates which grow differently and in a more 3-dimensional way will be incomplete even at nominal thicknesses of 10 microns, and will require very much thicker coatings to ensure complete coverage. Similarly if the coating cannot be applied uniformly then a significantly higher average weight/unit area must be laid down to ensure that the most lightly coated areas have a sufficient covering. It is obviously also important to provide a substantial thickness which has some mechanical resistance to minor surface damage in order to prevent ready penetration of the coating depth in general use. Coating thickness is readily determined from accurately prepared cross-sections, but care must be taken to select representative areas for examination. Average thickness can be estimated from coating weight over a known substrate area using theoretical density values. However, this obviously ignores effects arising from non-uniform deposit distribution. Both techniques have been used as appropriate in this study.

5.1.1.4. Surface finish

Surfaces which are rough to the touch are not usually acceptable as they are, but further finishing such as deburring, grinding or polishing can be carried out to improve the characteristic. Sufficient coating thickness must be available to allow removal of

material in these operations without risk of exposing the substrate. Surfaces which are smooth to the touch will vary in brightness according to the grain-size of the surface layers. The finest surfaces will be mirror-bright. This is not usually important for corrosion-protection purposes. Surface texture can be determined using stylus-type machines such as the Talysurf. This is described in chapter 6. Generally a visual examination together with information from microscopic examination of cross-sections was used here for assessment of surface finish.

5.1.1.5. Mechanical properties

Once a coating has been applied to a substrate, then subsequent manufacturing operations may need to be carried out to produce the finished article. An example might be bending of sheet material to construct a particular product. For the coating to be satisfactory it must have sufficient mechanical strength and ductility to deform with the substrate without peeling or cracking. Irrespective of the adhesion strength (see below), if the coating material is brittle, cracks or pores will appear on deformation in this way. Even if no post-coating operations are necessary, good mechanical strength and ductility will offer advantages in making the material less vulnerable to perforation as a result of mechanical damage. The determination of the mechanical properties of coatings is difficult because of the need to separate the coating from the substrate before testing, to ensure unambiguous results. In practice, testing of the coated material and examination for cracks, tears, etc. is more convenient in many cases. Hardness can be considered a composite property, depending on the material's capacity for deformation (ductility) as well as its mechanical strength (tensile